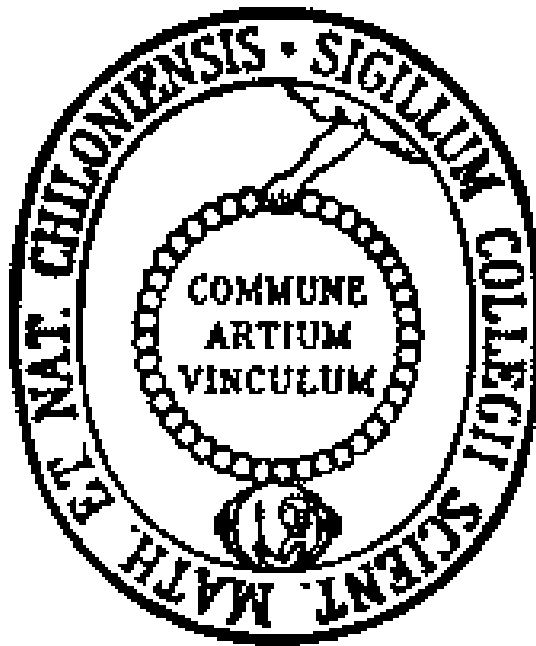


Proteolytic control of necroptosis



Dissertation zur Erlangung des Doktorgrades
der Mathematisch-Naturwissenschaftlichen
Fakultät der Christian-Albrechts-Universität
zu Kiel

vorgelegt von

Johaiber I. Fuchslocher Chico

Kiel

2017

Erster Gutachter: Prof. Dr. Dieter Adam

Zweiter Gutachter: Prof. Dr. Dr. Thomas C. G. Bosch

Inhaltsverzeichnis

A)	Eidesstattliche Erklärung.....	I
B)	Acknowledgements.....	II
C)	List of abbreviations.....	III
D)	List of figures.....	VIII
E)	List of tables.....	X
1	Summary.....	1
1.1	Zusammenfassung.....	2
2	Introduction.....	4
2.1	Caspase-dependent programmed cell death: Apoptosis.....	4
2.2	Caspase-independent programmed cell death.....	5
2.3	Necroptosis.....	6
2.3.1	The death receptor superfamily.....	7
2.3.2	The necroptotic pathway.....	7
2.3.3	HtrA2/Omi and necroptosis.....	10
2.3.4	Biological role of necroptosis.....	12
2.4	ADAM17 and necroptosis.....	13
2.5	Mouse model of DSS-Colitis.....	14
2.6	Acid sphingomyelinase and ceramide.....	15
3	Materials and Methods.....	17
3.1	Materials.....	17
3.1.1	Equipment.....	17
3.1.2	Reagents and chemicals.....	19

3.1.3	Antibodies	22
3.2	Methods.....	23
3.2.1	Cell lines and cytotoxicity assays.....	23
3.2.2	Animal experiments	24
3.2.3	Cell lysates	26
3.2.4	Protein quantification	27
3.2.5	SDS-PAGE and Western blot analysis.....	27
3.2.6	Flow cytometry.....	28
3.2.7	Transfection.....	28
3.2.8	Gene modification and sequencing	30
3.2.9	A-SMase activity assay	32
3.2.10	Immunofluorescence	32
3.2.11	Cell fractionation	33
4	Results	34
4.1	Contribution of necroptosis to intestinal inflammation in ADAM17 ^{ex/ex} /RIPK3 ^{-/-} mice 34	
4.1.1	Conclusion	41
4.2	Contribution of PGAM5 during necroptosis.....	43
4.2.1	Conclusion	44
4.3	Contribution of HtrA2/Omi to necroptosis	46
4.3.1	Conclusion	52
4.4	Localization of HtrA2/Omi during necroptosis.....	52
4.4.1	Conclusion	55
4.5	Role of known substrates of HtrA2/Omi	55
4.5.1	Conclusion	58

4.6	Role of acid sphingomyelinase in necroptosis	58
4.6.1	Localization of the necroptotic cleavage site of acid sphingomyelinase.....	58
5	Discussion	62
5.1	The relationship between ADAM17, RIPK3 and necroptosis in DSS-induced colitis.	62
5.2	The role of PGAM5 in necroptosis.....	64
5.3	The role of HtrA2/Omi in necroptosis	65
5.4	Identification of the cleavage site of acid sphingomyelinase in necroptosis.....	69
6	Citations.....	70
7	List of publications	90
8	Curriculum Vitae.....	91
9	Appendix.....	92

A) Eidesstattliche Erklärung

Hiermit erkläre ich, Johaiber Ilich Fuchslocher Chico, dass ich die vorliegende wissenschaftliche Abhandlung mit dem Titel:

„Proteolytic control of necroptosis“

nach den Regeln guter wissenschaftlicher Praxis eigenständig verfasst und keine anderen als die angegebenen Hilfsmittel und Quellen benutzt habe. Dabei habe ich keine Hilfe, außer der wissenschaftlichen Beratung durch meinen Doktorvater Prof. Dr. rer. nat. Dieter Adam, meinem zweiten Betreuer Prof. Dr. rer. nat. Stefan Schütze und durch die namentlich erwähnten Kooperationspartner in Anspruch genommen.

Diese Arbeit wurde bisher an keiner Stelle im Rahmen eines Prüfungsverfahrens vorgelegt. Teile dieser Arbeit wurden bereits publiziert.

B) Acknowledgements

Special thanks to my P.I. Prof. Dr. rer. nat. Dieter Adam for the chance he gave me by admitting me into his group to work on this very interesting topic and the trust he placed on me in the past years. Thank you also for all the suggestions and critical scientific discussions which helped to advance not only the project, but also contribute to my own scientific growth.

Prof. Dr. Dr. h.c. Thomas Bosch I give my thanks for his willingness to assess and correct my work.

I also want to thank the director of the Institute of Immunology, Prof. Dr. med. Dieter Kabelitz, for giving me the opportunity of working in his institute. It was like a second home to me for nearly 4 years, in no small part due to the excellent relationship with all my co-workers, for which I am deeply grateful.

Many thanks to the group of Prof. Dr. rer. nat Stefan Schütze; he himself and Dr. Jürgen Fritsch were always there with useful guidance and experimental expertise whenever I needed it.

Special thanks to Parvin Davarnia for always believing in me and all the teachings, conversations, support and care that made this work possible. She truly was my Labmom™. I also have to mention Carina Saggau and Justus Hoyer, thank you for your support -in and out of the laboratory. Your friendship kept me moving forward. To my former colleagues Dr. Justyna Sosna and Sabine Mathieu-Grützmacher, my thanks for their continued support, assistance and teachings.

Of course, this acknowledgement would not be completed without deeply thanking my family: my parents Aura Rosa and Andrei and my sister Yakora for their love, trust and support, for teaching me to fight and giving me the necessary tools to succeed in life; my aunt Isabel for making my German adventure possible by opening her home to me; and my girlfriend Wasifa for accompanying me at every step of the way and, through her love, kept me going through wind and weather. I love you all. Thank you so much.

C) List of abbreviations

ADAM17	A disintegrin and metalloproteinase 17
AIF	apoptosis inducing factor
Apaf-1	apoptotic protease activating factor-1
A-SMase	acid sphingomyelinase
ATP	adenosine-5'-triphosphate
Bcl-2	B-cell/ lymphoma-2
BMDM	bone marrow-derived macrophage
BSA	bovine serum albumin
BV6	a Smac mimetic
Cas9/Cas	CRISPR-associated 9
Caspase	cysteine-aspartate protease
CASP3/4/5/6/7/8/9	caspase-3/4/5/6/7/8/9
CD95	cluster of differentiation 95 (also known as Fas)
CHX	cycloheximide
ciAP	cellular inhibitor of apoptosis protein
CLSM	confocal laser scanning microscopy
CRISPR	clustered regularly interspaced short palindromic repeats
Ctrl/Ctrl	control
CYLD	cylindromatosis

DAMPs	damage associated molecular patterns
dATP	deoxyadenosine triphosphate
DBC1	deleted in bladder cancer protein 1
DD	death domain
DESC 1	transmembrane protease serine 11E
DISC	death inducing signaling complex
DPSYL 4	dihydropyrimidinase-like 4
DRs	death receptors
Drp 1	dynamamin 1 like protein
dsRNA	double-stranded RNA
DSS	dextran sulfate sodium
FACS	flow-analyser and cell sorter
FASR	Fas cell surface death receptor
FADD	Fas-associated protein with death domain
FCS	fetal calf serum
GFP	green fluorescent protein
GGT1	gamma-glutamyltransferase 1
HtrA2	high temperature requirement protein A2
IAP	inhibitor of apoptosis protein
IF	immunofluorescence
IFN	interferon

IL (-22, -23, -1 β)	interleukin (-22, -23, -1 β)
LONP1	Lon protease 1
LUBAC	linear ubiquitin chain assembly complex
MEF	mouse embryonic fibroblast
MLKL	mixed lineage kinase domain-like
MMP3	metalloproteinase 3 or stromelysin-1
MPP-A/PMPCA	mitochondrial-processing peptidase subunit alpha
Nec-1s	necrostatin 1 s
NF- κ B	nuclear factor- κ B
NOX1	NADPH oxidase-1
PAGE	polyacrylamide gel electrophoresis
PBS	phosphate buffered saline
PCD	programmed cell death
PDXDC1	pyridoxal dependent decarboxylase domain containing protein 1
PFA	paraformaldehyde
PGAM5	phosphoglycerate mutase family member 5
PI	propidium iodide
PMPCA	mitochondrial processing peptidase alpha
PRPF8	pre-mRNA processing factor 8
PSA1	proteasome subunit, alpha type-1

RHIM	RIPK homotypic interaction motif
RIPK1/RIP1	receptor-interacting serine-threonine protein kinase 1
RIPK3/RIP3	receptor-interacting serine-threonine protein kinase 3
RNAi	RNA interference
ROS	reactive oxygen species
RT	room temperature
SDS	sodium dodecyl sulfate
siRNA	small interfering RNA
Smac	second mitochondria-derived activator of caspases
SMase	sphingomyelinase
TLR	Toll-like receptor
TMPRSS11E	transmembrane protease serine 11E
TNF	tumor necrosis factor
TNF-R	TNF receptor
TRADD	TNF-R1-associated protein with death domain
TRAF	TNF-R-associated factor
TRAIL	TNF-related apoptosis inducing ligand
TRAILR	TRAIL-receptor
UCH-L1	ubiquitin C-terminal hydrolase 1
vMIA	viral mitochondrial inhibitor of apoptosis
VPS4B	Vacuolar Protein Sorting 4 Homolog B

wt/ WT	wild-type
WT1	Wilms' tumour suppressor protein 1
zVAD-fmk/ zVAD	benzyloxycarbonyl-Val-Ala-Asp-fluoromethylketone

Commonly used abbreviations are not listed.

D) List of figures

- Figure 1: Summary of apoptosis
- Figure 2: Summary of necroptosis
- Figure 3: Proposed model of HtrA2/Omi involvement in necroptosis
- Figure 4: Structure of ADAM17
- Figure 5: Schematic representation of the workflow of an overlap extension PCR
- Figure 6: Summary of DSS-induced acute colitis (ADAM17 ex/ex RIPK3^{-/-} and ADAM17 ex/ex mice)
- Figure 7: Histology of DSS-induced acute colitis colon samples (ADAM17 ex/ex RIPK3^{-/-} and ADAM17 ex/ex mice)
- Figure 8: Western blot analysis of DSS-induced acute colitis colon samples (ADAM17 ex/ex RIPK3^{-/-} and ADAM17 ex/ex mice)
- Figure 9: Summary of DSS-induced chronic colitis (ADAM17 ex/ex RIPK3^{-/-} and ADAM17 ex/ex mice)
- Figure 10: Histology of DSS-induced chronic colitis colon samples (ADAM17 ex/ex RIPK3^{-/-} and ADAM17 ex/ex mice)
- Figure 11: Western blot analysis of DSS-induced chronic colitis colon samples (ADAM17 ex/ex RIPK3^{-/-} and ADAM17 ex/ex mice)
- Figure 12: Western blot analysis of DSS-induced colitis colon samples (C57BL/6 mice)
- Figure 13: Functional assay of ADAM17^{-/-} MEF
-

-
- Figure 14: PGAM5 increase and siRNA
- Figure 15: CRISPR/Cas generation of PGAM5^{-/-} clones
- Figure 16: Time course of HtrA2/Omi^{-/-} MEF
- Figure 17: Rescue assay of HtrA2/Omi^{-/-} MEF
- Figure 18: CRISPR/Cas generation of HtrA2/Omi^{-/-} L929 cells
- Figure 19: Rescue Assay of HtrA2/Omi^{-/-} L929
- Figure 20: CRISPR/Cas generation of HtrA2/Omi^{-/-} HT-29 cells
- Figure 21: TRAIL-induced necroptosis of L929 and MEF cells
- Figure 22: Generation of vMIA expressing L929
- Figure 23: Immunofluorescence analysis of MEF and L929 cells
- Figure 24: Fractionation of MEF
- Figure 25: Western blot analysis of HtrA2/Omi substrates
- Figure 26: siRNA knock-down of HtrA2/Omi substrates
- Figure 27: Summary of A-SMase constructs generation
- Figure 28: CRISPR/Cas generation of A-SMase^{-/-} L929
- Figure 29: siRNA knockdown of cleaving candidates of A-SMase
- Figure 30: Actualized mode of action of HtrA2/Omi
-

E) List of tables

- Table 1: Breakdown of cell lines, media and stimulations used throughout the present work
- Table 2: Breakdown of primers and PCR conditions used in the genotyping of ADAM 17^{ex/ex} and ADAM 17^{ex/ex}-RIPK3^{-/-} mice
- Table 3: Genetic constructs used in this thesis

1 Summary

One of the most important processes governing the life of multicellular organisms is the regulated cellular death. It is important for maintaining cellular homeostasis, helping in foetal development, underpinning the working of the immune system and other biological processes. Cell death has been divided into accidental (necrosis) and regulated. This latter category has traditionally been occupied by apoptosis, a death form governed by the proteolytic activity of cysteine-aspartic proteases termed caspases (Kerr *et al.* 1972). In the last decades, other forms of cellular demise have been identified as being under the control of cellular signal cascades, thus expanding our understanding of regulated cell death.

The present work focuses on proteolytic processes underpinning a regulated cell death which is not under the control of caspases, specifically necroptosis. The name was created in 2005, by Degterev and colleagues to describe a form of cell death active even after suppressing caspase activity and being easily distinguishable from apoptosis on the morphological level due to distinct features: while apoptotic cells show membrane blebbing, nuclear fragmentation and cell shrinkage, this form showed the hallmarks of necrosis, cellular swelling, leading to bursting of the cells.

Necroptosis is a form of caspase-independent cell death, characterised by the activation of RIPK3 and MLKL. Multiple publications demonstrate that this pathway can be activated by a host of different receptors, such as tumor necrosis factor receptor 1, Fas cell surface death receptor, toll-like receptor 3 and 4 and interferon receptor. The group of Prof. Dr. Adam previously demonstrated the importance of acid sphingomyelinase and the possible role of the high temperature requirement protein A2 (HtrA2, also called Omi) in necroptosis.

The present works' aim has been to gain further insights into the proteolytic mechanisms present in necroptosis via multiple routes: investigating an *in-vivo* model for necroptosis in DSS-induced colitis in mice with an extremely reduced expression of the sheddase ADAM17, investigating the role of the phosphoglycerate mutase family member 5 (PGAM5) in necroptosis, analysis of the function of the protease HtrA2/Omi and its possible substrates in

necroptotic cell death and investigating the proteolytic cleavage of acid sphingomyelinase (A-SMase) as a component of necroptosis.

1.1 Zusammenfassung

Einer der wichtigsten Prozesse die das Leben von multizellulären Organismen beeinflussen, ist der regulierte Zelltod. Es ist wichtig für die Aufrechterhaltung der zellulären Homöostase, Beihilfe in der fötalen Entwicklung, als Basis für die Funktion des Immunsystems und andere biologische Prozesse. Der Zelltod wird in zufällig (Nekrose) und reguliert unterteilt. Letztere Kategorie wurde traditionell der Apoptose zugeschrieben, eine Form des Zelltodes unter der Kontrolle der proteolytischen Aktivität von Cystein-Aspartase Proteasen, genannt Caspasen (Kerr *et al.* 1972). In den letzten Jahrzehnten wurden andere Arten von Zelltod identifiziert, die unter der Kontrolle von zellulären Kaskaden liegen, womit unser Verständnis von reguliertem Zelltod expandiert wurde.

Diese Arbeit konzentriert sich auf proteolytische Prozesse die die Basis für eine regulierte Form von Zelltod sind, die nicht unter der Kontrolle von Caspasen ist, konkret: Nekroptose. Der Name entstand 2005 als Degterev und Kollegen eine Arte des Zelltodes beschrieben, die sogar nach Unterdrückung von Caspase Aktivität verlief, und morphologisch leicht von Apoptose zu unterscheiden ist: während apoptotische Zellen Blasenbildung in der Membran, nukleare Fragmentation und Schrumpfen vorweisen, zeigte diese Art die charakteristischen Merkmale von Nekrose, Anschwellen bis zum Bersten der Zellen.

Nekroptose ist eine Form von Caspase-unabhängigem Zelltod, die durch die Aktivierung von RIPK3 und MLKL charakterisiert. Eine Vielzahl von Publikationen haben gezeigt, dass der Signalweg von mehreren verschiedenen Rezeptoren aktiviert werden kann, wie Tumornekrosefaktor-Rezeptor-1, Fas-Zelloberflächen-Rezeptor, Toll-ähnliche Rezeptoren -3 und -4 und der Interferon-Rezeptor. Die AG von Prof. Dr. Adam hat auch die Wichtigkeit der sauren Sphingomyelinase und die mögliche Rolle des Hohen Temperatur benötigendes Protein A2 (HtrA2 auch Omi genannt) in Nekroptose gezeigt.

Das Ziel dieser Arbeit war es weitere Einsichten von proteolytischen Prozessen in der Nekroptose zu gewinnen. Dieses Ziel wurde in mehreren Ansätzen verfolgt: die Untersuchung eines *in-vivo* Modells der Nekroptose in Mäusen mit einer extremen Reduktion der Expression der „shedase“ ADAM17. Die Analyse einer möglichen Rolle der Phosphoglycerat Mutase Familienmitglied 5 (PGAM5) in Nekroptose, die Aufklärung der Funktion der Protease HtrA2/Omi und ihrer möglichen Substrate im nekroptotischen Zelltod, sowie die Untersuchung der proteolytischen Spaltung der sauren Sphingomyelinase (A-SMase) als Komponente der Nekroptose.

2 Introduction

2.1 Caspase-dependent programmed cell death: Apoptosis

Since the publication of the first paper describing the biochemical mechanisms underpinning its route (Kerr *et al.* 1972), apoptosis has quickly become the most studied and best understood form of cellular demise.

At the morphological level, apoptosis is characterized by exposure of phosphatidylserine on the outer layer of the cytoplasmic membrane, nuclear condensation, membrane blebbing, cell shrinkage, DNA fragmentation and finally disintegration into so-called apoptotic bodies, which are then eliminated by phagocytes (Nagata *et al.* 2017, Poon *et al.* 2014).

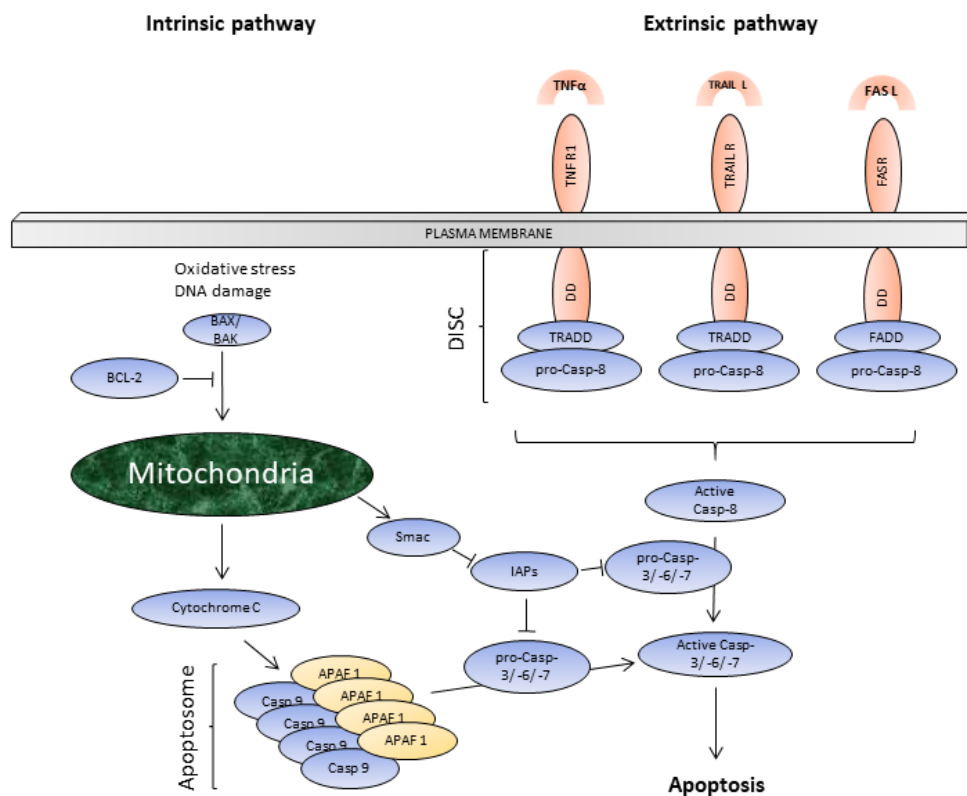


Figure 1

Summary of the two apoptosis pathways. The intrinsic pathway can be triggered by oxidative stress and/or DNA damage. This promotes the activation of pro-apoptotic BCL-2 family members such as BAX or BAK, which mediate cytochrome C release from mitochondria. Cytochrome C is able to promote the formation of the apoptosome by oligomerizing caspase 9 and Apaf-1, which then can activate the effector caspases 3, -6 and -7. The extrinsic pathway starts with the docking of death-inducing ligands to their receptor, leading to death-inducing signaling complex (DISC) formation, containing death-domain proteins such as TRADD/FADD and pro caspase 8, which is then activated by autoproteolysis. Active caspase 8 is in turn able to activate the effector caspases 3, -6 and -7. In both cases, release of Smac from mitochondria inhibits IAPs, permitting the execution of apoptosis.

At the molecular level, apoptosis can be triggered by two distinct pathways (see figure 1). The extrinsic pathway is activated by external signals docking on death receptors such as tumor necrosis factor receptor (TNF-R), TNF related apoptosis-inducing ligand-receptor (TRAILR) and cluster of differentiation 95 (CD95, also known as Fas), initiating a cascade through downstream adapter proteins such as TNF-associated death domain (TRADD) and Fas-associated death domain protein (FADD), the activation of initiator caspases-8 and -10 and effector caspases-3, -6, and -7 (Nagata *et al.* 2017, Poon *et al.* 2014). The intrinsic pathway is under the control of members of the B-cell lymphoma-2 (Bcl-2) family and activates in response to stimuli such as DNA damage, hypoxia or oxidative stress (Galluzzi *et al.* 2012). In this scenario, intracellular stimuli can induce the release of cytochrome c from mitochondria, which recruits the apoptotic protease activating factor 1 (Apaf-1) and the initiator caspase-9, forming a complex called “apoptosome”. The apoptosome is then able to activate the effector caspases-3, -6, and -7 (Dai *et al.* 2015, Nagata *et al.* 2017). In both pathways, the simultaneous release of second mitochondrial-derived activator of caspases (Smac) from mitochondria inhibits the activity of inhibitor of caspase proteins (IAP, Fuchs and Steller 2015), which permits the apoptotic process by inhibiting a crucial apoptotic inhibitor.

2.2 Caspase-independent programmed cell death

In contrast to apoptosis, caspase-independent programmed cell death is less well described. The reason for this is found in the common morphological features of these different forms of cellular demise: extreme organelle and cellular swelling leading to bursting cells and immunological alert due to the high amount of damage-associated proteins disseminated in the surroundings. This morphology coincides with necrosis, a term historically used for accidental forms of cellular death (Vanden Berghe *et al.* 2014), and as such lead to the initial dismissal of instances of necroptosis as merely accidental.

However, in recent years the search for and study of molecular mechanisms has led to the discovery of a host of different types of programmed cell death distinct from apoptosis such as necroptosis (Degterev *et al.* 2005), ferroptosis (Dixon *et al.* 2012), oxytosis (Tan *et al.* 2001),

pyroptosis (Cookson and Brennan 2001), pyronecrosis (Wilingham *et al.* 2007), mitochondrial permeability transition (MPT)-dependent necrosis (Baines *et al.* 2005), parthanatos (Andrabi *et al.* 2008) and NETosis/Etosis (Brinkman *et al.* 2004).

2.3 Necroptosis

The term necroptosis was coined in a study searching for a chemical compound able to inhibit a non-apoptotic form of cell death in a model of ischemic brain injury. While being morphologically necrotic, it was also triggered by the same stimuli as apoptosis, such as TNF (Degterev *et al.* 2005). An inhibitor was found and called necrostatin 1 (Nec1), and in a follow-up study shown to inhibit the kinase activity of receptor interacting protein kinase 1 (RIPK1 or RIP1) (Degterev *et al.* 2008).

Three further studies appearing in short succession showed that RIPK1 interacts with and phosphorylates receptor interacting protein kinase 3 (RIPK3 or RIP3) through their respective RIP homotypic interaction motif (RHIM) domains (Cho *et al.* 2009, He *et al.* 2009, Zhang *et al.* 2009). This marked the first finding of a molecular component unique to necroptosis, since RIPK1 was already known to act e.g. in apoptosis and inflammation signaling (Lin *et al.* 1999, Kelliher *et al.* 1998). Coupled with the previous discovery that RIPK3^{-/-} mice were viable (Newton *et al.* 2004). Finally, mixed lineage kinase domain-like protein (MLKL) was shown to be another protein unique to the necroptotic pathway (Sun *et al.* 2012), leading to the establishment of the term “Necroptosis” as referring to the type of regulated cell death mediated by RIPK3 and MLKL (Galluzzi *et al.* 2015).

A debated topic to this day is the role of mitochondria in necroptosis. Phosphoglycerate mutase family member 5 (PGAM5) has been identified as a key mediator in necroptosis (Wang *et al.* 2012) via its effect on Dynamin related protein-1 (Drp1) and thus mitochondrial fission. Further studies dismissed the necessity of Drp1 (Moujalled *et al.* 2014) and even mitochondria for necroptosis altogether.

This seminal work demonstrated the existence of an underlying molecular mechanism regulating a morphologically necrotic type of death, and opened the door to potential

therapeutic solutions to pathologic injuries that, up to that point, were believed to be the consequence of unregulated processes.

2.3.1 The death receptor superfamily

A lot of the work done in necroptosis, including this thesis, focuses on the pathway initiated by the TNF receptor 1 (TNF-R1), a member of the TNF receptor superfamily, which governs processes such as immune response, proliferation, hematopoiesis and cell death (Aggarwal 2003). Two different TNF receptors are known, TNF-R1 is ubiquitously expressed, while TNF-R2 has been shown to be expressed only by endothelial cells and some immune cells (Aggarwal and Natarajan. 1996).

Some receptors of the TNF superfamily possess a cysteine-rich domain in the extracellular portion of the receptor (the death domain or DD) thus belonging to the subgroup of death receptors or DR (Aggarwal, 2003). DR have been shown to be able to induce both caspase-dependent and -independent cell death (Leist and Jäättelä 2001) including TNF-R1, CD95, DR3, DR6 and TRAILR1/2 (Mahmood and Shukla 2010).

2.3.2 The necroptotic pathway

Once TNF-R1 is bound by the TNF ligand, it is able to recruit TNF-R1-associated death domain protein (TRADD), as well as TNF-R-associated factor (TRAF) 2/3/5/6, linear ubiquitin chain assembly complex (LUBAC) and cellular inhibitor of apoptosis protein 1 and 2 (cIAP1/2), which polyubiquitinate RIPK1, generating a stable complex called Complex I (Micheau and Tschopp 2003). The complex I pushes the balance of cellular survival/death in favor of the NF- κ B pathway and thus survival and cytokine production (Sun and Wang 2014).

The auto-ubiquitination of cIAP1/2, coupled with the interaction of Smac, compromises cIAP activity and thus elicits the dissociation of RIPK1 from the plasma membrane (Du *et al.* 2000), followed by the removal of the K63-linked polyubiquitin chain on RIPK1 by either cylindromatosis (CYLD) and/or the ubiquitin-modifying enzyme A20 (Wertz *et al.* 2004, Moquin *et al.* 2013). RIPK1 can then bind to the Fas-associated death domain (FADD), through which it recruits procaspase 8. Together with RIPK3 they form the so-called Complex IIb, which

subsequently leads to the activation of caspases and apoptosis (Pasparakis and Vandenabeele 2015). This can also happen under conditions initially compromising RIPK1 ubiquitination (Moquin *et al.* 2013).

Interestingly, the apoptotic initiator caspase 8 acts as a necroptotic repressor. This is shown by the fact that the embryonic lethality of *Casp 8*^{-/-} mice is rescued by concomitant homozygous deletion of RIPK3 (Kaiser *et al.* 2011, Oberst *et al.* 2011), because of the loss of caspase 8-triggered uncontrolled necroptosis being rescued. If caspase activity is compromised however, and given high enough cellular levels of RIPK3 and MLKL, necroptosis will ensue. RHIM-RHIM interactions between RIPK1 and RIPK3, lead to the phosphorylation of RIPK3 at Ser227 (Ser232 for mouse RIPK3) (Chen *et al.* 2013). Subsequently, its substrate MLKL is also phosphorylated at Thr357/Ser358 in humans and Ser345 in mouse (Rodriguez *et al.* 2016), all three elements forming a complex called necrosome (Pasparakis and Vandenabeele 2015).

Phosphorylation destabilizes the monomeric structure of MLKL, pushing it to an oligomeric state which enables the N-terminal helix bundle to bind phosphatidylinositol phosphate lipids (PIPs) and the mitochondria-specific cardiolipin (CL) (Wang *et al.* 2014a, Dondelinger *et al.* 2014). Oligomerized pMLKL then translocates to membranes, but the concrete mode of action of the pores formed by pMLKL is still debated, with Ca²⁺ influx (Murphy *et al.* 2014) and Na⁺ influx (Chen *et al.* 2013) being proposed, however, cells cultured in calcium and sodium-free media are still able to enter, a slightly delayed, necroptosis (He *et al.* 2011).

In addition to TNF, necroptosis can be triggered by other signals and receptors, such as the aforementioned members of the DR family Fas, TRAILR1/2 (Holler *et al.* 2000) and DR3 (Bittner *et al.* 2017), Toll-like receptors (TLRs, Ch'en *et al.* 2008), intracellular RNA (Schock *et al.* 2017) and DNA (Upton *et al.* 2012) sensors, interferons (IFNs, He *et al.* 2011, Thapa *et al.* 2013), proteasome inhibitors (Moriwaki and Chan 2016), ionizing radiation (Schildkopf *et al.* 2010), reactive oxygen species (ROS, Zhang *et al.* 2017), calcium overload (Nomura *et al.* 2014) and ischemia-reperfusion injury (Wen *et al.* 2017). All these processes are schematically shown in figure 2.

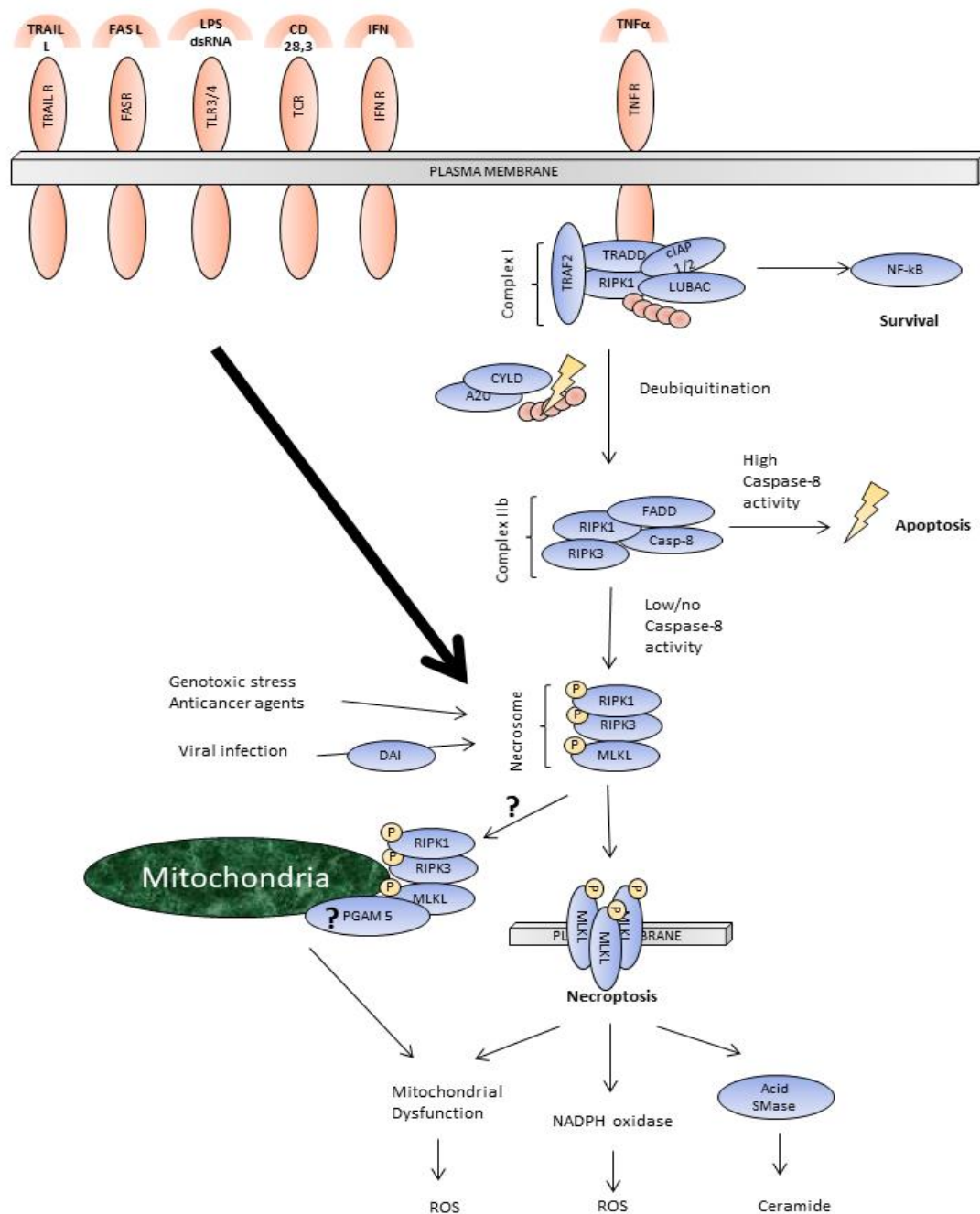


Figure 2

Summary of the necroptotic pathway, in which, activated by its ligand, TNF-R1 recruits RIPK1 into complex I formed also by TRADD, TRAF2, IAPs, and LUBAC, leading to the polyubiquitination of RIPK1 and typically to the activation of NF- κ B-dependent survival signals. If IAP activity is compromised, the ubiquitin chains attached to RIPK1 are proteolytically removed by CYLD or A20, enabling RIPK1 to associate with FADD and pro-caspase-8 in complex IIb. Canonically, high caspase-8 activity within complex IIb leads to proteolysis and inactivation of RIPK1 and RIPK3, thereby inducing apoptosis. Under conditions that compromise or reduce caspase-8 activity, RIPK1 and RIPK3 become activated by phosphorylation (P), promoting the recruitment of MLKL into the necrosome as well as its phosphorylation and thus activation. The involvement of the necrosome with mitochondria and PGAM5 remains unclear, but activated MLKL translocates to plasma and intracellular membranes, disrupting them and causing necroptotic death. Downstream effector mechanisms such as

mitochondrial dysfunction, NOX1 and A-SMase further enhance necroptosis by triggering the production of ROS or ceramide.

Necroptosis may also be triggered by stimuli other than TNF, such as triggers of the TCR, by the death ligands TRAIL and FasL, dsRNA or LPS via TLR3 and TLR4, respectively, or by interferons. Virus infections can directly activate RIPK3 (via the intracellular DNA sensor DAI), as can genotoxic stress and anti-cancer agents.

Lightning symbols indicate proteolytic cleavage events.

2.3.3 HtrA2/Omi and necroptosis

HtrA2/Omi is a ubiquitously expressed serine protease located in mitochondria with a reported chaperone activity (van Loo *et al.* 2002). HtrA2/Omi is known to promote apoptosis via translocation to the cytosol and subsequent release of active caspases from IAPs (van Loo *et al.* 2002, Suzuki *et al.* 2001, and Yang *et al.* 2003). In addition, our group has shown that HtrA2/Omi acts in necroptosis, since pharmacologically inhibited L929Ts, HT-29 and Jurkat I42 cells as well as HtrA2/Omi knock-out MEF are protected from TNF-induced necroptosis (Sosna *et al.* 2013). The concrete mode of action of HtrA2/Omi remains yet unknown. Since this enzyme doesn't seem to exit mitochondria under necroptosis (van Loo *et al.* 2002, Blink *et al.* 2004), the death signal must be relayed to and from the mitochondria via indirect means.

One of the possibilities regarding signal transduction is a cysteine protease that functions as a deubiquitinase: ubiquitin C-terminal hydrolase 1 (UCH-L1, Meyer-Schwesinger *et al.* 2011). UCH-L1 was demonstrated to play a role in necroptosis in kidney podocytes, where it is activated via monoubiquitination by yet unknown means but clearly through the indirect action of HtrA2/Omi (Sosna *et al.* 2013). The problem with this proposed pathway lays in the relatively narrow tissue distribution of UCH-L1, which is mainly expressed in the brain, synovial membranes and cells of testis, ovaries and kidney (Meyer-Schwesinger *et al.* 2011). It can thus not be the only mechanism of signal relay available, to the broader cell population (see figure 3 for the proposed mode of action of HtrA2/Omi and UCH-L1).

In a proteome-wide analysis (Vande Walle *et al.* 2007), the group of P. Vandenabeele found certain proteins to be substrates of HtrA2/Omi during apoptosis: DBC1 (Deleted in Bladder Cancer protein 1), PDXDC1 (Pyridoxal Dependent Decarboxylase Domain Containing protein 1) and VPS4B (Vacuolar Protein Sorting 4 Homolog B), the latter two identified in the study merely as fragments. These proteins are possible candidates for the role of signal transduction from mitochondria and were therefore studied in the present work.

Other candidates of interest are mitochondrial-processing peptidase subunit alpha (MPP-A, also called PMPCA), proteasome subunit alpha type-1 (PSA1) and the mitochondrial ATP-dependent serine protease (LONP1), all proteins that were identified in a proteomic screen by Susann Voigt during her PhD thesis in the group of Prof. Dr. Adam.

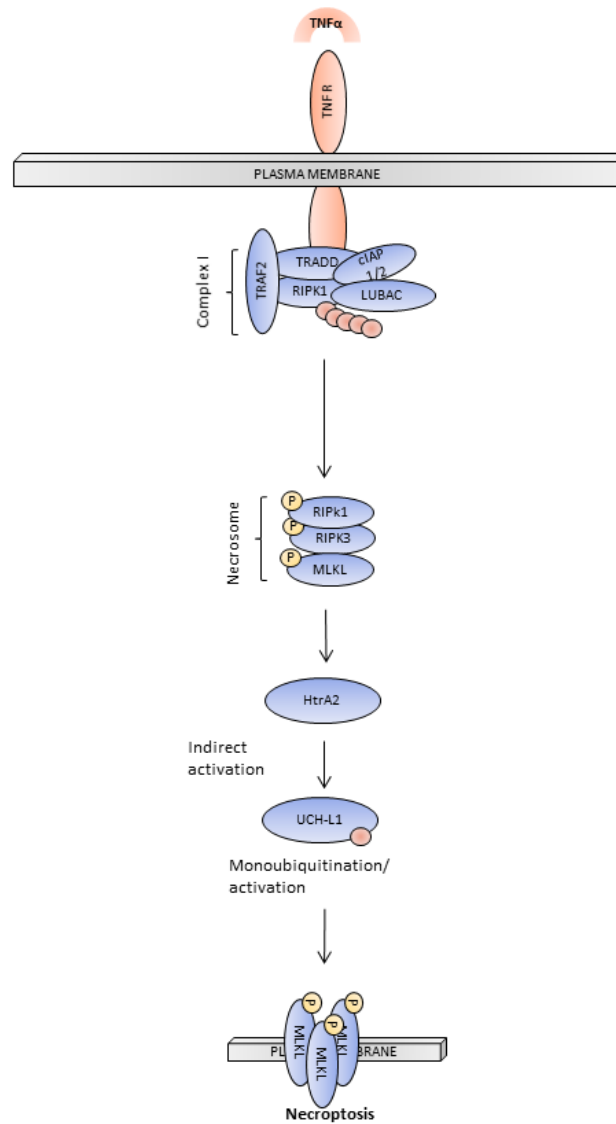


Figure 3

Summary of the proposed involvement of HtrA2/Omi in necroptosis. Upon formation of the necrosome, the necroptotic signal is relayed to the mitochondria by yet unknown means. HtrA2/Omi then cleaves an as yet unidentified protein, which would be able to relay the signal to monoubiquitinate UCH-L1 in tissue in which it is available through indirect means.

2.3.4 Biological role of necroptosis

Since the discovery that knock-out of either RIPK3 or MLKL has little effect on the development and fertility of mice, detailed analysis of the physiological and pathological roles of necroptosis has been possible (Sun and Wang 2014).

The primary role of necroptosis seems to be in viral (Cho *et al.* 2009), bacterial (McComb *et al.* 2012, González-Juarbe *et al.* 2015, Pearson *et al.* 2017) and parasitic infection (Osborn *et al.* 2010) defence, since the release of damage associated molecular patterns (DAMPs) from the bursting necroptotic cells alerts and mobilizes the host immune response. Thus, necroptosis contributes to physiological immunosurveillance (Cho *et al.* 2009, Huang *et al.* 2015, Pearson *et al.* 2017), although the conservation of several components of the pathway in the animal kingdom seems to be poor (Dondelinger *et al.* 2016).

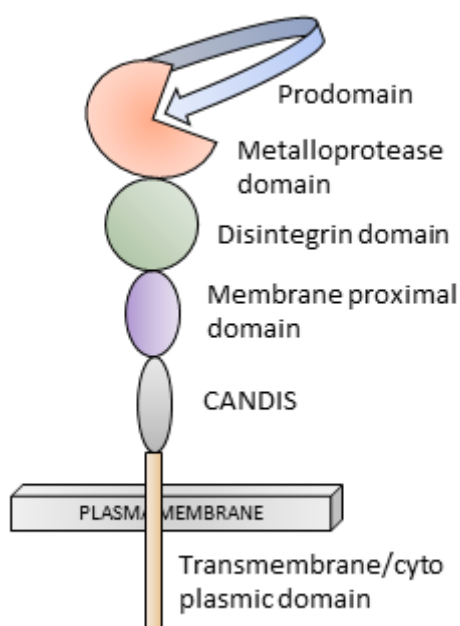
Nonetheless, there have been numerous publications addressing to the role of necroptosis in human and mice under multiple conditions, such as ischemia reperfusion injury (Rosenbaum *et al.* 2010, Zhang *et al.* 2016), sepsis (Linkerman *et al.* 2012), inflammatory bowel (Günther *et al.* 2011) and skin diseases (Bonnet *et al.* 2011), Gaucher's disease (Vitner *et al.* 2014), Morbus Alzheimer (Qinli *et al.* 2013), Morbus Huntington (Zhu *et al.* 2011), retinal disorders (Trichonas *et al.* 2010, Sato *et al.* 2013), traumatic brain (You *et al.* 2008, King *et al.* 2014) and spinal cord injury (Wang *et al.* 2014b, Fan *et al.* 2016), stroke (Degterev *et al.* 2005, Zhu *et al.* 2012), acute hepatitis (Deutsch *et al.* 2015), chronic alcoholic (Roychowdhury *et al.* 2013, Wang *et al.* 2016) and non-alcoholic liver diseases (Gautheron *et al.* 2014, Afonso *et al.* 2015), acute kidney injury (Linkerman *et al.* 2013), myocardial infarction (Luedde *et al.* 2014 and others) and atherosclerosis (Lin *et al.* 2013, Meng *et al.* 2015).

Necroptosis also plays a role in cancer (Aaes *et al.* 2016, Seifert *et al.* 2016, He *et al.* 2013 and others), with special regard to a potentially ground-breaking publication showing that endothelial cells dying of necroptosis might promote metastasis (Strilic *et al.* 2016).

2.4 ADAM17 and necroptosis

At least 10% of all cell surface proteins are suspected to be proteolytically cleaved leading to the release of soluble proteins (Fong *et al.* 2011, Kawahara *et al.* 2014). The first shedding protease to be molecularly described was a member of a family of disintegrin metalloproteases called ADAMalysins (Müllberg *et al.* 2000): a disintegrin and metalloprotease 17 (ADAM17).

In the years since that seminal publication, the structure of ADAM17 has been unraveled (see figure 4): Starting with an N-terminal signal sequence, followed by a pro-domain which acts as a chaperone and is thought to inhibit the enzymatic activity of the protein (Wong *et al.* 2015), a metalloproteinase or catalytic domain (Maskos *et al.* 1998), a disintegrin domain that recombinantly expressed is able to impair the interactions between fibroblasts and carcinoma cells (Trad *et al.* 2013), a membrane proximal domain shown to enable the protein to switch from an open to a closed conformation (Düsterhöft *et al.* 2013, Sommer *et al.* 2016), a short stalk sequence (highly conserved throughout the animal kingdom) called CANDIS (Conserved ADAM seventeen dynamic interaction sequence, Düsterhöft *et al.* 2014) and finally a transmembrane domain with a short cytoplasmic C-terminal tail (Black *et al.* 1997).



ADAM17 seems to be a vital protein, having more than 80 substrates; amongst them cytokine receptors such as interleukin-6 receptor (IL-6R), cell adhesion molecules such as CD44 and important proteins in development and differentiation such as transforming growth factor alpha (TGF α) (Scheller *et al.* 2011).

Figure 4

Structure of ADAM17 showing its six domains (adapted from Zunke and Rose-John (2017)).

The importance of ADAM17 was confirmed after the finding that knock-out mice are not viable (Peschon *et al.* 1998). Nonetheless, ADAM17

hypomorphic mice, called ADAM17^{ex/ex}, could be generated (Chalaris *et al.* 2010). These mice show greatly reduced ADAM17 mRNA and protein levels. Phenotypically, ADAM17^{ex/ex} mice show naked patches of skin and often blindness, impaired milk ducts, high susceptibility to dextran sulfate sodium (DSS)-induced inflammatory bowel disease (with impaired intestinal barrier and strongly reduced intestinal regeneration upon challenge) and a non-mendelian genotypical distribution due to higher pre- and post-natal mortality rate (Chalaris *et al.* 2010).

Despite the difficulties in breeding ADAM17^{ex/ex} mice, there is one fact that could turn them into an attractive model for the TNF-R1 activated necroptotic pathway *in vivo*: TNF is synthesized as a membrane protein that can be activated via proteolytical cleavage (Kriegler *et al.* 1988), shedding that was shown to be done by ADAM17 (Black *et al.* 1997, Moss *et al.* 1997, Müllberg *et al.* 2000).

2.5 Mouse model of DSS-Colitis

Ulcerative colitis is a chronic and relapsing disorder with an immunological component, since it is present in inflammatory lesions affecting various parts of the intestine such as rectum and colon (Carter *et al.* 2004). It is characterized by severe diarrhea, rectal bleeding, abdominal pain and fluid and electrolyte loss (Rhandhawa *et al.* 2014).

Dextran sulfate sodium (DSS)-induced colitis in mice and rats has long been used as a model for human ulcerative colitis, since it is easily reproducible, and courses with similar symptomatology and morphology as in humans (Gaudio *et al.* 1999, Jurjus *et al.* 2004). The direct toxic effect of DSS on epithelial cells manifests itself as erosions with complete loss of surface epithelium and a subsequent increase of the colonic mucosal permeability, allowing permeation of large molecules of up to 50 kDa (Ni *et al.* 1996).

At the cellular level, DSS-induced colitis disrupts the metabolism of phospholipids, decreasing phosphocholine and glycerophosphocholine levels in the colon of mice, thus probably disrupting membrane integrity (Michel *et al.* 2006, Dong *et al.* 2013). At the molecular level, DSS-induced colitis causes an increase in the production of inflammatory cytokines in both

mid and distal colon (Andújar *et al.* 2012), in addition to a marked increase in TNF levels (Dharmani *et al.* 2011) which makes this an attractive model of TNF-R-activated necroptosis.

The usual dosage for the study of acute colitis is of 3-5% DSS (w/v) in drinking water ad libitum for 5-8 days, followed by the same amount of days with unadulterated drinking water, whereas chronic colitis can be achieved by chaining 3-5 cycles of 1-2% DSS (w/v) in drinking water followed by the same amount of days with unadulterated drinking water (Rhandhawa *et al.* 2014). However, ADAM17^{ex/ex} mice, which were used in the present work, show a significant susceptibility to DSS-induced colitis (Chalaris *et al.* 2010), the high mortality rate forcing a lower dosage as described in Materials and Methods.

2.6 Acid sphingomyelinase and ceramide

First found in rat liver tissue (Kanfer *et al.* 1966), acid sphingomyelinase (henceforth A-SMase) is an enzyme that cleaves sphingomyelin into ceramide. It took 25 more years before the locus for the gene encoding the human A-SMase (SMPD1) was mapped to the short arm of chromosome 11 (da Veiga Pereira *et al.* 1991), which is, interestingly, close to other lysosomal proteins such as cathepsin D and acid phosphatase 2 (Zeidan & Hannun 2010). With the mouse version having 82% identical sequence to the human sequence, the gene seems to be highly conserved in mammals (Newrzella *et al.* 1992).

At a structural level, the A-SMase consists of two domains divided by a proline-rich region: an activator domain towards the N-terminus and a catalytic domain towards the C-terminus, the latter containing as much as 5 disulfide bonds (Lansmann *et al.* 2003), which can potentially serve as regulators depending on their oxidative status (Qiu *et al.* 2003). The enzyme can be found as a 75 kD precursor protein, that is cleaved within the Golgi to a 72 kD and a 57 kD form (Hurwitz *et al.* 1994), with heavy glycosylations being responsible for trafficking from the Golgi to the lysosome and protection from the lysosomal surrounding (Scheiffele *et al.* 2000).

Although the cleaving activity of the enzyme normally takes place in the lysosome on sphingomyelin transported from the plasma membrane (Schuchman *et al.* 1991), A-SMase can

also translocate to the plasma membrane via vesicular transport, provided there are intact lipid rafts (Charruyer *et al.* 2005).

At a functional level, A-SMase activity can be induced by a variety of signals, such as oxidative stress (Li *et al.* 2012), radiation, cytotoxic agents, pathogens (viral, bacterial and parasitic) and, relevant for the present work, ligation of death receptors such as TNF, FasL and TRAIL (Zeidan & Hannun 2010). In fact, our group and others have shown A-SMase-generated ceramide to be crucial for TNF-induced (Thon *et al.* 2005) and TRAIL-induced (Thon *et al.* 2006, Sosna *et al.* 2016) necroptosis, as well as in TNF-induced apoptosis (Dumitru *et al.* 2007).

A-SMase seems to be important in certain pathophysiological conditions, with a link found in ischemia (Soeda *et al.* 2004, Ohtani *et al.* 2004), possibly depression in mice (Gulbins *et al.* 2013) and Niemann-Pink disease, a syndrome caused by mutations in the SMPD1 gene, with varying degrees of A-SMase deficiencies leading to disturbed sphingomyelin degradation and accumulation of lipids in the cells (Levrán *et al.* 1991, Irun *et al.* 2013, Manshadi *et al.* 2015).

3 Materials and Methods

3.1 Materials

3.1.1 Equipment

Company	Equipment
AGFA, Mortsels, Belgium	AGFA CP1000 film processing machine
BD Biosciences, Heidelberg, Germany	FACSCalibur flow cytometer FACS Aria sorter Software: BD CellQuest™ Pro V. 4.0.2 5 mL polystyrene round-bottom FACS tubes
Bio Rad, Munich, Germany	GenePulser™ X Cell Mini PROTEAN® System Casting Stand and Mini PROTEAN® tetra system Mini PROTEAN® II Glass Plates mm 10-well comb Power Pack 3000 protein blotting cell SmartSpec™ 3000 spectrometer
Biometra, Göttingen, Germany	Rocking platform WT12 Thermocycler T3000 Standard Power Pack P25
Black Diamond Technologies, Lower Hutt, New Zealand	Mitsubishi P90
Carl Roth, Karlsruhe, Germany	Microscope slides

CORNING, Wiesbaden, Germany	10 CC Tissue Culture Dish
Eppendorf, Hamburg, Germany	Refrigerated centrifuge 5417R Bench-top Centrifuge 5415D Thermomixer compact Pipettes (10, 100, 200, 1000 µL)
Excelitas Technologies, Waltham, MA, USA	X-Cite® Series120 Mercury Lamp
GE Healthcare, Munich, Germany	Amersham Hyperfilm™ Hypercassette™ 18x24 cm
GFL, Wunstorf, Germany	Water Bath1003
Gilson, Middletown, WI, USA	Pipettes (10, 20, 1000 µL)
Greiner Bio-One, Frickenhausen, Germany	Serological pipettes (1, 2, 5, 10, 25, 50 mL) 15 and 50 mL tubes 6 and 12-Well Plates (transparent, flat bottom) 96-Well Plates (White, round bottom) CRYO.S® PP with screw cap, sterile
Heraeus, Osterode, Germany	Megafuge 1.0 Minifuge RF Lamin Air HA2472GS
Hirschmann Laborgeräte, Eberstadt, Germany	Pipetus-Akku
IKA Labortechnik, Staufen, Germany	RCT Basic magnetic stirrer
Kaiser Fototechnik, Buchen, Germany	Kaiser RT1
KERN & SOHN, Balingen, Germany	Scale 440-47N
Kisker Biotech, Steinfurt, Germany	Microcentrifuge
Life Technologies, Carlsbad, CA, USA	Horizon® 58 Gibco BRL Horizontal Gel Electrophoresis Apparatus Horizon® 11-14 Gibco BRL Horizontal Gel Electrophoresis Apparatus
Lonza Group, Basel, Switzerland	Amaxa® Nucleofector™ Device

PeqLab Biotechnologie, Erlangen, Germany	NanoDrop® ND-1000 Spectrophotometer Software: ND-1000 v. 3.7.9
Petra Electric, Ense, Germany	Water heater
Sarstedt, Nümbrecht, Germany	Polystyrene cuvettes (10x4x45)
Sartorius Analytic, Göttingen, Germany	A120S Scale E2000D Scale
Scientific Industries, Bohemia, NY, USA	Vortexgenie2™
SI Analytics, Mainz, Germany	Ph meter
Sony, Tokio, Japan	Black and White monitor SSM-S30CE
Stuart, Staffordshire, UK	SRT9 Analogue tube roller
Tecan Group, Männedorf, Germany	Infinite M200 ELISA Microplate Reader Software: i-Control 1.3
Thermo Scientific	HERAcell 150i CO2 Incubator SpeedVac Centrifuge Haake C1 thermo circulator 96-Well plates (transparent, flat bottom) Molecular Probes® MitoTracker Orange
UVP, Upland, CA, USA	High Performance Transilluminator
Wheaton, Millville, NY, USA	2 ml Tissue Grinder, Douncer
Zeiss, Göttingen, Germany	Axiovert 135 Microscope Axiovert 200M Laserscanning Microscope

3.1.2 Reagents and chemicals

Company	Product
Abcam, Cambridge, UK	Cell fractionation Kit- Standard (ab109719)
Bachem, Heidelberg, Germany	zVAD-fmk
BASF Bioresearch, Ludwigshafen, Germany	hTNF
Bemis Flexible Packaging, Oshkosh, WI, USA	Parafilm®

Biochrom, Berlin, Germany	PBS Dulbecco w/o Ca ²⁺ w/o Mg ²⁺ G418 Trypsin/EDTA (10x) L-Glutamine McCoy's SA Modified Medium Penicillin/Streptomycin
Carl Roth, Karlsruhe, Germany	Saponin Methanol ≥99% Hydrogen Peroxide 30% Ethanol 96% Ethanol ROTIPURAN® ≥99,8%
Cell Signaling Technologies, Danvers, MA, USA	LumiGLO® chemiluminescent substrate
Echelon Bioscience, Salt Lake City, UT, USA	A-SMase Assay Kit
Ecolab, Mannheim am Rhein, Germany	Sekusept® forte
GE Healthcare, Munich, Germany	TEMED
Invitrogen, Darmstadt, Germany/Carlsbad, CA, USA	Agarose electrophoresis grade Zeocin™ PCDNA 3.1 Vector T4 DNA Ligase
Life Technologies, Darmstadt, Germany	GIBCO® RPMI Medium 1640 (1x) GIBCO® Sodium Pyruvate 100nm (100x) GIBCO® StemPro® Accutase® Cell Dissociation Reagent GIBCO® Fetal Bovine Serum GIBCO® DMEM
Lonza Cologne, Cologne, Germany	Amaya™ Cell Line Nucleofactor™ Kit V, Kit T, Kit C, Kit R, Primary Fibroblast Kit
Merck, Darmstadt, Germany	Glycerol 85% SeccoSolv® Dimethyl sulfoxide

	RIPK3 inhibitor GSK'872 Paraformaldehyde
MP Biomedicals, CA, USA	Dextran Sulfate Sodium Salt (36000-50000 M. Wt) Colitis Grade
New England Biolabs, Ipswich, Massachusetts, USA	BsmBI endonuclease PshA1 endonuclease
Qiagen, Hilden, Germany	QIAGEN® Plasmid Maxi Kit (25) QIAprep Spin Miniprep Kit (250) RNeasy® Mini Kit (50)
Roche, Basel, Switzerland	Complete® Protease inhibitor cocktail
Serva, Heidelberg, Germany	Acrylamide/Bis Solution (40%)
Sigma-Aldrich, Munich, Germany	TWEEN®20 Poly-L-Lysine Cycloheximide Propidium Iodide Ponceau S
Stratagene, CA, USA	QuikChange® Site-Directed Mutagenesis Kit
Thermo Scientific, Waltham, USA	Coomassie Blue Protein Assay Albumin Standard Mitochondrial Isolation Kit for Mammalian Cells PhireTissue Direct PCR Master Mix Pierce® BCA Protein Assay Kit PAGE Ruler Prestained Protein Ladder Mitotracker®Orange CMTMRos
Vector Laboratories, Burlingame, CA, USA	Vectashield® mounting medium with DAPI
VWR Chemicals, Fontenay-seurs-Bois, France	TechniSolv ethanol 70%

3.1.3 Antibodies

Company	Target	Used dilution
	Primary antibody (unless otherwise noted, for human and mouse both)	
Sigma Aldrich, Heidelberg, Germany	B-Actin (A1978) MLKL (human, SAB2103620) RIPK3 (PRS2283)	1:10000 1:1000
Cell Signaling Technologies, Danvers, MA, USA	COX IV (#4850) AsM Rabbit (#3687s) p65 NF- κ B (#3033S) Cleaved Caspase3 (#9661L)	1:10000 1:1000 1:1000 1:1000
Biomol, Hamburg, Germany	PARP(SA-253)	1:1000
Biorbyt, Cambridge, UK	MLKL (mouse, orb32399)	1:1000
Abcam, Cambridge, UK	pMLKL (ab196436) pRIPK3 (ab195117) PGAM5 (ab126534)	1:1000 1:1000 1:2500
OriGene Europe-Acris Antibodies, Herford, Germany	HtrA2 (15775-1-AP)	1:1000
R&D Systems, Minneapolis, MN, USA	HtrA2 (AF1458)	0.25 μ g/mL
Invitrogen, Darmstadt, Germany	V5 (PN 46-0705)	1:5000
	Secondary Antibody	
Abcam, Cambridge, UK	Alexa Fluor 488 donkey-anti rabbit IgG	1:200
Jackson ImmunoResearch Europe, Suffolk, UK	Donkey anti-rabbit IgG peroxidase-conjugated	1:10000
Jackson ImmunoResearch Europe, Suffolk, UK	Donkey anti-mouse IgG peroxidase-conjugated	1:10000

3.2 Methods

3.2.1 Cell lines and cytotoxicity assays

The murine fibrosarcoma cell line L929sA was kindly provided by Peter Vandenabeele (Ghent University, Ghent, Belgium) and has been described previously (Vanhaesebroeck *et al.* 1992). A TRAIL-sensitive subset of those cells (L929Ts) was generated in the Laboratory of Dieter Adam (Christian-Albrecht University, Kiel, Germany), described earlier (Thon *et al.* 2005) and is the cell line being referenced throughout this work as L929. Murine embryo fibroblasts (MEF) and HtrA2 deficient MEF lines have been previously described (Martins *et al.* 2004). Hamster embryonic kidney cells constitutively expressing the simian virus 40 (SV40) large T antigen cells (HEK293T) and human colorectal cancer cells (HT-29) were obtained from the American Type Culture Collection (ATCC, Manassas, VA, USA), the latter being gifted to us by Holger Kalthoff (Christian-Albrecht University, Kiel, Germany). During the course of the present work, HtrA2/OMI deficient HT-29 and L929 were generated via CRISPR/Cas, as were A-SMase deficient L929. For further information on the media used in the cell cultures, see table 1.

Every 2 to 4 days, cells were detached using phosphate buffered saline (PBS) containing 0.5% (v/v) trypsin and 0.2% (v/v) EDTA and re-seeded in fresh medium for passaging purposes. For long-term storage, cells were frozen in liquid nitrogen after resuspension in FCS containing 10% (v/v) DMSO.

For cytotoxicity assays, cell death was induced with TNF. If necessary, a pre-stimulation (30 min before adding TNF) with cycloheximide (CHX), a eukaryotic protein synthesis inhibitor, was performed to sensitize the cells to the cell death stimulus. Since the purpose of this work was to examine necroptosis, the vast majority of experiments also included z-Val-Ala-DL-Asp-fluoromethylketone (henceforth zVAD-fmk or zVAD). Being a pan-caspase inhibitor, it was used to prevent apoptosis, exceptions being made when explicitly comparing results with apoptosis. For further information on the concentrations used, see table 1.

Table 1

Detailed breakdown of cell lines, media and stimulants used throughout the present work.

Cell line	System	Medium	Stimulation
L929 (including HtrA2 and A-SMase ^{-/-})	Mouse	Click's/RPMI 1640 (50/50% v/v) supplemented with 10% (v/v) FCS, 2mM L-glutamine, 50 µg/L penicillin/streptomycin	100 ng/mL TNF or TRAIL 20 mM zVAD-fmk
MEF (including HtrA2 ^{-/-})	Mouse	DMEM supplemented with 10% (v/v) FCS, 50 µg/L penicillin/streptomycin and 50 µg β-mercaptoethanol in 0,9% (w/v) NaCl	100 ng/mL TNF or TRAIL 20 mM zVAD-fmk 1 µg/mL CHX
HT-29 (including HtrA2 ^{-/-})	Human	RPMI 1640 supplemented with 10% (v/v) FCS and 1 mM sodium pyruvate	100 ng/mL TNF or TRAIL 20 mM zVAD-fmk 10 µg/mL CHX

3.2.2 Animal experiments

3.2.2.1 Animal treatment

Mice were kept under standardized conditions with a controlled temperature of 21 °C and 55-65% relative humidity on a 12 h light/12 h dark cycle and housed individually in ventilated cages with free access to drinking water and standard diet. All experiments were performed in accordance with the German Regulations of Animal Welfare approved by the Ministerium für Energiewende, Landwirtschaft, Umwelt, Natur und Digitalisierung, Schleswig-Holstein (Kiel, Germany; V 312-7224.121-20 (18-1/13)).

3.2.2.2 ADAM17^{ex/ex} and ADAM17^{ex/ex} – RIP3^{-/-} mice

ADAM17^{ex/ex} animals generated in Chalaris *et al* (2010) were used as basis, and crossed with RIPK3^{-/-} obtained from Genentech.

3.2.2.3 Mouse genotyping

Mice tails were clipped at the central animal facility (UKSH, Kiel) according to the animal care guidelines of Kiel University. Afterwards, the DNA was extracted using the PhireTissue Direct PCR Mix according to the manufacturer's instructions. PCR was performed with the same kit, using conditions as shown in Table 2. The PCR product was run on a 2% Agarose (w/v) gel electrophoresis and the genotype visualized via ethidium bromide under UV light.

Table 2

Breakdown of primers and PCR conditions used in the genotyping of ADAM 17^{ex/ex} and ADAM 17^{ex/ex}-RIPK3^{-/-} mice.

Gene of interest	Primers	PCR conditions
Adam 17	1: CTTATTATTCTCgTggTC 2: TATgTgATAgTgTAATg	1: Preheating 98°C 5 min 2: Denaturation 98°C 5 sec 3: Annealing 46°C 5 sec 4: Elongation 72°C 20 sec, back to 2 x40 5: Final Elongation 72°C 1 min 6: End 4°C infinite
Ripk3	1: CgCTTTAgAAgCCTTCAggTTgAC 2: gCCTgCCCATCAgCAACTC 3: CCAgAggCCACTTgTgTAgCg	1: Preheating 98°C 5 min 2: Denaturation 98°C 5 sec 3: Annealing 57°C 5 sec 4: Elongation 72°C 20 sec, back to 2 x40 5: Final Elongation 72°C 1 min 6: End 4°C infinite

3.2.2.4 DSS colitis

Experiments were done on 14-20 weeks-old mice. Acute Colitis was induced by administration of 1,5% DSS (mol wt: 36000-50000; MP Biomedicals) in the drinking water for 5 d followed by 5 d of regular drinking water.

Chronic Colitis was induced by administration of 0,5% DSS in the drinking water for 5 days, followed by 5 days of regular drinking water. This cycle was repeated twice more using 0.75% DSS in each administration phase.

In both cases a disease activity index (DAI) was measured by the sum of three scores each from 0-4 in ascending order of gravity assessing stool consistency, blood in stool and bodyweight.

3.2.2.5 Organ and tissue sample handling

Spleen, caecum, colon, small intestine and liver were harvested immediately after killing the animals according to the guidelines mentioned above. Organs were weighted and split in two, one part being shock-frozen in liquid nitrogen for further protein, DNA and RNA analyses, while the other was fixed in 4% formalin or 4% PFA (colon) and embedded in paraffin for further histological examination.

3.2.2.6 Histological examination

Kindly performed by Christoph Becker and Barbara Ruder from the University of Erlangen, samples prepared above that are shown in the thesis were stained with hematoxylin/eosin (H&E) and β -catenin as well as myeloperoxidase (MPO) in immunofluorescence.

3.2.2.7 Organ lysates

Tissue samples were homogenized in RIPA lysis buffer (150 mM NaCl, 1% Triton X-100, 0.5% Sodium Deoxycholate, 0.1% SDS, 50 mM tris-HCl, pH 8,0) containing 10 μ g/mL Complete[®] protease inhibitor. Samples were centrifuged for 10 min at maximum speed and supernatant was stored for further use at -20°C.

3.2.3 Cell lysates

Supernatant and detached cells were collected in 50 mL tubes. Starting from here, the whole process was done at 4°C. Cells were centrifuged at 400 x g for 5 min. The cell pellets were transferred to 1.5 mL reaction tubes and washed once with PBS (centrifugation at maximum speed for 1 min). Cells were lysed for 10 min with TNE lysis buffer (50 mM Tris pH 8.0, 150 mM NaCl, 1% (v/v) NP-40, 3 mM EDTA) containing 10 μ g/mL complete protease inhibitor. Samples were centrifuged for 10 min at maximum speed and supernatant was stored for further use at -20°C.

3.2.4 Protein quantification

Lysate concentrations were measured depending on the amount of material at hand. A BCA-Protein Assay Kit was used (according to the instructions of the manufacturer) if a low amount was present, due to the high sensitivity of the kit permitting it to detect low quantities. Having a medium or high amount of material, concentration was measured using Coomassie Blue Protein Assay. In this method, 1-5µg lysate was added to 1 mL reagent in a polystyrene cuvette and mixed thoroughly. Absorbance was measured at 595 nm with a spectrometer and compared to a previously done standard.

3.2.5 SDS-PAGE and Western blot analysis

12% SDS-PAGE gels were poured according to standard protocols (Laemmli, 1970). Whenever possible, 20 µg of lysate in 20 µL buffer were used in each case, further mixed with 5 x sample buffer (10% v/v β-mercaptoethanol, 125 mM Tris-HCL pH 6.8, 4% w/v SDS, 20% v/v glycerol, 0.02% w/v bromophenol blue) to a final volume of 25µL. After boiling for 5 min at 100°C, the samples were loaded into the gel, previously mounted on the mini PROTEAN® tetra system, and submitted to an electrical current of 25 mA per gel for an hour.

The proteins were then transferred to a membrane via (wet) Western blotting, after which they were placed under constant gentle agitation for an hour in blocking solution: PBST (PBS with 0.1% v/v TWEEN 20) with 5% (w/v) milk-powder. The membranes were then placed in blocking solution containing primary antibody (see 3.1.3) over night at 4°C. Excess of primary antibody was washed with 3 cycles of 10 min PBST under constant gentle agitation, after which the secondary antibody (see 3.1.3) would be added, also diluted in blocking solution. The membranes would roll for an hour at RT, after which they were washed again. The membranes were developed using LumiGLO® reagent, the proteins being detected by exposure on an X-ray film for 10 seconds up to 1 hour.

In case of a re-blot, the peroxidase coupled to the secondary antibody was inactivated with H₂O₂ for an hour, followed by 30 min of PBST washing and incubation overnight with a new primary antibody, restarting the cycle.

3.2.6 Flow cytometry

To analyze cell death via loss of membrane integrity, 5×10^5 cells were seeded in 6-well plates and left to attach for a minimum of 5 hours (usually overnight). After treatment (see Table 1), cells were detached with accutase and collected (including the supernatant). After resuspension, 1/3 of those cells were used to generate lysates as explained above. The rest were centrifuged at 400g for 10 min at 4°C. The cell pellet was washed once in ice-cold PBS/5 mM EDTA, centrifuged again and finally resuspended in 200µL of PBS/5 mM EDTA containing 2 µg/mL propidium iodide (PI). PI, being a fluorescent intercalating agent only able to penetrate the cells showing a compromised membrane integrity, was used to assess cell death.

At this point the cells were analyzed on a FACSCalibur flow cytometer. Excluding cellular debris for the analysis, 10000 cells were examined for each measurement in triplicate. Values were calculated as [(100-PI negative cells) %]; to account for already disintegrated cells losing PI staining at the time of measurement.

3.2.7 Transfection

All constructs used for transfections are listed in table 2. The constructs were propagated in *E. coli* (XL Blue) and DNA was isolated via the Quiagen® Plasmid Maxi Kit following the manufacturer's instructions with kind assistance by Parvin Davarnia.

Table 3
Constructs used throughout the present work.

Company/source	Vector	Construct
Sigma-Aldrich, Munich, Germany	pCMV-GFP CRISPR/Cas	HtrA2 CRISPR/Cas human HtrA2 CRISPR/Cas mouse PGAM5 CRISPR/Cas human PGAM5 CRISPR/Cas mouse
Received from Dr. Edward MocarSKI, Atlanta, GA, USA	LNCX	vMIA

Received from Dr. Edward MocarSKI, Atlanta, GA, USA	PCDNA 3.1	HtrA2 WT HtrA2 protease inactivated
Received from Dr. Yusuf Hannun, Stony Brook, NY, USA	pEF6/V5-His-TOPO®	V5-tagged A-SMase WT
Based on the previous V5-tagged A-SMase WT	pEF6/V5-His-TOPO®	V5-tagged A-SMase modified through overlap extension PCR

3.2.7.1 Nucleofection

Several Amaxa® Cell line Nucleofector Kits specific for the respective cell line were used, according to the recommendations of the manufacturers. 1×10^6 cells were harvested and resuspended in 100 μ L solution, transferred into a cuvette (also part of the kit) and transfected with 5 μ g DNA/ 150 pmol siRNA. After applying the corresponding program, cells were gently transferred into 10 cm³ plates containing prewarmed medium and cultured further. The downstream handling of the cells was performed as either of the options outlined below.

3.2.7.2 Transient transfection

After 24 hours, cells were detached and seeded into 6-well plates (5×10^5 cells per well), after which stimulation and, usually, FACS measurements would follow.

3.2.7.3 Stable transfection

After 24 hours, cells were detached and re-seeded in usually five 10 cm petri dishes, after which fresh medium and antibiotic was added to select transfected clones. In a period of usually 4-6 weeks, medium and antibiotic would be renewed every week until colonies were spotted, at which point individual ones would be picked and transferred to individual wells in 6-well plates. After reaching 80-90% confluence, cells were harvested and portioned such that, 2/3rd were frozen, 1/3rd were used to generate lysates for screening purposes and a drop supplemented with medium remained in the individual wells for easy access in case of a positive screening result.

3.2.7.4 Transfection of CRISPR/Cas constructs

After 48 hours, cells were selected using a FACS Aria sorter, the GFP tag of clustered regularly interspaced short palindromic repeats / CRISPR-associated 9 (CRISPR/Cas) constructs being the marker. Single clones were seeded by the sorter in individual wells in 96-well plates containing 100 μ L of prewarmed medium. After usually 4-5 weeks, colonies would form. Those colonies were transferred to individual wells in 12-well plates. Upon reaching 80-90% confluence, cells were harvested and portioned such that, 2/3rd were stored frozen and 1/3rd were used to generate lysates for screening purposes. A drop with additional medium remained in the individual wells for easy access in the event of a positive screening result.

3.2.8 Gene modification and sequencing

3.2.8.1 Overlap extension PCR

To identify the cleavage site of A-SMase in necroptosis, an overlap extension PCR (OE-PCR) was performed on a previously generated pEF6/V5-His-TOPO[®] vector containing A-SMase.

The OE-PCR starts with a first PCR, using two primer pairs, AB and CD, with B and C having overlapping endings. This generates two complementary sequences after annealing occurs. In a following ligation step, the sequence between them is ignored due to lack of complementary sequence on annealing, effectively deleting it. A second PCR provides enough of the gen with the desired deletion to use for further cloning experiments (see figure 5). In our setup, a 50-amino acid region surrounding the suspected cleavage site of A-SMase in necroptosis was deleted, both completely and in 10 aa portions (primers were designed by myself while constructs were kindly generated by Parvin Davarnia). Furthermore, various 10 aa portions were combined, as shown in Results, to generate larger deletions (primers were kindly designed by Prof. Dr. Adam while constructs were kindly generated by Parvin Davarnia).

With the OE-PCR completed, the newly mutated region was cut out with BsmB1 and PshA1 endonucleases, and inserted back with a ligation into a new pEF6/V5-His-TOPO[®] vector containing A-SMase treated with BsmB1 and PshA1 endonuclease. Finally constructs were

expanded, extracted via a QIAprep spin Miniprep kit according to the manufacturer's instructions and sequenced to verify the constructs and the newly mutated regions.

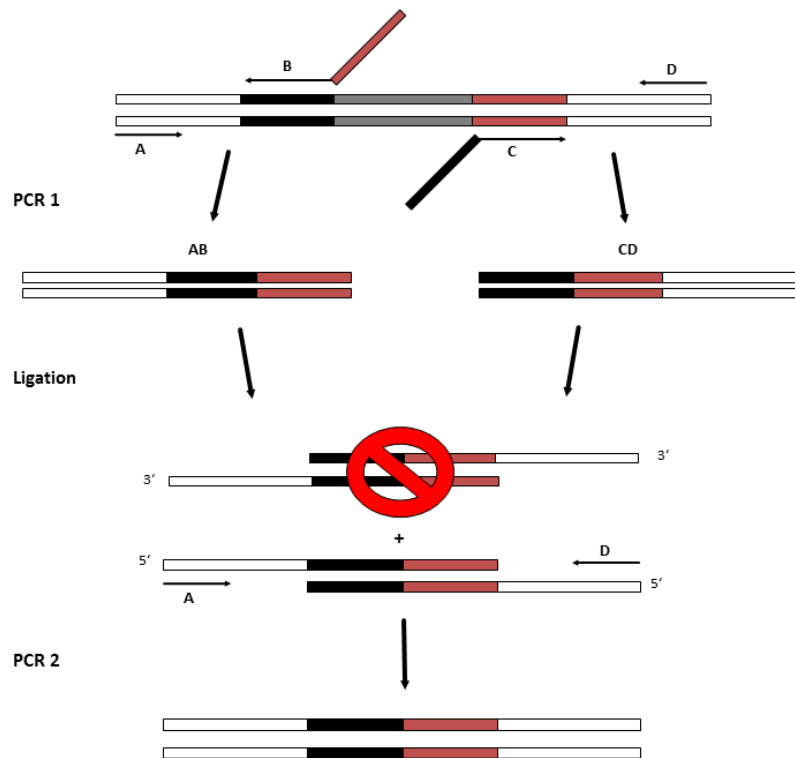


Figure 5
Schematic representation of the workflow of an overlap extension PCR.

3.2.8.2 DNA extraction, PCR and sequencing

To assess the validity of the generated CRISPR/Cas clones and A-SMase mutants by sequencing, DNA was extracted:

- In the case of the CRISPR/Cas clones, with the PhireTissue Direct PCR Mix according to the manufacturer's instructions, and subjected to a PCR to amplify the sequence of interest for the CRISPR clones. When needed, DNA was re-extracted from PCR product after Agarose gel electrophoresis via Quiaquick® gel extraction Kit.
- In the case of the A-SMase mutant constructs, a PCR was performed directly to expand the quantity.

In both cases, DNA was measured using a Nanodrop® and sent to the Institute of Clinical Molecular Biology (IKMB, Kiel) for Sanger sequencing.

3.2.9 A-SMase activity assay

The assay was performed using the A-SMase Assay Kit (Echelon) according to the manufacturer's instructions. The readout was performed on white flat-bottomed 96-well plates via a Tecan reader.

3.2.10 Immunofluorescence

To analyze the subcellular localization during cell death of HtrA2/OMI, 1.5×10^5 cells were seeded on cover slides in 12-well plates and left to attach for a minimum of 5 hours before being stimulated. 30 min before treatment end, mitotracker was added to the medium to 300nM final concentration. Starting with the addition of mitotracker, the whole experiment was performed with lights in the room switched off in order to minimize bleaching effects.

On treatment end, supernatant was discarded, and the individual wells washed thrice with PBS, after which 500 μ L 4% (w/v) PFA was added for 15 min at RT. Alternatively, 500 μ L supernatant was kept in the individual wells and 500 μ L 8% (w/v) PFA were added for 10 min at 30°C, after which it would be discarded and the wells washed thrice gently with PBS, to avoid the loss of dying, detaching cells (for further information on the topic, see Results and Discussion).

For permeabilization, the cells were washed thrice with PBS containing 0.5% (w/v) saponin (freshly made), followed by 10 min of incubation at RT and additional 10 min of incubation at RT with PBS/0.5% saponin containing 0.12% (v/v) glycerin to saturate possible free aldehyde groups left from the PFA. Afterwards, cells were washed once with PBS/0.5% saponin and blocked for an hour at RT with PBS/0.5% saponin/1% (v/v) BSA. At this point, primary antibody would be placed on parafilm, diluted in PBS/0.5% saponin/1% BSA according to the manufacturer's recommended concentrations (usually around 1/200), and the cover slides with the cells placed face-down on it. This was then placed in a humid chamber, covered to protect it from light, and incubated for an hour on RT, followed by overnight incubation at 4°C.

The next day, the cover slides were placed on new 12-well plates and washed thrice with PBS/0.5% saponin. Afterwards, secondary antibody was placed on parafilm, diluted in PBS/0.5% saponin/1% BSA (1/200), in a humid chamber for an hour at 37°C. After being placed again in a new 12-well, and washing thrice with PBS/0.5% saponin, the cover slides were placed face-down on a drop of DAPI placed on microscope slides and sealed with nail polish.

Samples could be stored at this point for several months in a dark box at 4°C without bleaching, but were usually visualized within a week via confocal laser scanning microscopy (CLSM).

3.2.11 Cell fractionation

Cells were fractionated using the Cell Fractionation Kit- standard (Abcam, UK) following the manufacturer's instructions.

4 Results

4.1 **Contribution of necroptosis to intestinal inflammation in ADAM17^{ex/ex} /RIPK3^{-/-} mice**

To gain insight into the biological role of necroptosis, we collaborated within our CRC 877 in an established model system of proteolysis. ADAM17^{ex/ex} mice have been previously shown to be highly susceptible to DSS induced colitis (Chalaris *et al.* 2010) and thus necroptosis was blocked to assess whether the mice would fare better. To accomplish this, ADAM17^{ex/ex} mice were cross-bred with RIPK3^{-/-} mice. RIPK3 being a fundamental protein in the necroptotic pathway, its deletion generates mice unable to perform necroptosis as described in Cho *et al.* 2009, He *et al.* 2009 and Zhang *et al.* 2009. After cross-breeding and selection, the mice were subjected to acute DSS-induced colitis (as explained in Materials and Methods).

The experiment had to be interrupted prematurely due to the loss of more than 20% body weight in some mice, as prescribed by the German Animal Protection Act. In figure 6, the lack of significant difference between genotypes is shown as measured both by body weight loss percentage and Disease Activity Index (DAI). Similar results were obtained comparing the weight or length of various organs (intestine, colon, caecum, spleen and liver), except for slight significance in liver and colon (raw) that disappeared once the body weights of the individual mice were considered.

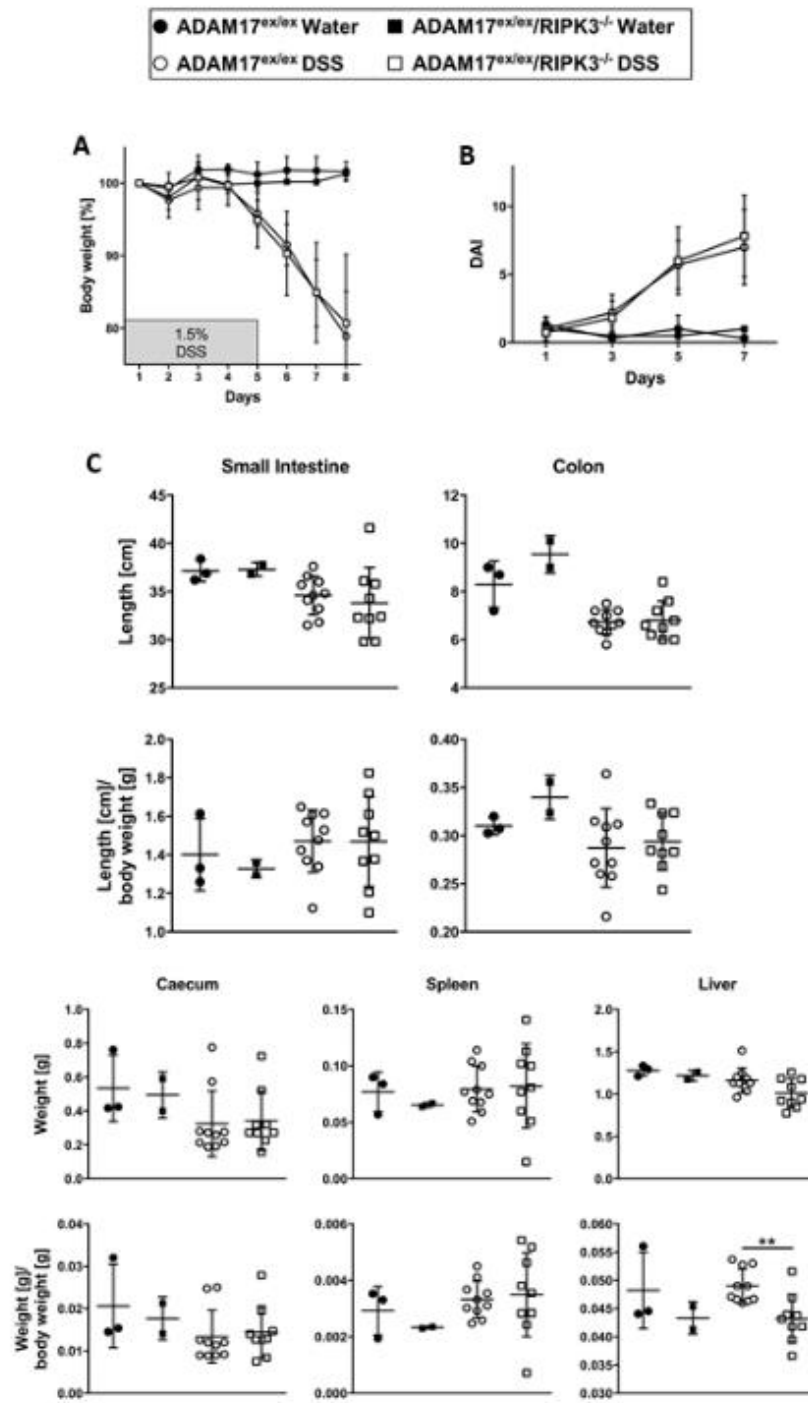


Figure 6

- A) Bodyweight shift throughout the DSS-induced acute colitis experiment.
 B) Disease activity index as measured by the sum of scores for stool consistency, blood in stool and bodyweight.
 C) Comparison of lengths and weights of the indicated organs without and with bodyweight considered.

Histological analysis of colon distal samples showed no significant differences between genotypes (see figure 7) as measured by:

- Haematoxylin/eosin (H&E) staining to assess the general status of the tissue.
- β -catenin immunofluorescence staining to assess the structural integrity of the epithelial barrier.
- Myeloperoxidase (MPO) immunofluorescence staining to detect lymphocyte infiltration and thus inflammatory response.

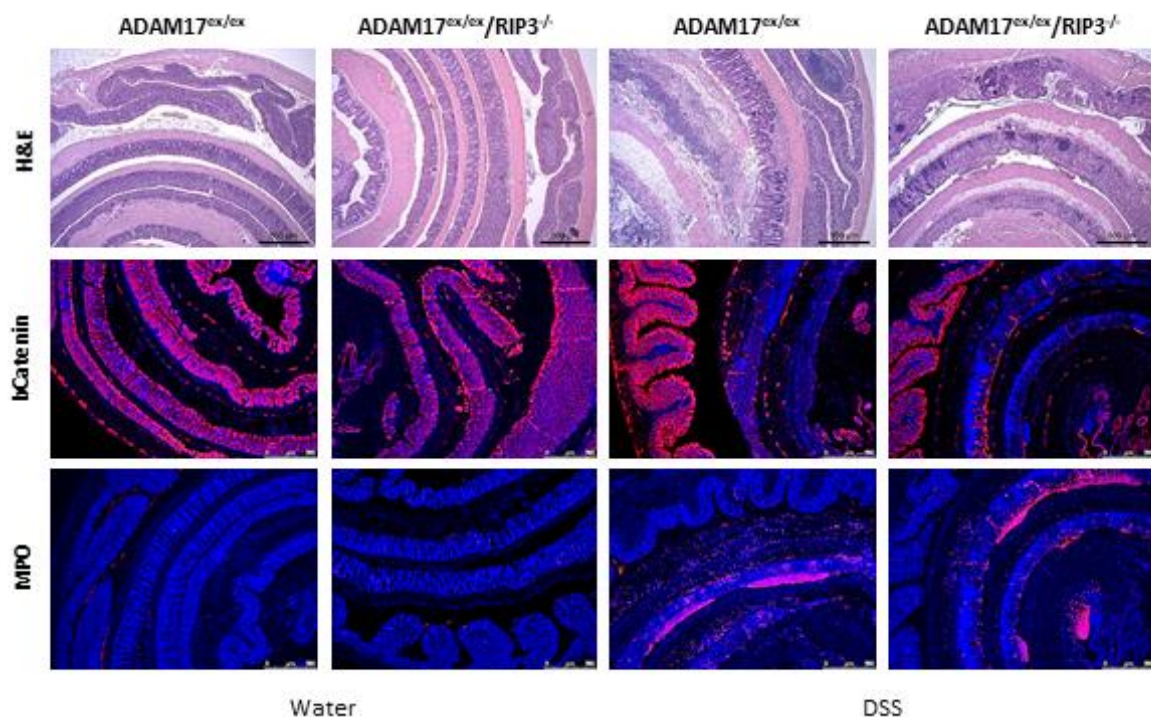
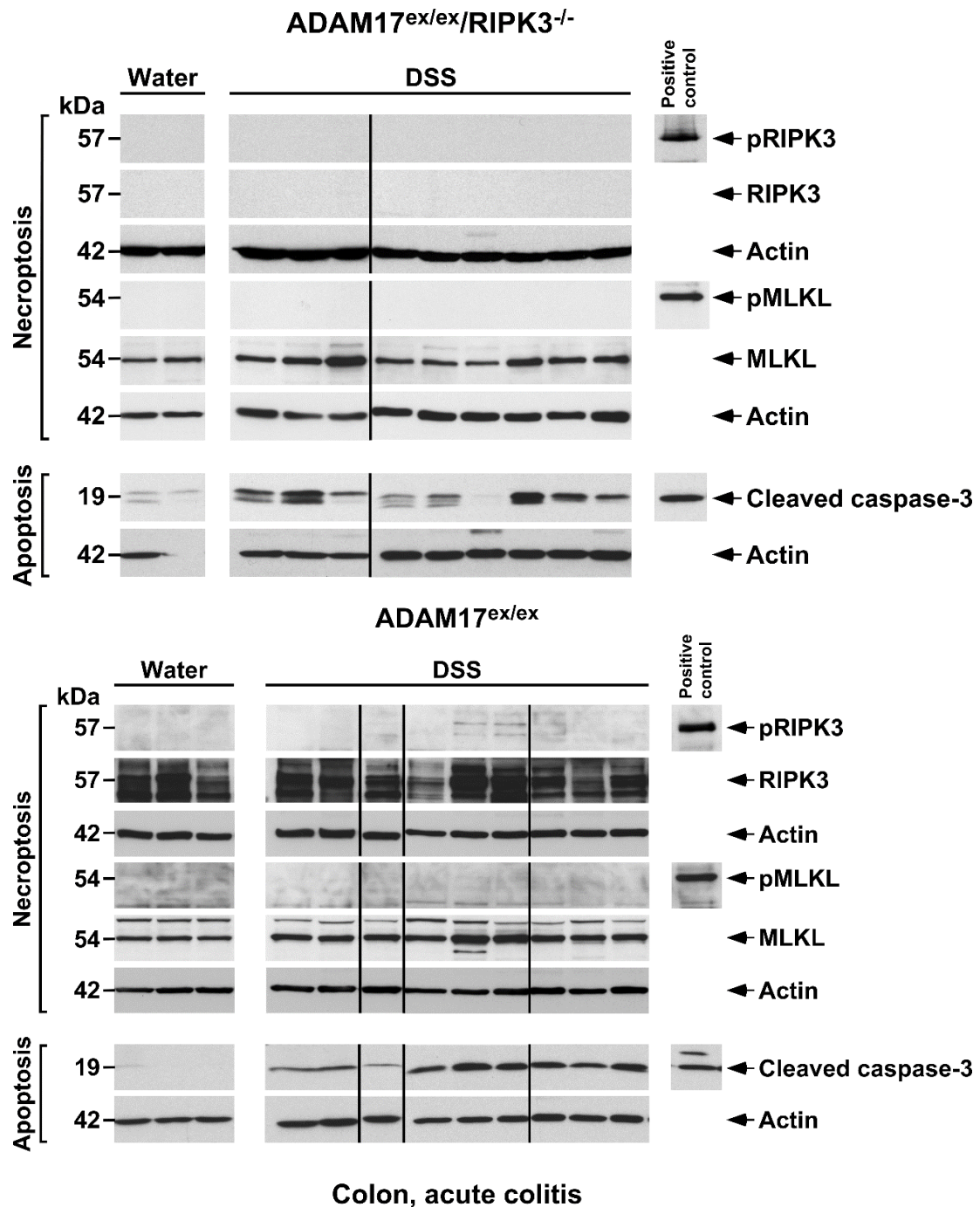


Figure 7

Kindly performed by Christoph Becker and Barbara Ruder from the University of Erlangen, DSS-induced acute colitis samples prepared above were stained with H&E and β -catenin as well as MPO in immunofluorescence.

Western blot analysis of liver and colon samples yielded no necroptotic signal as measured by either pRIPK3 or pMLKL expression. Apoptosis could be shown, as measured by Caspase 3 cleavage (see figure 8). Similar results could be observed in liver tissue, which was studied as an independent organ (see Appendix).

**Figure 8**

Western blot analysis of lysates generated from colon tissue samples of the ADAM17^{ex/ex} RIPK3^{-/-} and ADAM17^{ex/ex} mice participating in the DSS-induced acute colitis experiment. Performed in separate gels to avoid overlapping of pMLKL/MLKL and pRIPK3/RIPK3. Western blots for actin were performed to verify equal loading.

Positive control for necroptosis consists of lysates from MEF pre-stimulated with 1 μ g/mL CHX and 20 μ M zVAD for 30 min, and then stimulated with 100 ng/mL TNF for 16 h. Positive control for apoptosis consists of lysates from MEF pre-stimulated with 1 μ g/mL CHX for 30 min, and then stimulated with 100 ng/mL TNF for 16 h.

It was considered that the high susceptibility of the ADAM17^{ex/ex} phenotype in DSS-induced colitis could possibly lead to cellular and tissue damage onset before the hypothetical onset of necroptosis. Thus, a new experiment was started. This time chronic colitis was induced, as described in Materials and Methods, at lower DSS concentrations. However, as seen in figure 9, there was no significant difference in body weight loss percentage between genotypes, and hardly any effect in the DAI from the treatment at all.

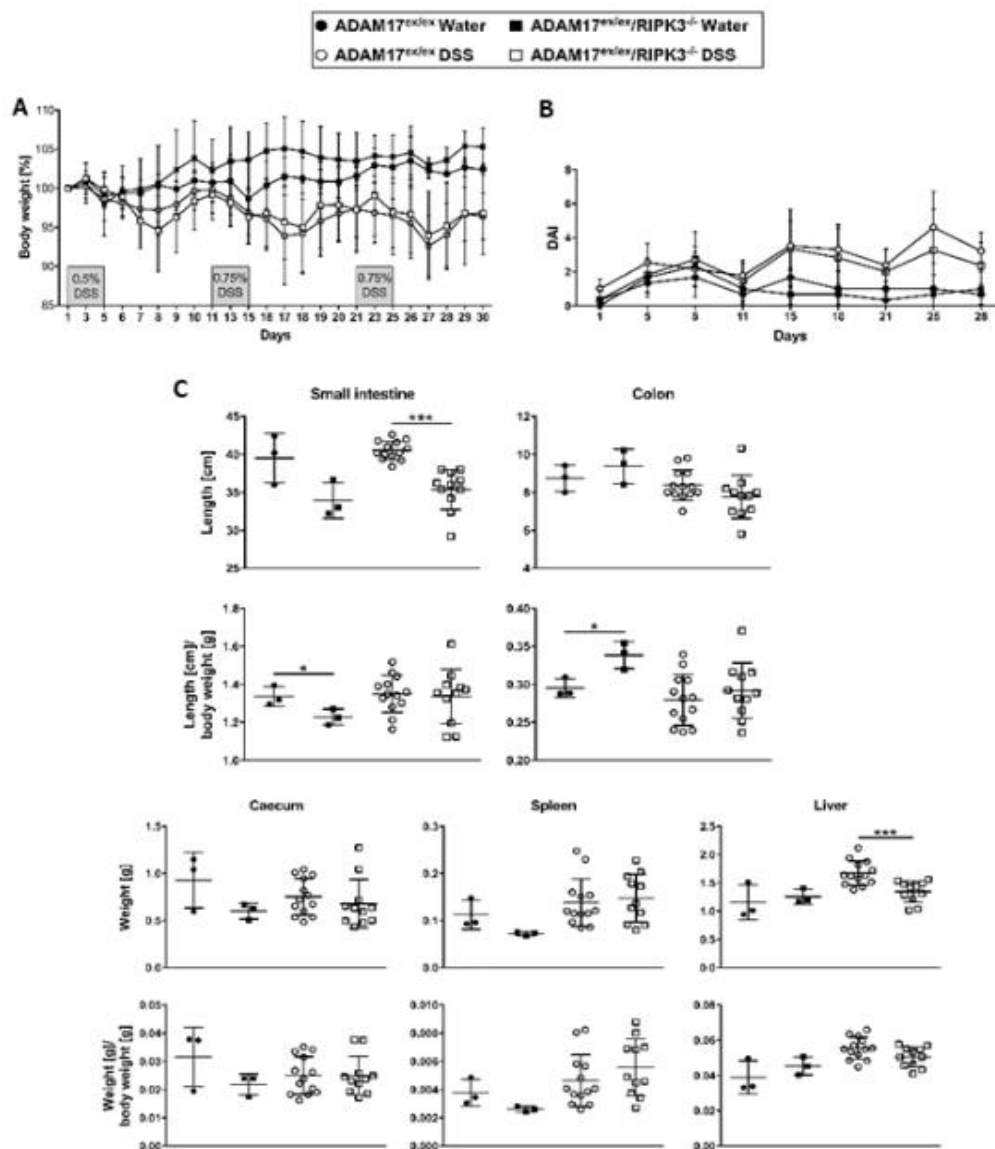


Figure 9

- A) Bodyweight shift throughout the DSS-induced chronic colitis experiment.
 B) Disease activity index as measured by the sum of scores for stool consistency, blood in stool and bodyweight.
 C) Comparison of lengths and weights of the indicated organs without and with bodyweight considered.

Histological analysis of colon distal samples showed no significant difference between genotypes again, as measured by H&E, β -catenin and MPO staining (see figure 10). In contrast to the histological examination of the acute colitis samples, these show less damage to the tissue overall.

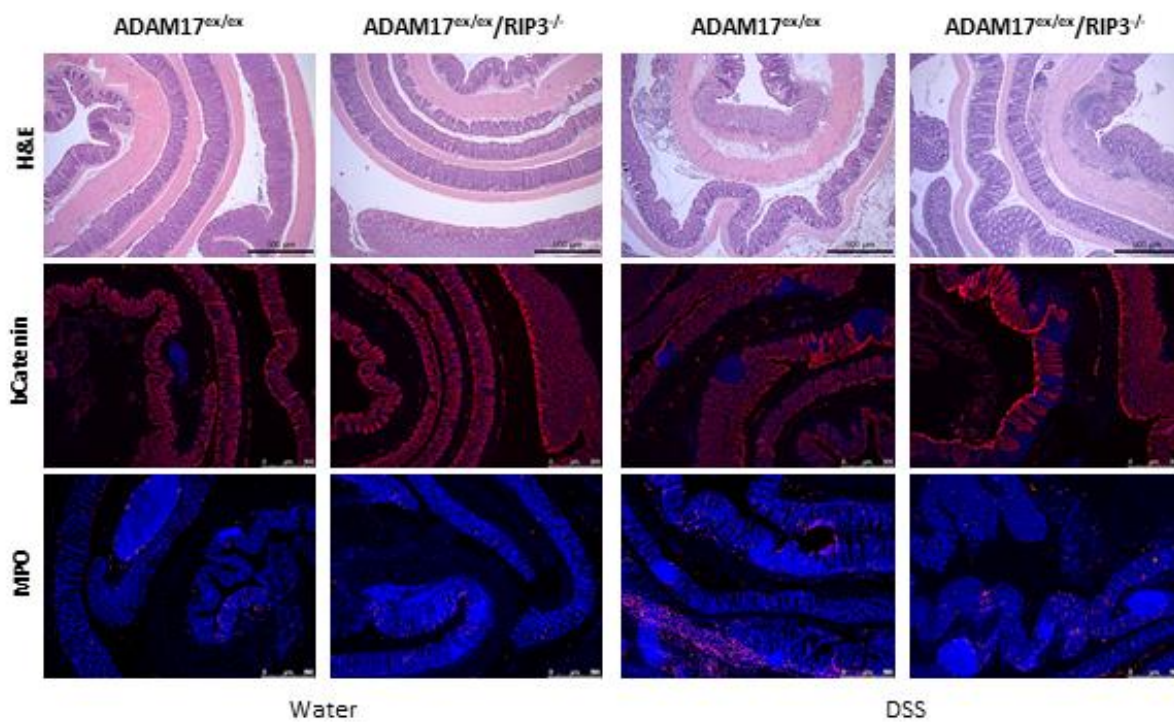
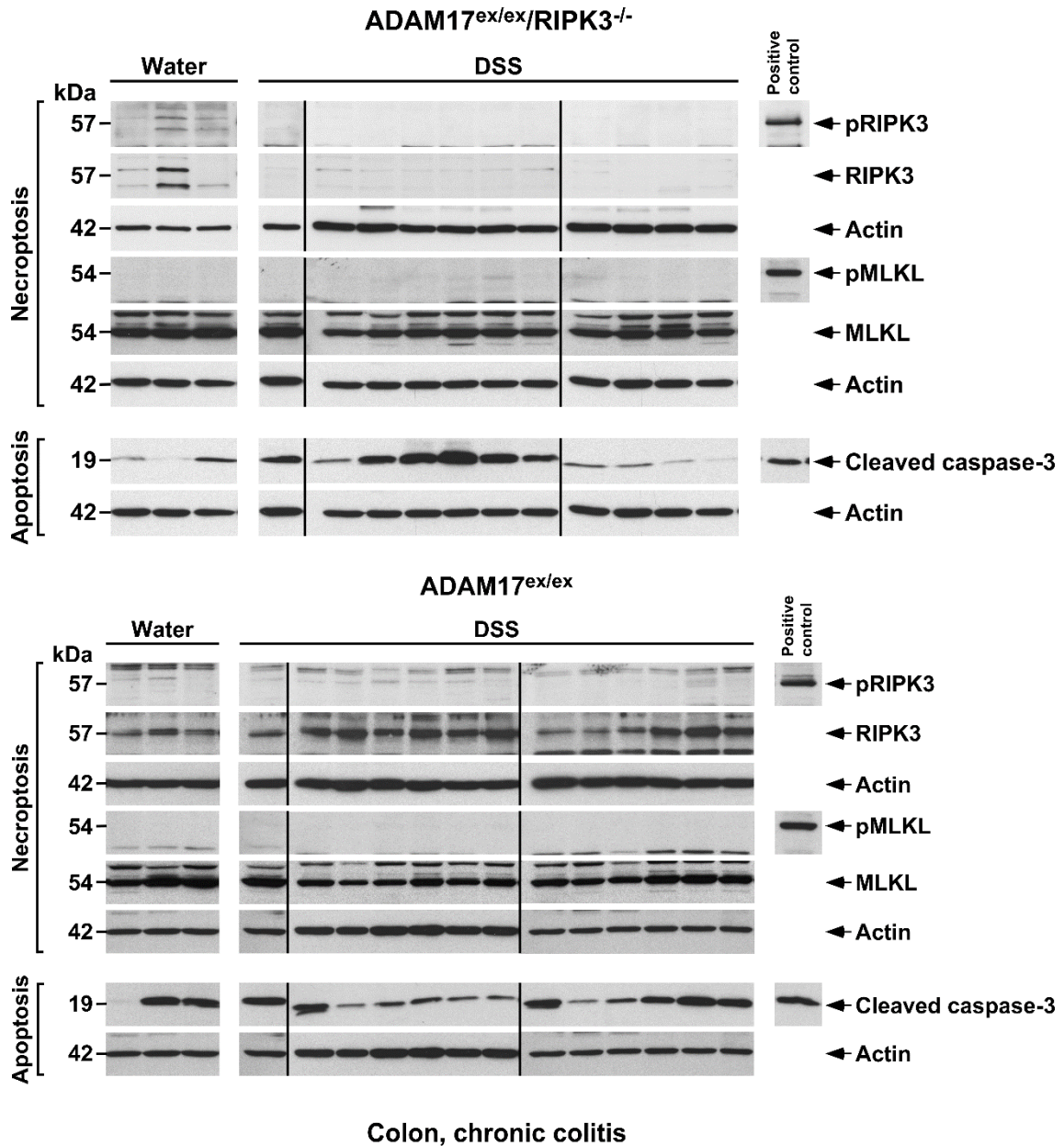


Figure 10

Kindly performed by Christoph Becker and Barbara Ruder from the University of Erlangen, DSS-induced chronic colitis samples prepared above were stained with H&E and β -catenin as well as MPO in immunofluorescence.

Western blot analysis of colon samples showed no necroptotic signal as measured by either pRIPK3 or pMLKL expression. Despite the relative lack of tissue damage compared to the acute colitis, apoptosis could still be shown, as measured by Caspase 3 cleavage (see figure 11). Here too, liver tissue was analysed, yielding similar results (see Appendix).

**Figure 11**

Western blot analysis of lysates generated from colon tissue samples of the ADAM17^{ex/ex} RIPK3^{-/-} and ADAM17^{ex/ex} mice participating in the DSS-induced chronic colitis experiment. Performed in separate gels to avoid the overlapping of pMLKL/MLKL and pRIPK3/RIPK3. Western blots for actin were performed to verify equal loading. Positive control for necroptosis consists of lysates from MEF pre-stimulated with 1 μ g/mL CHX and 20 μ M zVAD for 30 min, and then stimulated with 100 ng/mL TNF for 16 h. Positive control for apoptosis consists of lysates from MEF pre-stimulated with 1 μ g/mL CHX for 30 min, and then stimulated with 100 ng/mL TNF for 16 h.

Intrigued by the results, Western blot analysis of DSS-induced colitis WT mice was performed. As shown in figure 12, necroptotic and apoptotic signals as measured by pRIPK3/pMLKL and Caspase 3 cleavage respectively, are indeed present.

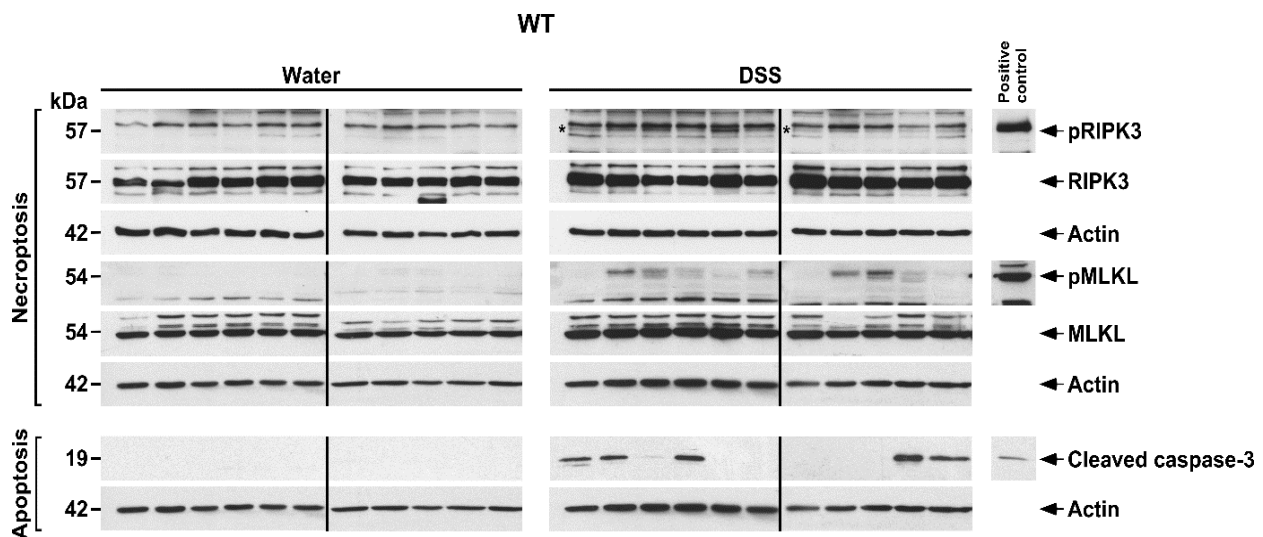


Figure 12

Western blot analysis of lysates generated from colon tissue samples of C57BL/6 mice. Western blots were done in separate gels to avoid overlapping of pMLKL/MLK and pRIPK3/RIPK3. Western blots for actin were performed to verify equal loading. Positive control for necroptosis consists of lysates from MEF pre-stimulated with 1 μ g/mL CHX and 20 μ M zVAD for 30 min, and then stimulated with 100 ng/mL TNF for 16 h. Positive control for apoptosis consists of lysates from MEF pre-stimulated with 1 μ g/mL CHX for 30 min, and then stimulated with 100 ng/mL TNF for 16 h.

To further corroborate and analyse these results, previously generated MEF from ADAM17^{ex/ex} mice (Chalaris *et al.* 2010) were used. Those cells were then analysed in a TNF-induced necroptosis assay. As seen in figure 13, ADAM17^{ex/ex} cells are protected against TNF-induced necroptosis. As in the DSS-colitis experiments, Western blot analysis showed neither pRIPK3 nor pMLKL signal in ADAM17^{ex/ex} cells as opposed to WT MEF.

4.1.1 Conclusion

ADAM17 plays a role in necroptosis *in vivo*, since both ADAM17^{ex/ex} and ADAM17^{ex/ex}/RIPK3^{-/-} mice failed to show necroptotic signals that WT mice do display. The lack of necroptotic signals, tied with a protective effect, can be reproduced at a cellular level with external TNF stimulation.

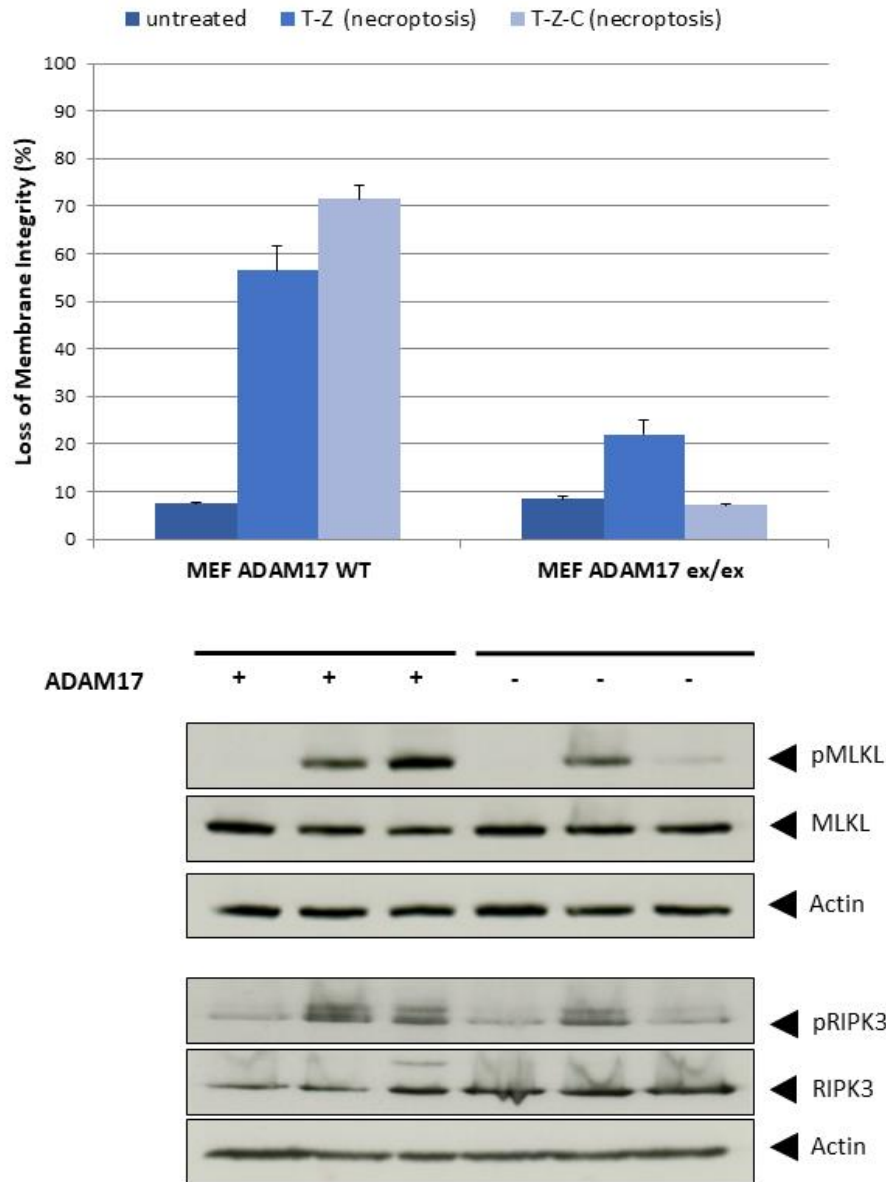


Figure 13

Functional assay to determine the effect of ADAM17 loss on necroptosis in MEF. Cells were pre-stimulated with 1 $\mu\text{g}/\text{mL}$ CHX and 20 μM zVAD for 30 min, and then stimulated with 100 ng/mL TNF for 16 h to elicit necroptosis. Loss of membrane potential was measured via PI staining and FACS. Western blot analysis of the corresponding lysates, done in two separate gels to avoid overlapping of pMLKL/MLKL and pRIPK3/RIPK3 signals. Western blots for actin were performed to verify equal loading.

Error bars represent the standard deviation from N=3 measurements.

4.2 Contribution of PGAM5 during necroptosis

Involvement of PGAM5 in necroptosis has been a contentious topic in the literature. In our hands, we could show that the amount of PGAM5 increases during necroptosis in mouse and human cells, coupled in the latter case with a shift to the lower of the two bands (see figure 14 A and B). It remained unclear whether this increase was a consequence of necroptosis or rather a necessary part of the necroptotic pathway, thus, to elucidate the matter, PGAM5 was downregulated on HT-29 cells via siRNA. As seen in figure 14 C, PGAM5 knock-down had no significant effect on necroptosis.

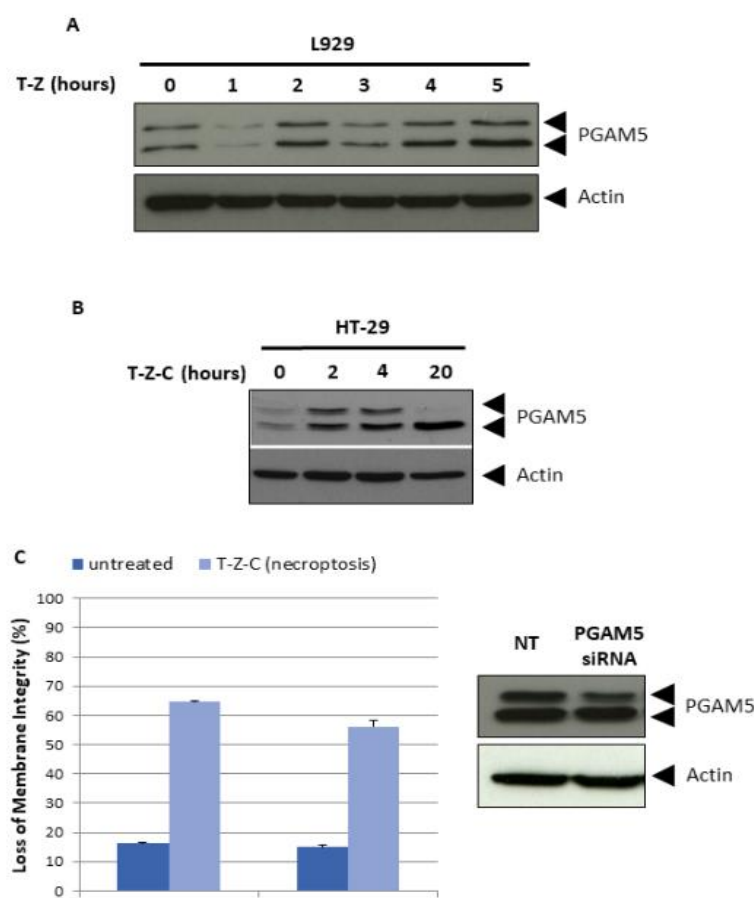


Figure 14

- A) Western blot analysis of lysates corresponding to L929 cells showing the increase of PGAM5 during necroptosis. Cells were pre-stimulated with 20 μ M zVAD for 30 min, and then stimulated with 100 ng/mL TNF for the indicated times to elicit necroptosis. Western blots for actin were performed to verify equal loading.
- B) Western blot analysis of lysates corresponding HT-29 cells showing the increase of PGAM5 during necroptosis. Cells were pre-stimulated with 10 μ g/mL CHX and 20 μ M zVAD for 30 min, and then stimulated with 100 ng/mL TNF for the indicated times to elicit necroptosis. Western blots for actin were performed to verify equal loading. Blots kindly performed by Sabine Mathieu-Grützmaier.
- C) PGAM5 downregulation with siRNA in HT-29 cells. 48 hours after the siRNA transfection, cells were pre-stimulated with 1 μ g/mL CHX and 20 μ M zVAD for 30 min, and then stimulated with 100 ng/mL TNF for the indicated times to elicit necroptosis. Western blot analysis of the corresponding lysates was done to determine the knock-down efficiency. Western blots for actin were performed to verify equal loading. Error bars represent the standard deviation from N=3 measurements.

Nonetheless, since the knock-down efficiency was low and even a small amount could still be sufficient to perform its function, PGAM5^{-/-} HT-29 and L929 were generated using CRISPR/Cas (figure 15). PGAM5^{-/-} L929 cells were preferred for further experiments due to the Western blots showing clear knock-outs, while the HT-29 Western blots still showed significant PGAM5 signal. As seen in figure 15 in measurements kindly performed by Justus Hoyer, PGAM5^{-/-} L929 cells show no significant difference in regard to TNF-induced necroptosis compared to WT L929 cells, and inconsistent or no effects under TRAIL-induced necroptosis.

4.2.1 Conclusion

PGAM5 doesn't seem to play any significant role in necroptosis.

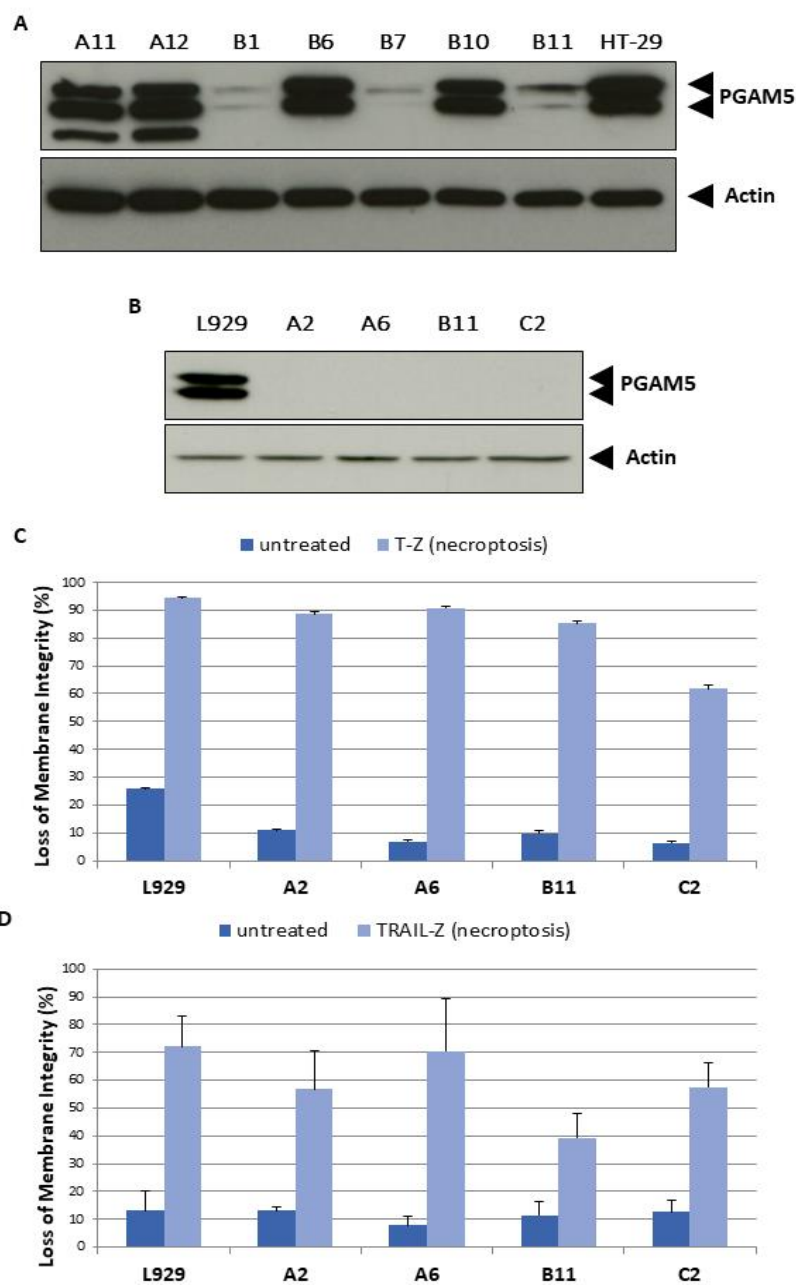


Figure 15

- A) Western blot showing lysates corresponding to HT-29 CRISPR/Cas clones for PGAM5. The names used for the clones are a combination of a letter and a number, corresponding to the respective place in the 12-well in which the clone grew. Western blots for actin were performed to verify equal loading. Not used in further experiments.
- B) Western blot showing lysates corresponding to L929 CRISPR/Cas clones for PGAM5. The names used for the clones are a combination of a letter and a number, corresponding to the respective place in the 12-well in which the clone grew. Western blots for actin were performed to verify equal loading.
- C) Flow cytometric analysis to determine the effect of PGAM5 loss on TNF-induced necroptosis in the L929 CRISPR/Cas clones for PGAM5 generated in B). Cells were pre-stimulated with 20 μ M zVAD for 30 min, and then stimulated with 100 ng/mL TNF for 4 h to elicit necroptosis. Loss of membrane potential was measured via PI staining. Measurement kindly performed by Justus Hoyer. Error bars represent the standard deviation from N=3 measurements.
- D) Flow cytometric analysis to determine the effect of PGAM5 loss on TRAIL-induced necroptosis in the L929 CRISPR/Cas clones for PGAM5 generated in B). Cells were pre-stimulated with 20 μ M zVAD for 30 min, and then stimulated with 100 ng/mL TRAIL for 16 h to elicit necroptosis. Loss of membrane potential was measured via PI staining. Measurement kindly performed by Justus Hoyer. Error bars represent the standard deviation from N=6 measurements across 2 experiments.

4.3 Contribution of HtrA2/Omi to necroptosis

HtrA2/Omi has been previously reported to play an important role in necroptosis (Sosna *et al.* 2013). The exact mechanism or position within the signalling pathway being unknown, both pMLKL and pRIPK3 were examined in HtrA2/Omi^{-/-} MEF cells under necroptotic conditions. As seen in figure 16, these cells show an extremely delayed pMLKL and pRIPK3 signal compared to WT cells, correlating with the previously shown necroptotic death resistance.

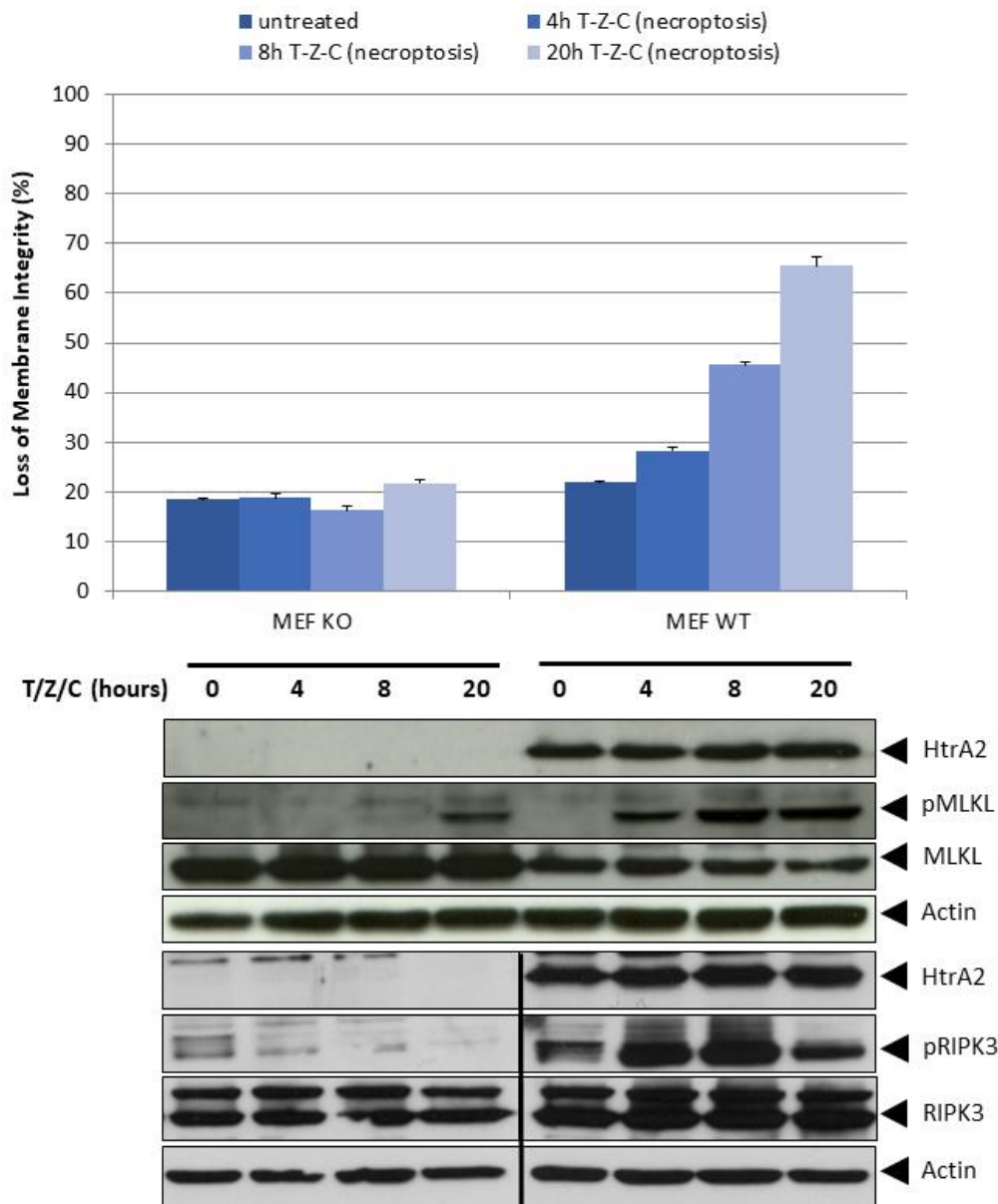


Figure 16

Upper panel: Flow cytometric analysis of a time-course of necroptosis in HtrA2/Omi^{-/-} and WT MEF. Cells were pre-stimulated with 1 μ g/mL CHX and 20 μ M zVAD for 30 min, and then stimulated with 100 ng/mL TNF for the indicated times to elicit necroptosis. Loss of membrane potential was measured via PI staining.

The lower panel shows the Western blot analysis of the corresponding lysates, which was done in two separate gels to detect pMLKL/MLKL and pRIPK3/RIPK3 signals that would otherwise overlap. Western blots for actin were performed to verify equal loading. Error bars represent the standard deviation from N=3 measurements.

To further corroborate and investigate this result, a four-pronged approach was used:

- 1) HtrA2/Omi^{-/-} MEF stably re-transfected with WT HtrA2/Omi (“rescue”) were generated as described in Materials and Methods. HtrA2/Omi^{-/-} MEF re-transfected with WT HtrA2/Omi showed a significant increase in cell death and pMLKL/pRIPK3 signal similar to WT MEF (see figure 17), confirming the causal relationship between the knock-out and the effect on pMLKL/pRIPK3.

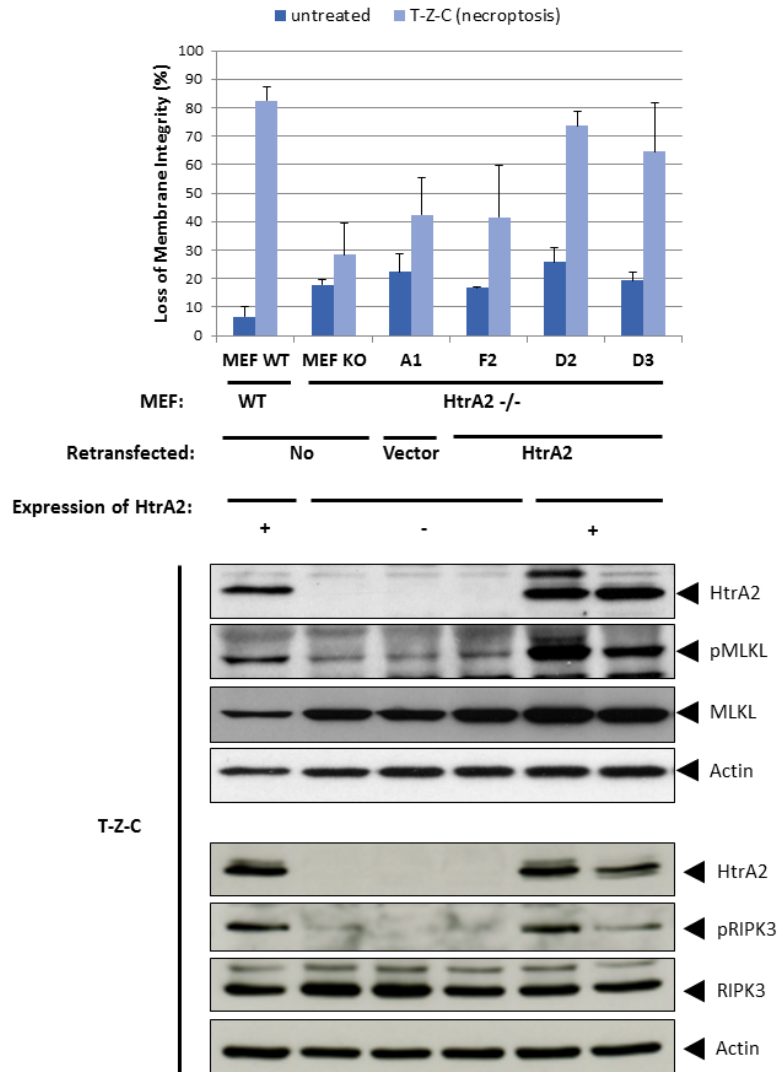


Figure 17

The upper panel shows the flow cytometric analysis of a rescue assay; showing the effect on necroptosis of WT, HtrA2/Omi^{-/-}, HtrA2/Omi^{-/-} vector-transfected (A1), HtrA2/Omi^{-/-} non-expressing WT transfected (F2), and two HtrA2/Omi^{-/-} - WT transfected (D2 and D3) MEF. Cells were pre-stimulated with 1 µg/mL CHX and 20 µM zVAD for 30 min, and then stimulated with 100 ng/mL TNF for 16 h to elicit necroptosis. Loss of membrane potential was measured via PI staining.

The lower panel shows the Western blot analysis of the corresponding lysates, which was done in two separate gels to detect pMLKL/MLKL and pRIPK3/RIPK3 signals that would otherwise overlap. Western blots for actin were performed to verify equal loading. Error bars represent the standard deviation from N=6 measurements across 2 experiments.

- 2) HtrA2/Omi^{-/-} L929 cells were generated via CRISPR/Cas as described in Materials and Methods. As can be seen in figure 18, the HtrA2/Omi^{-/-} clones C2 and C10 consistently showed the same phenotype as the HtrA2/Omi^{-/-} MEF, unlike clone B9 who inconsistently shifted between phenotypes (sometimes showing HtrA2/Omi signal and sometimes not doing so). After sequencing the three clones, C2 was selected for further studies due to it having the earliest STOP codon inserted.

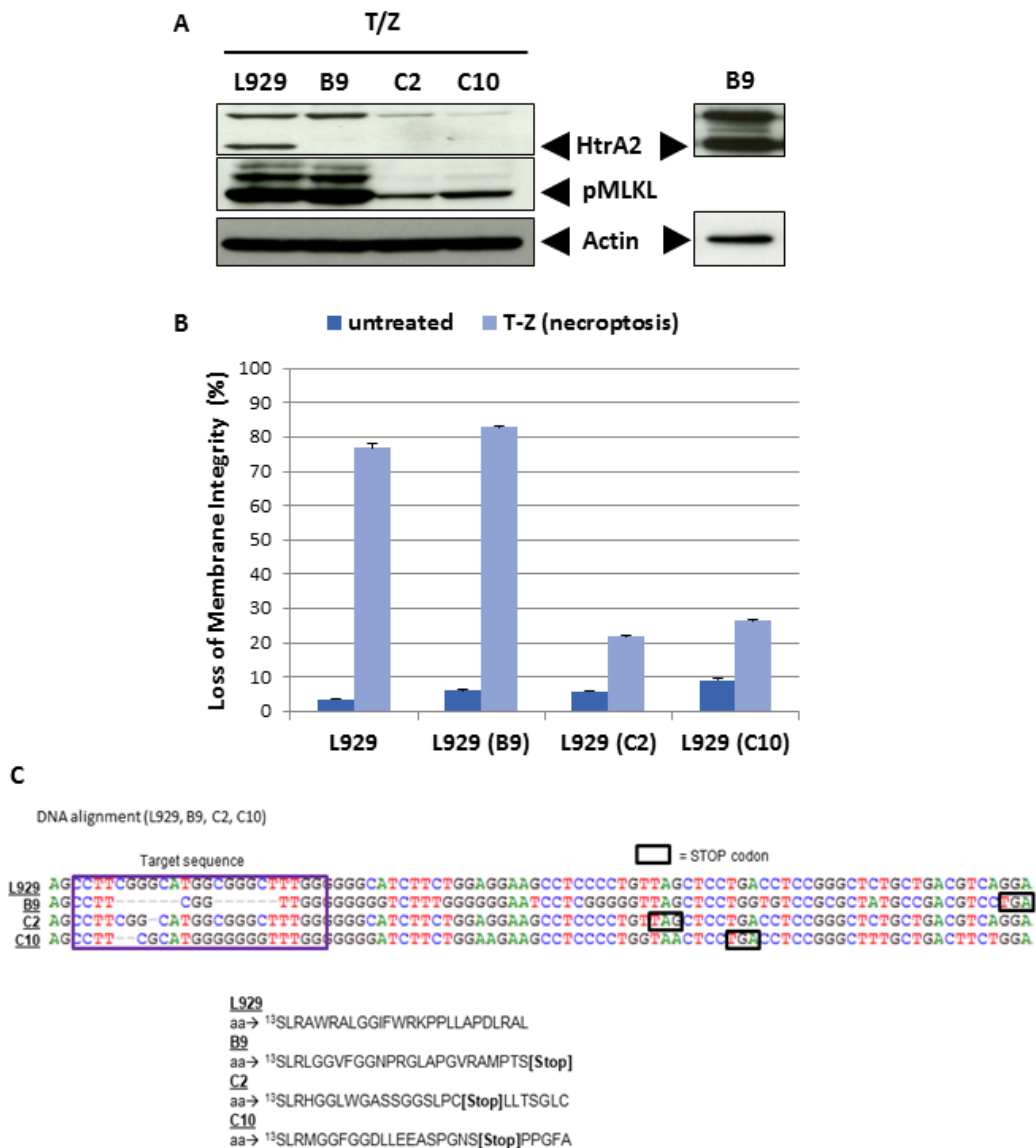


Figure 18

- A) Western blot showing lysates corresponding to L929 CRISPR/Cas clones for HtrA2/Omi. The names used for the clones are a combination of a letter and a number, corresponding to the respective place in the 12-well in which the clone grew. Western blots for actin were performed to verify equal loading.
- B) Flow cytometric analysis to determine the effect of HtrA2/Omi loss on TNF-induced necroptosis in the L929 CRISPR/Cas clones for HtrA2/Omi generated in A). Cells were pre-stimulated with 20 μ M zVAD for 30 min, and then stimulated with 100 ng/mL TNF for 4 h to elicit necroptosis. Loss of membrane potential was measured via PI staining. Error bars represent the standard deviation from N=3 measurements.
- C) Sequencing of the CRISPR/Cas clones generated in A), showing the nucleotide sequence and the corresponding amino acid sequence.

This final candidate (C2) was also stably re-transfected (“rescued”) with WT HtrA2/Omi. As shown in figure 19, the results are analogous to the ones in MEF cells, confirming that the protection observed is not limited to one cell line.

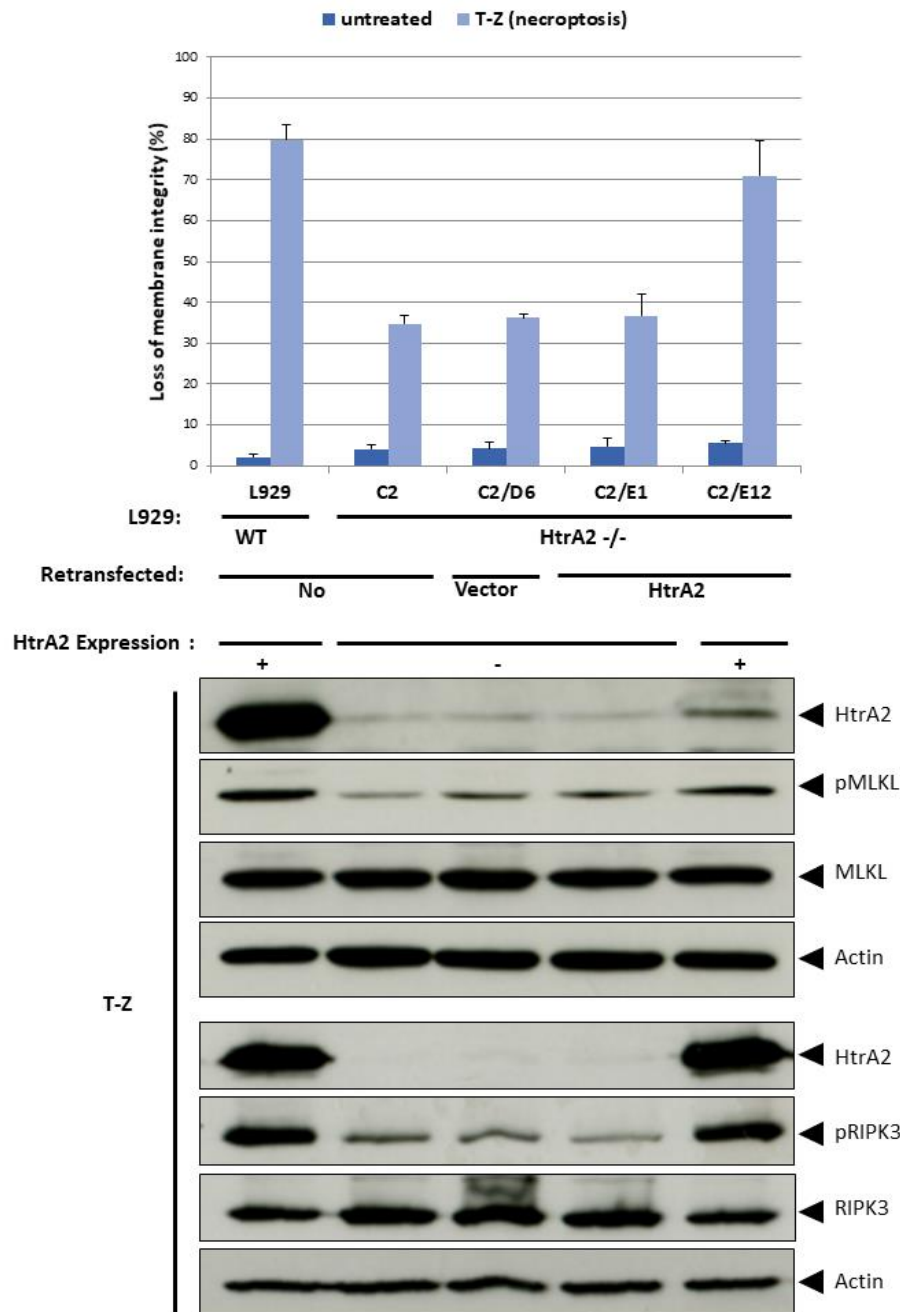


Figure 19

The upper panel shows the flow cytometric analysis of a rescue assay; showing the effect on necroptosis of WT, HtrA2/Omi^{-/-} (C2), HtrA2/Omi^{-/-} vector transfected (C2/D6), HtrA2/Omi^{-/-} non-expressing WT transfected (C2/E1), and HtrA2/Omi^{-/-} - WT transfected (C2/E12) L929. Cells were pre-stimulated with 20 μ M zVAD for 30 min, and then stimulated with 100 ng/mL TNF for 5 h to elicit necroptosis. Loss of membrane potential was measured via PI staining.

The lower panel shows the Western blot analysis of the corresponding lysates, which was done in two separate gels to detect pMLKL/MLKL and pRIPK3/RIPK3 signals that would otherwise overlap. Western blots for actin were performed to verify equal loading. Error bars represent the standard deviation from N=6 measurements across 2 experiments.

- 3) TRAIL-induced necroptosis with a selection of the clones generated in 1) and 2) was performed to assess whether the results seen in L929 cells and MEF could be reproduced under another kind of necroptotic stimulus. As can be seen in figure 21, similar results to the ones shown for TNF-induced necroptosis were obtained.

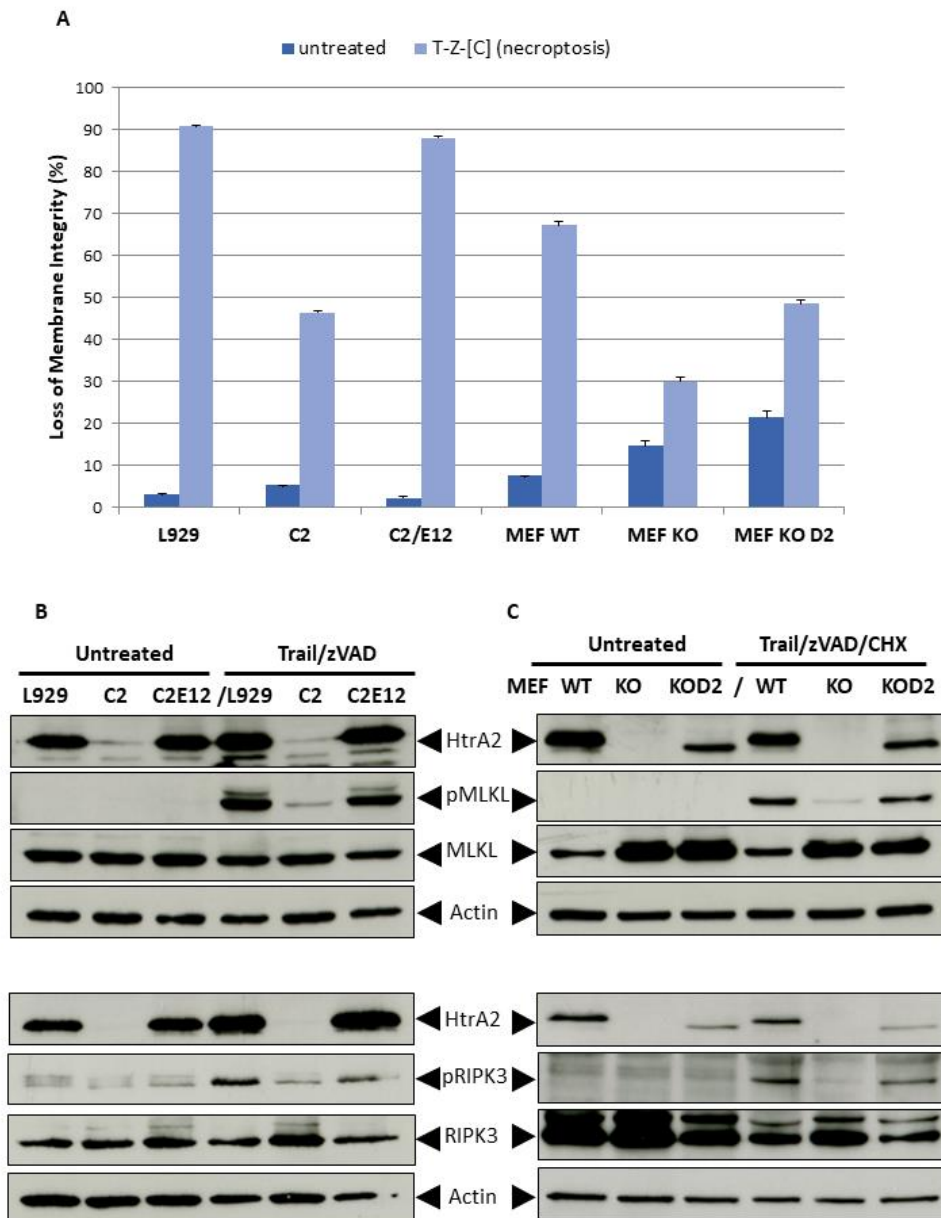


Figure 20

- A) Flow cytometric analysis with L929 cells and MEF WT, HtrA2/Omi^{-/-} (C2 for L929, KO for MEF), HtrA2/Omi^{-/-} WT re-transfected (C2E12 for L929 cells and KOD2 for MEF). L929 cells were pre-stimulated with 20 μ M zVAD for 30 min, and then stimulated with Trail for 16 h to elicit Trail-induced necroptosis. MEF cells were pre-stimulated with 1 μ g/mL CHX and 20 μ M zVAD for 30 min, and then stimulated with Trail for 16 h to elicit Trail-induced necroptosis. Loss of membrane potential was measured via PI staining. Error bars represent the standard deviation from N=3 measurements.
- B) Western blot analysis of L929 cell-lysates (corresponding to the flow cytometric analysis performed in A)) which was done in two separate gels to detect pMLKL/MLKL and pRIPK3/RIPK3 signals that would otherwise overlap. Western blots for actin were performed to verify equal loading.
- C) Western blot analysis of MEF lysates (corresponding to the flow cytometric analysis performed in A)), each done in two separate gels to avoid overlapping of pMLKL/MLKL and pRIPK3/RIPK3 signals. Western blots for actin were performed to verify equal loading.

- 4) HtrA2/Omi^{-/-} HT-29 cells were generated via CRISPR/Cas as described in Materials and Methods, to assess whether the results seen in L929 cells and MEF could be reproduced in a human cell line. As can be seen in figure 20, and unlike in L929, we were unable to elucidate a consistent causal relationship between the amount of HtrA2/Omi signal and protection against TNF-induced necroptosis. This was due to inconsistent results, such as clones still expressing HtrA2/Omi and showing protection (e.g. A8) or not (e.g. B9) and clones without HtrA2/Omi signal showing protection (e.g. A12) or not (e.g. B2).

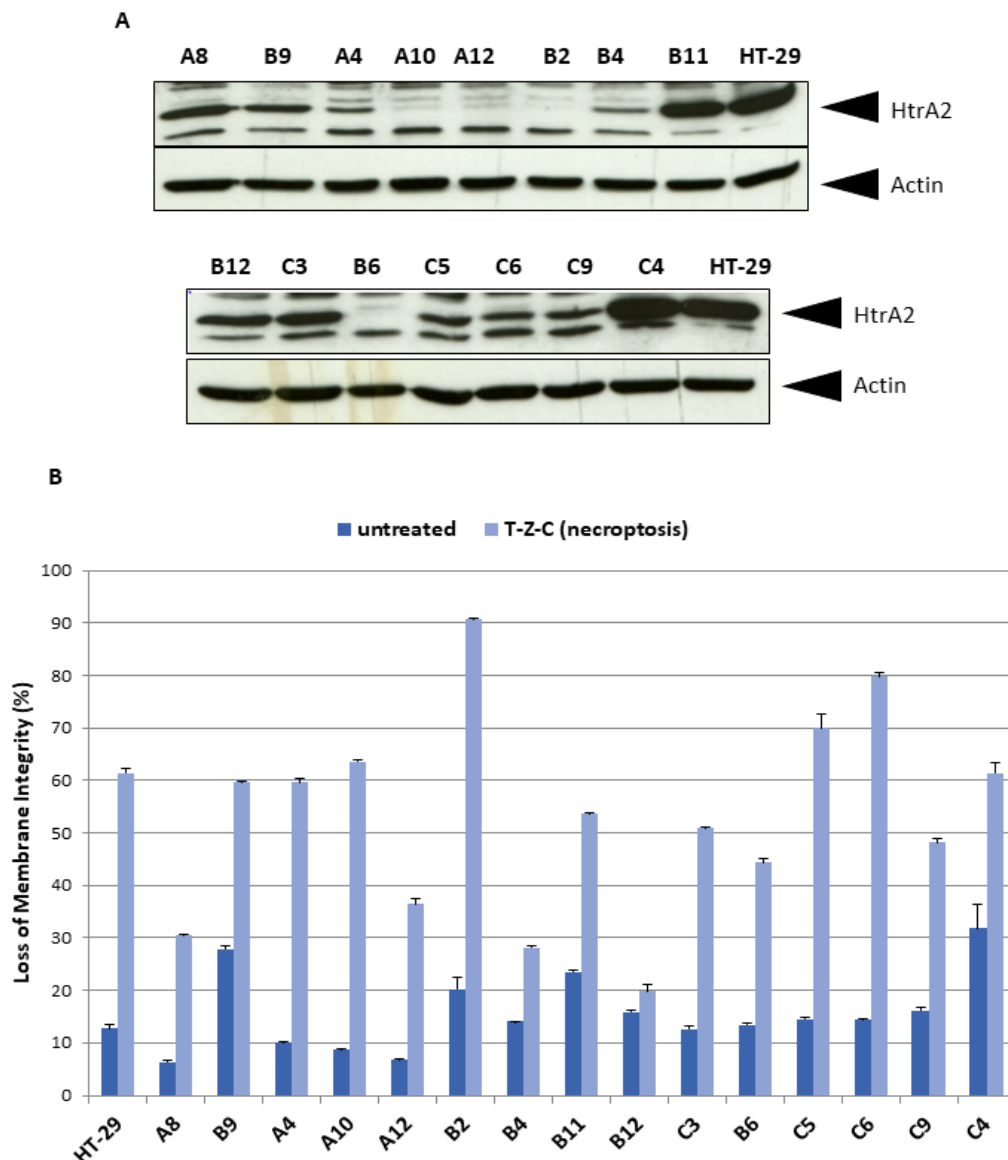


Figure 21

- A) Western blot showing lysates belonging to HT-29 CRISPR/Cas clones for HtrA2/Omi. The names used for the clones are a combination of a letter and a number, corresponding to the place in the 12-well in which each clone grew. Western blots for actin were performed to verify equal loading.
- B) Flow cytometric analysis to determine the effect of HtrA2/Omi loss on TNF-induced necroptosis in the HT-29 CRISPR/Cas clones generated in A). Cells were pre-stimulated with 10 $\mu\text{g}/\text{mL}$ CHX and 20 μM zVAD for 30 min, and then stimulated with 100 ng/mL TNF for 20 h to elicit necroptosis. Loss of membrane potential was measured via PI staining. Error bars represent the standard deviation from N=3 measurements.

4.3.1 Conclusion

HtrA2/Omi seems to act in some form upstream of RIPK3 (and thus also MLKL) phosphorylation in murine L929 cells and MEF necroptosis.

4.4 Localization of HtrA2/Omi during necroptosis

HtrA2/Omi is known to exit mitochondria during apoptosis, where it inhibits IAPs, thereby permitting cell death (van Loo *et al.* 2002). In contrast, HtrA2/Omi has been reported to stay in mitochondria under necroptotic conditions (van Loo *et al.* 2002, Blink *et al.* 2004). To confirm this in our system, a three-pronged approach was used.

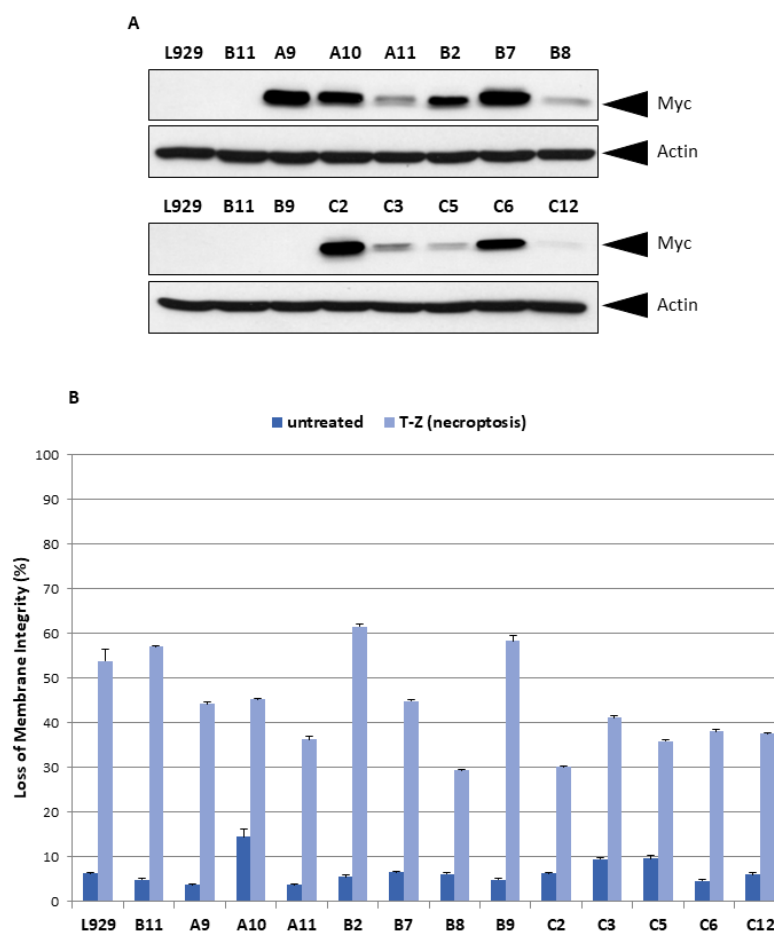


Figure 22

- A) Western blot showing lysates belonging to L929 clones stably transfected with Myc-tagged vMIA. Western blots for actin were performed to verify equal loading.
- B) Flow cytometric analysis to determine the effect of vMIA transfection on necroptosis. Cells were pre-stimulated with 20 μ M zVAD for 30 min, and then stimulated with 100 ng/mL TNF for 5 h to elicit necroptosis. Loss of membrane potential was measured via PI staining. Error bars represent the standard deviation from N=3 measurements.

-
- 1) Generation of clones stably expressing vMIA (cytomegalovirus Mitochondrial Inhibitor of Apoptosis) in L929 cells. vMIA is known to block the transit of various mitochondrial proteins into the cytosol, amongst them HtrA2/Omi (Goldmacher 2002). This protects cells against apoptosis, simultaneously protecting the virus from clearance. As shown in figure 22, the expression of vMIA does not protect cells from necroptosis.

 - 2) Immunofluorescence experiments in MEF and L929 cells were performed, in which the co-localization of HtrA2/Omi with MitoTracker® signal was confirmed. As shown in figure 23, the HtrA2/Omi signal seems to co-localize with the MitoTracker® signal before and after necroptotic stimulation in MEF and L929 cells, sometimes showing signal in and around the nuclei as well.

This indicates that HtrA2/Omi, for the most part, does not leave the mitochondria. Under apoptotic stimulus (figure 23 C), the HtrA2/Omi signal is completely lacking from the mitochondria, being instead in or around the nucleus. The nuclear or perinuclear localization of the HtrA2 signal, especially in apoptosis, are in accordance with a publication showing that HtrA2/Omi cleaves the Wilms' tumour suppressor protein 1 (WT1) under apoptotic conditions, and does so in the nucleus and cytoplasm of M15 cells (Hartkamp *et al.* 2010). Also, the NCBI entry for HtrA2/Omi mentions the nuclear localization of the protein (<https://www.ncbi.nlm.nih.gov/gene/27429>).

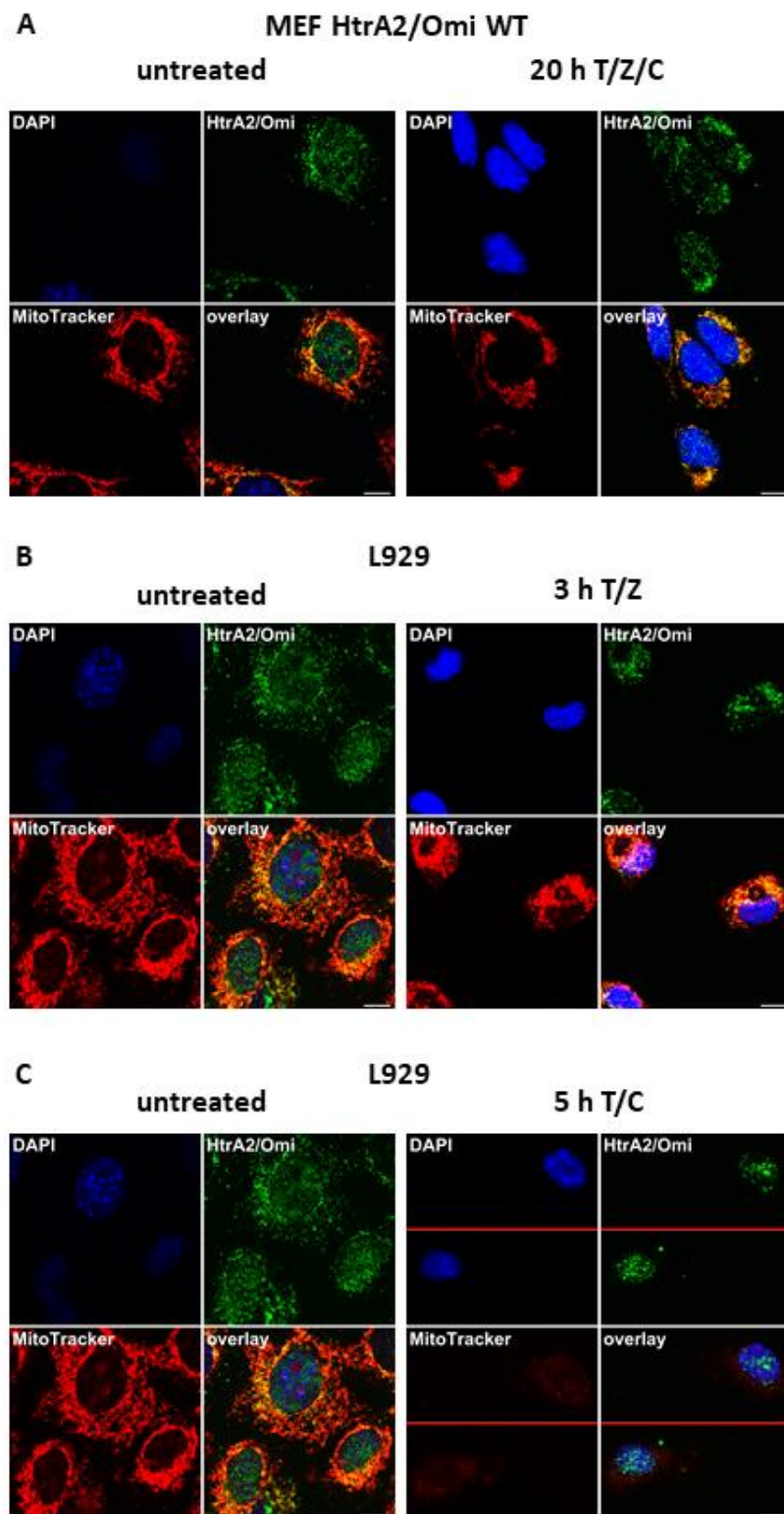


Figure 23

- A) Immunofluorescence of MEF cells, either left untreated or pre-stimulated with 1 $\mu\text{g}/\text{mL}$ CHX and 20 μM zVAD for 30 min, and then stimulated with TNF for 20 h to elicit necroptosis.
- B) Immunofluorescence of L929 cells, either left untreated or pre-stimulated with 20 μM zVAD for 30 min, and then stimulated with TNF for 3 h to elicit necroptosis.
- C) Immunofluorescence of L929 cells, either left untreated or pre-stimulated with 10 $\mu\text{g}/\text{mL}$ CHX for 30 min, and then stimulated with TNF for 5 h to elicit apoptosis.

- 3) Fractionation experiments in MEF were performed. Despite difficulties in re-blotting membranes to show control signals, the results point towards HtrA2/Omi staying in the mitochondrial fraction (see figure 24).

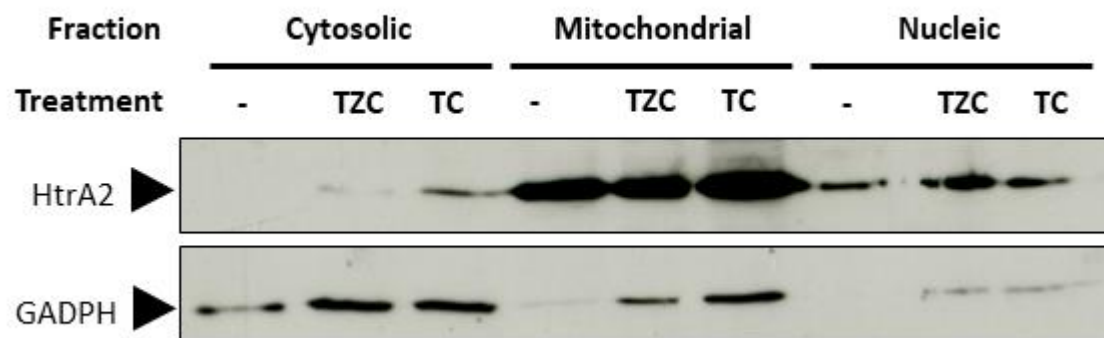


Figure 24

Western blot analysis corresponding to a fractionation experiment with WT MEF showing HtrA2/Omi signal and GADPH (localization control for cytosolic fraction) from the Mitochondrial Fraction Antibody cocktail (Abcam, UK). Neither ATP5 nor Histone 3 could be detected (not shown). Cells were either left untreated or pre-stimulated with 1 $\mu\text{g}/\text{mL}$ CHX and 20 μM zVAD for 30 min, and then stimulated with 100 ng/mL TNF for 16 h to elicit necroptosis or pre-stimulated with 1 $\mu\text{g}/\text{mL}$ CHX for 30 min, and then stimulated with TNF for 20 h to elicit apoptosis. After stimulation, cells were fractionated using the Fractionation Kit-Standard (Abcam, UK).

4.4.1 Conclusion

Taken together, these results suggest that HtrA2/Omi doesn't need to exit mitochondria during necroptosis to perform its function.

4.5 Role of known substrates of HtrA2/Omi

In a proteome-wide analysis (Vande Walle *et al.* 2007), the group of P. Vandenabeele found certain proteins to be substrates of HtrA2/Omi during apoptosis: DBC1 (Deleted in Bladder Cancer 1 protein), PDXDC1 (Pyridoxal Dependent Decarboxylase Domain Containing protein 1); and VPS4B (Vacuolar Protein Sorting 4 Homolog B), the latter two identified in the study merely as fragments.

To investigate whether these proteins are also cleaved by HtrA2/Omi during necroptosis, HtrA2/Omi WT, HtrA2/Omi^{-/-} and HtrA2/Omi^{-/-} reconstituted with HtrA2/Omi, MEF and L929 cells were analysed by Western blotting. As seen in figure 25, DBC1 showed a marked decrease under necroptotic conditions in MEF HtrA2/Omi WT and HtrA2/Omi^{-/-} reconstituted with HtrA2/Omi but not in L929 cells. PDXDC1 shows no difference in either cell line, with the possibility of a cleavage band appearing under necroptotic conditions in MEF HtrA2/Omi WT and WT re-transfected. VPS4B shows multiple bands in both cell lines, opening the question whether there is some form of cleavage taking place, but here too the results differ between MEF and L929.

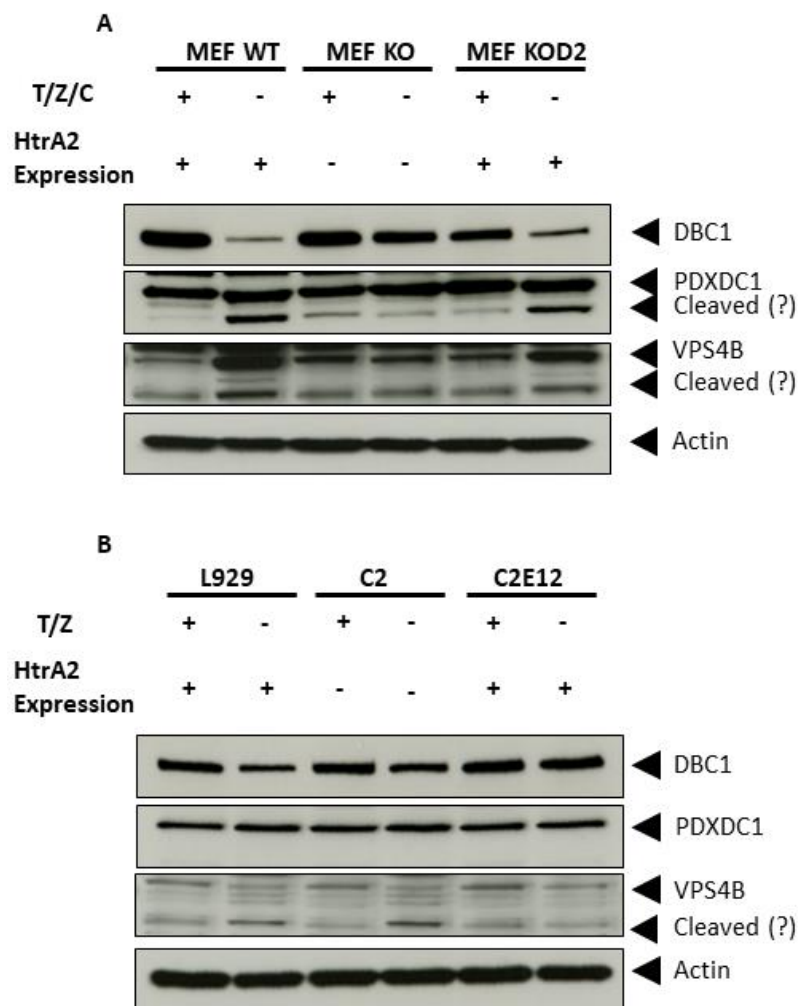


Figure 25

- A) Western blot analysis of HtrA2/Omi WT, HtrA2/Omi^{-/-} (KO) and HtrA2/Omi^{-/-} reconstituted with HtrA2/Omi (KOD2) MEF. Cells were pre-stimulated with 1 µg/mL CHX and 20 µM zVAD for 30 min, and then stimulated with TNF for 16 h to elicit necroptosis. Western blots for actin were performed to verify equal loading.
- B) Western blot analysis of HtrA2/Omi WT, HtrA2/Omi^{-/-} (C2) and HtrA2/Omi^{-/-} reconstituted with HtrA2/Omi (C2E12) L929 cells. Cells were pre-stimulated with 20 µM zVAD for 30 min, and then stimulated with TNF for 3 h to elicit necroptosis. Western blots for actin were performed to verify equal loading.

To corroborate whether this effect is a direct consequence of a lack of cleavage by HtrA2/Omi in HtrA2/Omi^{-/-} MEF or is indirectly caused by the necroptosis resistance of HtrA2/Omi^{-/-} MEF, a siRNA knockdown control experiment was performed with MEF HtrA2/Omi WT. If either of DBC1, PDXDC1 or VPS4B were downstream effectors of HtrA2/Omi, we would expect a protective effect analogous to the one seen in HtrA2^{-/-} MEF. As seen in figure 26, the knock-down of either of DBC1, PDXDC1 or VPS4B has no effect on cell death, but the efficiency of the knock-down is too low to draw any conclusions regarding a direct cleavage by HtrA2/Omi.

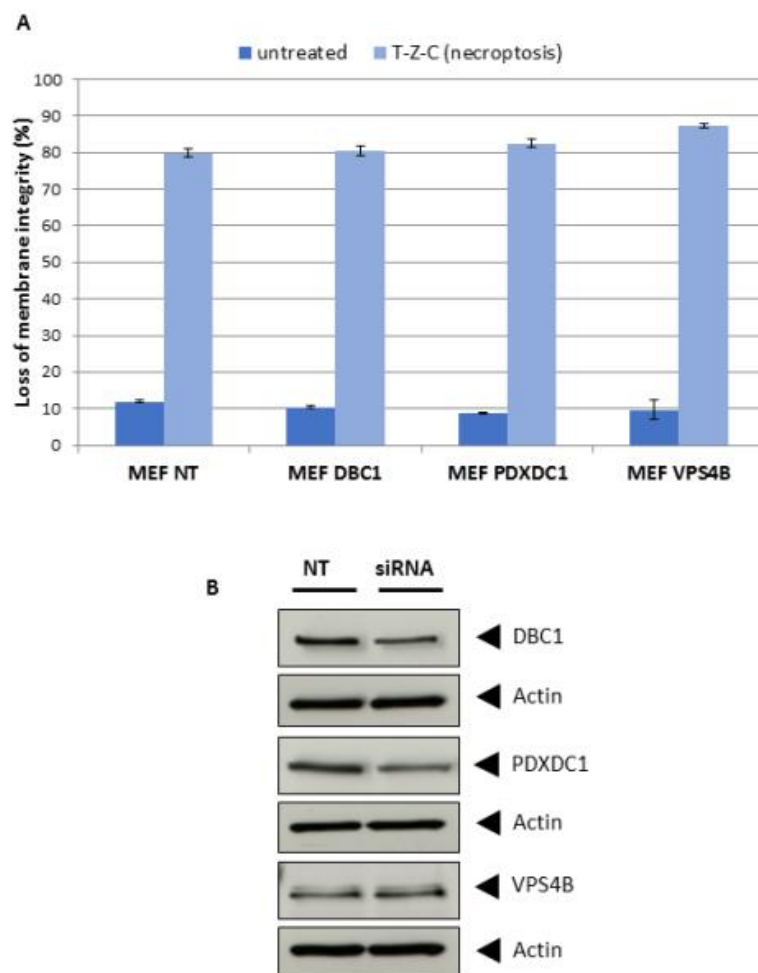


Figure 26

A) Flow cytometric analysis of HtrA2/Omi WT MEF transfected with non-targeting siRNA or against DBC1, PDXDC1 and VPS4B. 48 hours after the transfection, cells were pre-stimulated with 1 μ g/mL CHX and 20 μ M zVAD for 30 min, and then stimulated with TNF for 16 h to elicit necroptosis. Loss of membrane potential was measured via PI staining. Error bars represent the standard deviation from N=3 measurements.

B) Western Blot analysis lysates corresponding to A), comparing non-targeting control to siRNA transfected cells. Western blots for actin were performed to verify equal loading.

Experiment kindly performed by Carina Saggau.

4.5.1 Conclusion

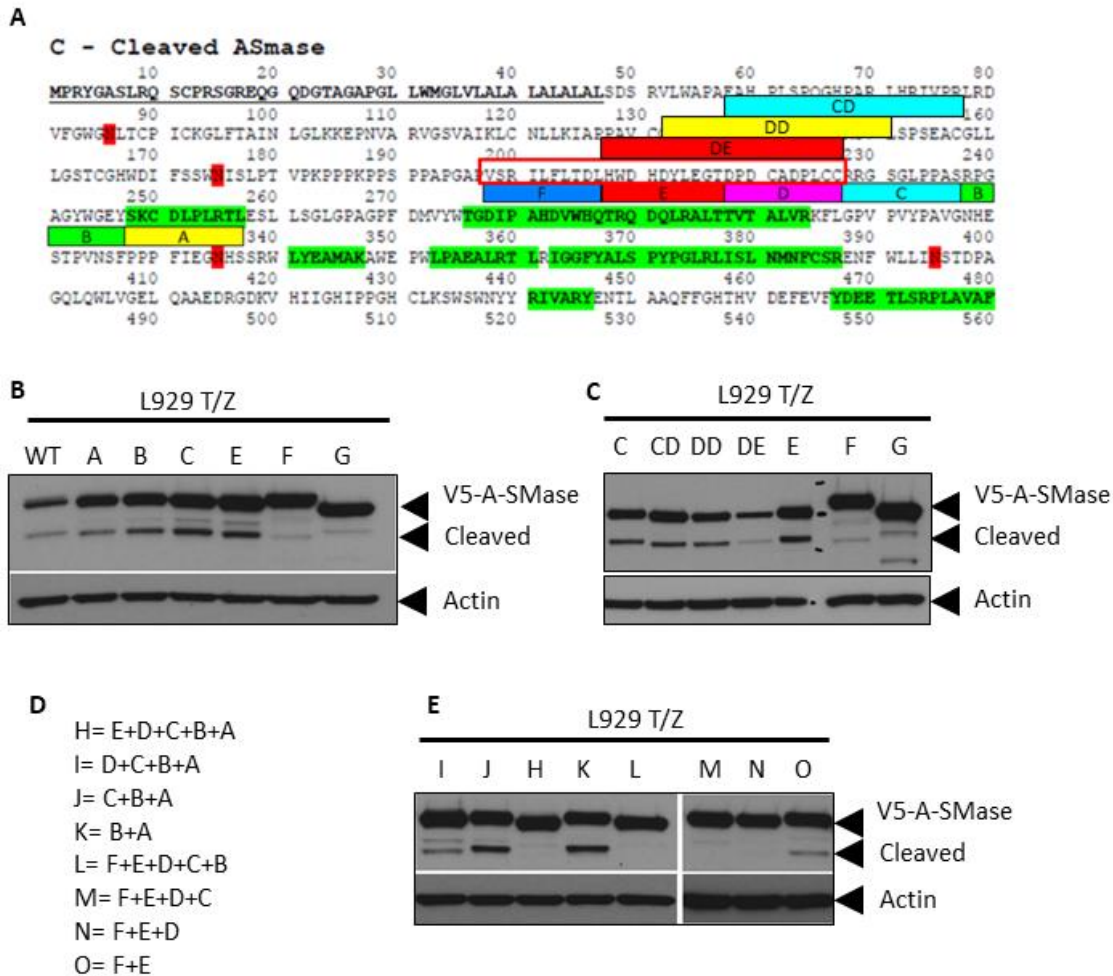
DBC1, PDXDC1 and VPS4B do not seem to be downstream mediators of HtrA2/Omi during necroptosis. Alternatively, the downregulation performed was not sufficient to block the function.

4.6 Role of acid sphingomyelinase in necroptosis

The importance of acid sphingomyelinase as a possible downstream effector in necroptosis has previously been shown (Thon *et al.* 2005). Cleaving the inactive pre-form is a vital step to the activation of the A-SMase, and while the cleavage site as well as the responsible protease (caspase 7) have both been found for the proteolytic activation of A-SMase in apoptosis (Edelmann *et al.* 2011), those cannot - per definition, be the ones responsible during a caspase independent form of cell death such as necroptosis. As such, the localization of the cleavage site was attempted, while the identification of the activating protein is currently being researched by the group of Prof. Dr. Adam.

4.6.1 Localization of the necroptotic cleavage site of acid sphingomyelinase

In previous work, mass spectrometric analysis had not revealed the exact cleavage site due to limits of detection. However, peptides of cleaved A-SMase had been identified. Based on this information, deletion by overlap extension PCR was performed as described in Materials and Methods. Thus, A-SMase mutants were generated that span a region of 50 deleted amino acids upstream of the most N-terminally located peptide, as well as mutants spanning partial deletions of the suspected region. These constructs were then transfected into L929 cells and lysates analysed via western blotting. As seen in figure 27, changes in the cleavage bands could be shown, suggesting not a single cleavage site, but a compound one, since cleavage is abrogated only under deletion of a larger portion of the sequence.

**Figure 27**

- A) Starting at the location of the most N-terminal fragment previously identified via mass spectrometry (identified fragments are shown in green), groups of 10 amino acids were deleted via overlap extension PCR in the region N-terminal to the peptide and called A-C and E-F (represented via the coloured boxes; clones containing deletion D could not be obtained). The region containing the cleavage sites is framed by a red box.
- B) Western blot analysis of lysates of L929 cells that were transfected with V5-tagged A-SMase containing deletions A-C and E-F plus deletion G, spanning the entire region covered by A-F. 48 hours after transfection, cells were pre-stimulated 30 min with 20 mM zVAD and stimulated for 4 hours with TNF. Lysates were analysed with V5 antibody. Cells in which the cleaved form of A-SMase disappeared were considered to encompass the cleavage site. Western blots for actin were performed to verify equal loading.
- C) Since no D deletion could be produced, 3 further constructs containing deletions spanning 20 amino acids, called CD, DD and DE were generated. Stimulation and western blot analysis were performed as in B).
- D) V5-tagged A-SMase constructs containing combinations of previous deletions were generated via overlap extension PCR and called I-O.
- E) L929 cells were transfected with V5-tagged A-SMase generated in D). Stimulation and western blot analysis were performed as in B).

Constructs were designed in collaboration with Prof. Dr. Adam, and the analysis of the deletion mutants was kindly performed by Parvin Davarnia.

To assess the functionality of the constructs generated in the above experiments via enzymatic activity assays, A-SMase^{-/-} L929 cells were generated via CRISPR/Cas as described in Materials and Methods. As can be seen in figure 28, the results are inconclusive, since deletions in and around the cleavage region completely blocked the A-SMase activity, regardless of the cleavage status seen in figure 27.

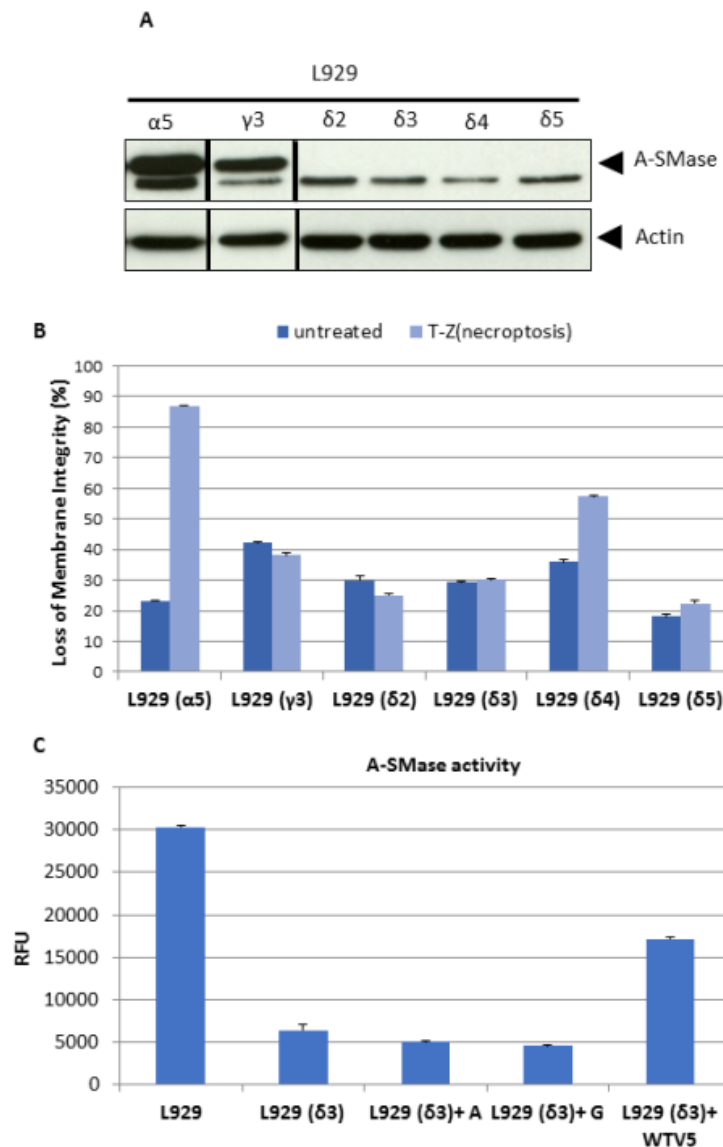


Figure 28

- A) Western blot analysis of generated L929 cells deficient for A-SMase by CRISPR/Cas. The $\delta 3$ clone was selected for further experiments. Western blots for actin were performed to verify equal loading.
- B) Flow cytometric analysis to determine the effect of A-SMase deletion on necroptosis in the L929 cells generated in A). Cells were pre-stimulated with 20 μ M zVAD for 30 min, and then stimulated with 100 ng/mL TNF for 4 h to elicit necroptosis. Loss of membrane potential was measured via PI staining. Error bars represent the standard deviation from N=3 measurements.
- C) A-SMase activity assay measured in relative fluorescent units (RFU). Analysis was performed using L929 cells expressing WT A-SMase, A-SMase deficient L929 cells ($\delta 3$) and A-SMase deficient L929 cells ($\delta 3$) reconstituted with construct A and with construct G, or A-SMase deficient ($\delta 3$) reconstituted with V5-tagged A-SMase. Error bars represent the standard deviation from N=3 measurements.

4.6.1.1 Conclusion

The cleavage site of A-SMase during necroptosis is probably a compound one, but the lack of enzymatic activity in the generated clones makes a definitive statement difficult.

5 Discussion

5.1 The relationship between ADAM17, RIPK3 and necroptosis in DSS-induced colitis

The aim of establishing an *in vivo* model for necroptosis using DSS-induced colitis was motivated by publications implicating necroptosis in intestinal inflammation in mice (Welz *et al.* 2011, Günther *et al.* 2011) and inflammatory bowel disease in children (Pierdomenico *et al.* 2013). Accordingly, some groups have tried a similar approach to the one we describe in the present work to investigate the role of necroptosis in bowel inflammation, namely the usage of RIPK3^{-/-} mice.

In one work (Moriwaki *et al.* 2014), the knock-out of RIPK3 increased DSS-induced colitis damage. They suggested that the damage was independent of the necroptotic functions of RIPK3. The impairment of non-necroptotic functions of RIPK3 important for subsequent tissue repair (namely activating IL-23, IL-1 β and IL-22) would then lead to the described situation. These non-necroptotic functions of RIPK3 in inflammation have just been recently described (Newton *et al.* 2016a, Moriwaki *et al.* 2017), and enhance the difficulty of analysing the obtained results. In contrast, the other work (Newton *et al.* 2016b) found no significant differences between RIPK3^{-/-} and WT mice under DSS-induced colitis. Differences in the exact treatment and microbiota of the mice have been posited as possible reasons for the disparity of results (Newton *et al.* 2016b, Moriwaki *et al.* 2016).

All that being said, our own study was performed with ADAM17^{ex/ex} and ADAM17^{ex/ex}/RIPK3^{-/-} mice as opposed to WT and RIPK3^{-/-} mice. As can be seen in this thesis, lack of ADAM17 impairs necroptotic signalling, an unexpected result that adds another layer of complexity to the data analysis. The drastic phenotype of ADAM17^{ex/ex} mice under DSS-induced colitis makes it unclear whether non-necroptotic functions of RIPK3 are playing a role. Our results, however, align with the study of Newton *et al.*, with no difference seen between ADAM17^{ex/ex} and ADAM17^{ex/ex}/RIPK3^{-/-} mice.

Necroptosis seems to be consequence rather than a cause in DSS-induced colitis, since both, ADAM17^{ex/ex}, and ADAM17^{ex/ex}/RIPK3^{-/-} mice suffered from colitis despite lacking the ability to perform necroptosis. Moreover, the consistent cleaved caspase 3 signal present in our experiments seems to point to apoptosis as a more probable cause for the observed tissue damage. In addition, our data shows that the necroptotic impairment of the ADAM17^{ex/ex} genotype is not limited to the colon, since similar results were obtained after examination of liver tissue; nor limited to DSS-induced colitis, since MEF isolated from ADAM17^{ex/ex} mice are indeed protected from necroptosis.

This last result aligns to a certain extent with the work of Cai *et al.* 2016, in which ADAM9, 10 and 17 were studied and implicated in necroptosis. The authors see an early activation of ADAMs downstream of MLKL promoting the shedding of various surface proteins. Notably the effects are readily apparent in adherent cells, but not in suspension cells, pointing to the shedding being effected on adherence proteins. Compared to our results, the clearest difference arises in the positioning of ADAM17 in a possible pathway, with our work pointing to a role upstream of RIPK3 and MLKL activation, whereas the work of Cai and colleagues place it downstream of MLKL. Further studies will have to elucidate the matter.

Another question that arises is the mechanism by which ADAM17 participates in the necroptotic pathway. TNF is synthesized as a membrane protein that can be activated via proteolytical cleavage (Kriegler *et al.* 1988), which was shown to be done by ADAM17 (Black *et al.* 1997, Moss *et al.* 1997, Müllberg *et al.* 2000). Whether this is the mechanism by which ADAM17 influences the necroptotic pathway remains to be seen, although our data suggests that this is not the case, since externally added TNF still failed to induce necroptosis in ADAM17^{ex/ex} MEF.

In any case, the relationship between ADAM17 and necroptosis seems to be a promising future target of study.

5.2 The role of PGAM5 in necroptosis

PGAM5 has been described as being at the convergence point for necroptotic signaling (Wang *et al.* 2012). In Immunoprecipitation experiments using HeLa cells overexpressing Flag-tagged RIPK3, the group found associated bands under necroptotic conditions corresponding to RIPK1, MLKL and the upper band of PGAM5. PGAM5 had been previously shown to be associated with the mitochondrial membrane (Lo and Hannink 2008). In further experiments with two different siRNAs against PGAM5, HeLa cells showed some resistance to necroptotic cell death (between 60 and 70% cell death instead of 90%). HT-29 cells stably expressing shRNA against PGAM5 showed even more resistance against necroptotic cell death (between 50 and 60% cell death instead of 90%).

In contrast to the results obtained by Wang and colleagues, Moriwaki, Farias Luz *et al.* (2016) found no protection against necroptosis in their setting. They generated PGAM5^{-/-} mice, from which they generated PGAM5^{-/-} MEF. They then tested the response to various cell death inducers including TNF, zVAD and BV6 (a Smac mimetic) finding no difference compared to WT MEF. They also generated RIPK1^{-/-}, RIPK3^{-/-} and PGAM5^{-/-} bone marrow-derived macrophages (BMDMs) and compared them to each other under LPS and zVAD-induced necroptosis, finding that the RIPK1^{-/-} and RIPK3^{-/-} BMDMs were protected against cell death, while the PGAM5^{-/-} BMDMs were not.

Wang and colleagues follow the lead of Lo and Hannink (2006) and describe a long and short form of PGAM5 (PGAM5L and PGAM5S respectively). These forms are only present in humans, while mouse cells only show the short form. Regardless, both forms show a double band. Using necrosulfonamide (NSA), Wang *et al.* showed necroptosis could be blocked in HeLa cells, specifically downstream of RIPK3 phosphorylation. This also blocked the interaction of PGAM5S with the rest of the complex (RIPK1/RIPK3/MLKL/PGAM5S) in immunoprecipitation experiments done in HeLa cells, which lead Wang and colleagues to conclude that PGAM5S is the downstream effector of the complex, and the next step in the necroptotic pathway. In contrast, Tait and colleagues (2013), testing the necroptotic route downstream of RIPK3, showed that mitochondria, and thus PGAM5 (in line with its mitochondrial localization), are not required for the induction of cell death.

Our results align with the results from Moriwaki, Farias Luz and colleagues, as well as the observations from Tait and colleagues. As seen in Results, neither siRNA knock-down of PGAM5 in HT-29 cells, nor CRISPR/Cas knock-out of PGAM5 in L929 cells provided any significant protection against necroptosis.

5.3 The role of HtrA2/Omi in necroptosis

The dramatic protection of HtrA2/Omi^{-/-} MEF and L929 cells, and the partial reconstitution of a necroptosis-susceptible phenotype under re-transfection, point to a clear function of HtrA2/Omi in necroptosis in murine cells, comparable to the importance of RIPK3 and/or MLKL phosphorylation. Despite the dismissal of the importance of mitochondria in some of the literature (Tait *et al.* 2013), it must be pointed out that the authors themselves insist that this holds true downstream of RIPK3. Since RIPK3 phosphorylation is abrogated in HtrA2/Omi^{-/-} MEF and L929 cells, it seems that HtrA2/Omi and thus mitochondria, do play a role upstream of RIPK3.

The concrete point of action in which HtrA2/Omi acts is still unclear, but I would put forward the following options:

Option 1: HtrA2/Omi cleaves RIPK1, releasing the RHIM homotypic domain, thus promoting the union with the RHIM domain of RIPK3. In favor of this hypothesis is a publication showing RIPK1 to be cleaved by HtrA2/Omi in caspase-independent death of Ba/F3 cells (Vande Walle *et al.* 2010), resulting in a 25 kDa band that is unable to induce NF- κ B activation and instead permits cell death. Thus, HtrA2/Omi function is necessary for Ba/F3 cells to activate caspase-independent cell death induced by IL-3 withdrawal, the suppression of HtrA2/Omi or its protease activity acting in a protective manner.

Although the work of Vande Walle *et al.* shows in principle that RIPK1 can be cleaved by HtrA2/Omi, the case is very specific, with cells that enter into caspase-independent cell death through removal of growth factors and are thus not regulated by the TNF-R1. A preliminary attempt to replicate this result in our necroptotic system (MEF and L929 cells) showed no such cleavage, but this may be due to the time points selected (data not shown). Another difficulty that may be important down the line is that Vande Walle and colleagues observed the cleavage of RIPK1 by HtrA2/Omi only in mouse cells: unlike mouse, human RIPK1 was not

cleaved by recombinant HtrA2/Omi *in vitro*, suggesting that this cleavage might be species-specific.

Option 2: HtrA2/Omi inactivates cIAP1/2, abrogating the ubiquitination of RIPK1 and thus pushing the system into cell death. The capacity of HtrA2/Omi to bind and inactivate IAPs is well known (van Loo *et al.* 2002, Suzuki *et al.* 2001, Yang *et al.* 2003 and others). The question remains whether this holds true in this case and how exactly the death signal is relayed into mitochondria, with two possibilities:

- Very early, and by an unknown relay mechanism, HtrA2/Omi is alerted of an incoming death signal and inactivates cIAP1/2. This mode of action, however, would not distinguish between apoptosis and necroptosis, and would entail that HtrA2/Omi^{-/-} cells would be resistant to apoptosis. Apoptotic resistance has been shown in siRNA downregulation of HtrA2/Omi (Martins *et al.* 2002), but to my knowledge, studies with genetically deleted HtrA2/Omi have not been done.
- A small amount of necrosome docking on mitochondria alerts HtrA2/Omi of the incoming death signal, promoting the inactivation of cIAP1/2 in a positive feedback loop.

Option 3: HtrA2/Omi activates LUBAC and/or A20, promoting the deubiquitination of RIPK1 and thus pushing the system into cell death. The importance of LUBAC and A20 in the deubiquitination of RIPK1 is well established (see Fuchslocher Chico *et al.* 2017 for an overview). Like in option 2, it is unclear how the death signal would relay into mitochondria, with two possibilities:

- Very early, and by an unknown relay mechanism, HtrA2/Omi is alerted of an incoming death signal and activates LUBAC and/or A20. As in option 2, this mode of action would act equally in apoptosis and necroptosis.
- HtrA2/Omi is reached by a small amount of necrosome arriving to the mitochondria, relaying the incoming death signal and promoting the activation of LUBAC and/or A20 in a positive feedback loop.

Option 4: HtrA2/Omi activates a yet unknown protein that is able to influence RIPK3 phosphorylation in a positive feedback loop.

Of all these options, and independently of the actual target of HtrA2/Omi, a positive feedback loop seems to be the most probable of the afore-mentioned possibilities (see figure 30). It would be specific to necroptosis and make use of oligomerized pMLKL's affinity to cardiolipin containing membranes e.g. the mitochondrial membrane (Wang *et al.* 2014a, Dondelinger *et al.* 2014), and thus explain how the necrosome initially reaches the mitochondria. The necrosome however, would act only as a signal transducer and not destroy the mitochondria, since observation of the mitochondrial transmembrane potential ($\Delta\Psi_m$) show no loss until after the permeabilization of the plasma membrane (Tait *et al.* 2013). That being said, while a positive feedback loop is able to quickly amplify incoming signals, it may still be overridden by persisting death signaling. This would also explain the very late appearance of pMLKL and cellular demise in HtrA2/Omi^{-/-} cells (see Results).

However well established the importance of HtrA2/Omi is in mouse cells, the results are more modest in human cells. It is unclear why the removal of HtrA2/Omi with CRISPR/Cas showed such varied results. Two possibilities arise:

- There is an inherent difficulty in transfecting HT-29 cells with CRISPR/Cas in our experimental setting, augmenting the chance of off-target effects, thus masking real effects.
- HtrA2/Omi is not equally important for necroptosis in human cells and thus the varied results are due to off-target effects.

Finding out which of the possibilities is true will prove vital to the possible therapeutic value of HtrA2/Omi in a clinical setting. A refinement of the current CRISPR/Cas technology seems to be the key point, since as of now off-target and contradicting (Woo Cho *et al.* 2014 & Zhang *et al.* 2015) effects seem to mask at least some results.

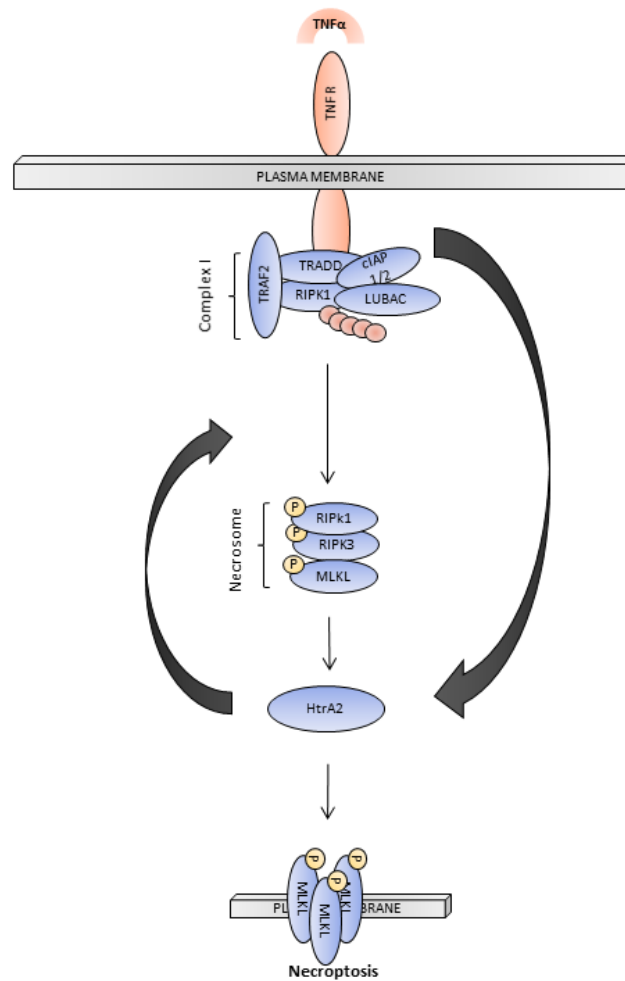


Figure 29

Actualized mode of action of HtrA2/Omi in the necroptotic pathway. The death signal is relayed to mitochondria via unknown mechanisms. HtrA2/Omi is then able to enhance phosphorylation of RIPK3 via unknown mechanisms in a positive feedback loop in which pMLKL is also able to target mitochondria and thus HtrA2/Omi, further enhancing its signalling.

5.4 Identification of the cleavage site of acid sphingomyelinase in necroptosis

We were able to define a region of 30 amino acids within the N-terminus of A-SMase that must contain at least two independent cleavage sites. The regulation of this cleavage seems to be rather complex, or tightly dependent on the three-dimensional structure of A-SMase, given that the results of this thesis show that any modification in and around the suspected site abrogates the activity of A-SMase. In the future, our group will study the effect of mutants containing stretches of randomized amino acids, rather than deletions, in the cleavage region on the activity of A-SMase.

Bioinformatic analysis of the 3-dimensional structure of A-SMase might also help in answering both the question of the cleavage site and give an approximate idea of the protease involved. This will help pin-pointing the role of A-SMase in the necroptotic pathway, and thus open new possibilities in the treatment of conditions in which it plays a role.

6 Citations

Aaes T.L, Kaczmarek A, Delvaeye T, De Craene B, De Koker S, Heyndrickx L, Delrue I, Taminau J, Wiernicki B, De Groote P, Garg A.D, Leybaert L, Grooten J, Bertrand M.J, Agostinis P, Berx G, Declercq W, Vandenabeele P, Krysko D.V (2016) Vaccination with necroptotic cancer cells induces efficient anti-tumor immunity. *Cell Rep.* 15, 274–287.

Afonso M.B, Rodrigues P.M, Carvalho T, Caridade M, Borralho P, Cortez-Pinto H, Castro R.E, Rodrigues C.M (2015) Necroptosis is a key pathogenic event in human and experimental murine models of non-alcoholic steatohepatitis. *Clin. Sci. (Lond.)* 129, 721–739.

Aggarwal B.B (2003) Signaling pathways of the TNF superfamily: a double-edged sword. *Nat Rev. Immunol.* 2, 745-756.

Aggarwal B.B and Natarajan K (1996) Tumor necrosis factors: Developments during the last decade. *Eur. Cytokine Netw.* 7, 93-124.

Andrabi S.A, Dawson T.M, Dawson V.L (2008) Mitochondrial and nuclear cross talk in cell death: parthanatos. *Ann. NY Acad. Sci.* 1147, 233–241.

Andújar I, Ríos J.L, Giner R.M, Miguel Cerdá J, Recio Mdel (2012) Beneficial effect of shikonin on experimental colitis induced by dextran sulfate sodium in BALB/C mice. *Evid. Based Complement Alternat. Med.*, 271606.

Baines C.P, Kaiser R.A, Purcell N.H, Blair N.S, Osinska H, Hambleton M.A, Brunskill E.W, Sayen M.R, Gottlieb R.A, Dorn G.W, Robbins J, Molkentin J.D (2005) Loss of cyclophilin D reveals a critical role for mitochondrial permeability transition in cell death. *Nature* 434, 658–662.

Bittner S, Knoll G, Ehrenschwender M (2017) Death receptor 3 mediates necroptotic cell death. *Cell. Mol. Life Sci.* 74, 543–554.

Black R.A, Rauch C.T, Kozlosky C.J, Peschon J.J, Slack J.L, Wolfson M.F, Castner B.J, Stocking K.L, Reddy P, Srinivasan S, Nelson N, Boiani N, Schooley K.A, Gerhart M, Davis R, Fitzner J.N,

Johnson R.S, Paxton R.J, March C.J, Cerretti D.P (1997) A metalloproteinase disintegrin that releases tumour-necrosis factor-alpha from cells. *Nature* 385, 729-733.

Blink E, Maiani N.A, Alnemri E.S, Zervos A.S, Roos D, Kuijpers T.W (2004) Intramitochondrial serine protease activity of Omi/HtrA2 is required for caspase-independent cell death of human neutrophils. *Cell Death Differ.* 11, 937–939.

Bonnet M.C, Preukschat D, Welz P.S, van Loo G, Ermolaeva M.A, Bloch W, Haase I, Pasparakis M (2011) The adaptor protein FADD protects epidermal keratinocytes from necroptosis in vivo and prevents skin inflammation. *Immunity* 35, 572–582.

Brinkmann V, Reichard U, Goosmann C, Fauler B, Uhlemann Y, Weiss D.S, Weinrauch Y, Zychlinsky A (2004) Neutrophil extracellular traps kill bacteria. *Science* 303, 1532–1535.

Cai Z, Zhang A, Choksi S, Li W, Li T, Zhang X.M, Liu Z.G (2016) Activation of cell-surface proteases promotes necroptosis, inflammation and cell migration. *Cell Res.* 26, 886-900.

Carter M.J, Lobo A.J, Travis S.P, British Society of Gastroenterology IBD Section (2004) Guidelines for the management of inflammatory bowel disease in adults. *Gut* 53, Suppl 5: V1-16.

Chalaris A, Adam N, Sina C, Rosenstiel P, Lehmann-Koch J, Schirmacher P, Hartmann D, Cichy J, Gavrilova O, Schreiber S, Jostock T, Matthews V, Häslér R, Becker C, Neurath M.F, Reiss K, Saftig P, Scheller J, Rose-John S (2010) Critical role of the disintegrin metalloproteinase ADAM17 for intestinal inflammation and regeneration in mice. *J. Exp. Med.* 207, 1617-1624.

Charruyer A, Grazide S, Bezombes C, Muller S, Laurent G, Jaffrezou J.P (2005) UV-C Light Induces Raft-associated Acid Sphingomyelinase and JNK Activation and Translocation Independently on a Nuclear Signal. *J. Biol. Chem.* 280, 19196-19204.

Ch'en I.L, Beisner D.R, Degterev A, Lynch C, Yuan J, Hoffmann A, Hedrick S.M (2008) Antigen-mediated T cell expansion regulated by parallel pathways of death. *Proc. Natl. Acad. Sci. U. S. A.* 105, 17463–17468.

Chen W, Zhou Z, Li L, Zhong C.Q, Zheng X, Wu X, Zhang Y, Ma H, Huang D, Li W, Xia Z, Han J (2013) Diverse sequence determinants control human and mouse receptor interacting protein

3 (RIPK3) and mixed lineage kinase domain-like (MLKL) interaction in necroptotic signalling. *J. Biol. Chem.* 288, 16247–16261.

Cho, Y.S, Challa S, Moquin D, Genga R, Ray T.D, Guilford M, Chan F.K (2009) Phosphorylation-driven assembly of the RIPK1– RIPK3 complex regulates programmed necrosis and virus-induced inflammation. *Cell* 137, 1112–1123.

Cookson B.T, Brennan M.A (2001) Pro-inflammatory programmed cell death. *Trends Microbiol.* 9, 113–114.

da Veiga Pereira L, Desnick R.J, Adler D.A, Disteché C.M, Schuchman E.H (1991) Regional assignment of the human acid sphingomyelinase gene (SMPD1) by PCR analysis of somatic cell hybrids and in situ hybridization to 11p15.1---p15.4. *Genomics* 9, 229-234.

Dai X, Zhang J, Arfuso F, Chinnathambi A, Zayed M.E, Alharbi S.A, Kumar A.P, Ahn K.S, Sethi G (2015) Targeting TNF-related apoptosis-inducing ligand (TRAIL) receptor by natural products as a potential therapeutic approach for cancer therapy. *Exp. Biol. Med. (Maywood)* 240, 760–773.

Degterev A, Hitomi J, Gernscheid M, Ch'en I.L, Korkina O, Teng X, Abbott D, Cuny G.D, Yuan C, Wagner G (2008) Identification of RIPK1 kinase as a specific cellular target of necrostatins. *Nat. Chem. Biol.* 4, 313-321.

Degterev A, Huang Z, Boyce M, Li Y, Jagtap P, Mizushima N, Cuny G.D, Mitchison T.J, Moskowitz M.A, Yuan J (2005) Chemical inhibitor of nonapoptotic cell death with therapeutic potential for ischemic brain injury. *Nat. Chem. Biol.* 1, 112–119.

Deutsch M, Graffeo C.S, Rokosh R, Pansari M, Ochi A, Levie E.M, Van Heerden E, Tippens D.M, Greco S, Barilla R, Tomkötter L, Zambirinis C.P, Avanzi N, Gulati R, Pachter H.L, Torres-Hernandez A, Eisenthal A, Daley D, Miller G (2015) Divergent effects of RIPK1 or RIPK3 blockade in murine models of acute liver injury. *Cell Death Dis.* 6, e1759.

Dharmani P, Leung P, Chadee K (2011) Tumor necrosis factor- α and Muc2 mucin play major roles in disease onset and progression in dextran sodium sulphate-induced colitis. *PLoS One* 6, e25058.

Dixon S.J, Lemberg K.M, Lamprecht M.R, Skouta R, Zaitsev E.M, Gleason C.E, Patel D.N, Bauer A.J, Cantley A.M, Yang W.S, Morrison B 3rd, Stockwell B.R (2012) Ferroptosis: an iron-dependent form of nonapoptotic cell death. *Cell* 149, 1060–1072.

Dondelinger Y, Declercq W, Montessuit S, Roelandt R, Goncalves A, Bruggeman I, Hulpiau P, Weber K, Sehon C.A, Marquis R.W, Bertin J, Gough P.J, Savvides S, Martinou J.C, Bertrand M.J, Vandenabeele P (2014) MLKL compromises plasma membrane integrity by binding to phosphatidylinositol phosphates. *Cell Rep.* 7, 971–981.

Dondelinger Y, Hulpiau P, Saeys Y, Bertrand M.J, Vandenabeele (2016) An evolutionary perspective on the necroptotic pathway. *Trends Cell Biol.* 26, 721–732.

Dong F, Zhang L, Hao F, Tang H, Wang Y (2013) Systemic responses of mice to dextran sulfate sodium-induced acute ulcerative colitis using ^1H NMR spectroscopy. *J. Proteome. Res.* 12, 2958-2966.

Du C, Fang M, Li Y, Li L, Wang X (2000) Smac, a mitochondrial protein that promotes cytochrome c-dependent caspase activation by eliminating IAP inhibition. *Cell* 102, 33–42.

Dumitru CA, Carpinteiro A, Trarbach T, Hengge UR, Gulbins E (2007) Doxorubicin enhances TRAIL-induced cell death via ceramide-enriched membrane platforms. *Apoptosis* 12, 1533–1541.

Düsterhöft S, Höbel K, Oldenfest M, Lokau J, Waetzig G.H, Chalaris A, Garbers C, Scheller J, Rose-John S, Lorenzen I, Grötzinger J (2014) A disintegrin and metalloproteinase 17 dynamic interaction sequence, the sweet tooth for the human interleukin 6 receptor. *J. Biol. Chem.* 289, 16336-16348.

Düsterhöft S, Jung S, Hung C.W, Tholey A, Sonnichsen F.D, Grötzinger J, Lorenzen I (2013) Membrane-proximal domain of a disintegrin and metalloproteinase-17 represents the

putative molecular switch of its shedding activity operated by protein-disulfide isomerase. *J. Am. Chem. Soc.* 135, 5776-5781.

Edelmann B, Bertsch U, Tchikov V, Winoto-Morbach S, Perrotta C, Jakob M, Adam-Klages S, Kabelitz D, Schütze S (2011) Caspase-8 and caspase-7 sequentially mediate proteolytic activation of acid sphingomyelinase in TNF-R1 receptosomes. *EMBO J.* 30, 379-394.

Fan H, Zhang K, Shan L, Kuang F, Chen K, Zhu K, Ma H, Ju G, Wang Y.Z (2016) Reactive astrocytes undergo M1 microglia/macrophages-induced necroptosis in spinal cord injury. *Mol. Neurodegener.* 11, 14.

Fong K.P, Barry C, Tran A.N, Traxler E.A, Wannemacher K.M, Tang H.Y, Speicher K.D, Blair I.A, Speicher D.W, Grosser T, Brass L.F (2011) Deciphering the human platelet sheddome. *Blood* 117, e15-e26.

Fuchs Y, Steller H (2015) Live to die another way: modes of programmed cell death and the signals emanating from dying cells. *Nat. Rev. Mol. Cell Biol.* 16 329–344.

Fuchslöcher Chico J, Saggau C, Adam D (2017) Proteolytic control of regulated necrosis. *Biochim Biophys Acta* 1864, 2147-2161.

Galluzzi L, Bravo-San Pedro J.M, Vitale I, Aaronson S.A, Abrams J, Adam D, Alnemri E.S, Altucci L, Andrews D, Annicchiarico-Petruzzelli M, Baehrecke E.H, Bazan N.G, Bertrand M.J, Bianchi K, Blagosklonny M.V, Blomgren K, Borner C, Bredesen D, Brenner C, Campanella M, Candi E, Cecconi F, Chan F.K, Chandel N.S, Cheng E.H, Chipuk J.E, Cidlowski J.A, Ciechanover A, Dawson T.M, Dawson V.L, De Laurenzi V, De Maria R, Debatin K.M, Di Daniele N, Dixit V, Dynlacht B.D, El-Deiry W.S, Fimia G.M, Flavell R.A, Fulda S, Garrido C, Gougeon M.L, Green D.R, Gronemeyer H, Hajnoczky G, Hardwick J.M, Hengartner M.O, Ichijo H, Joseph B, Jost P.J, Kaufmann T, Kepp O, Klionsky D.J, Knight R.A, Kumar S, Lemasters J.J, Levine B, Linkermann A, Lipton S.A, Lockshin R, Lopéz-Otín C, Lugli E, Madeo F, Malorni W, Marine J.-C, Martin S, Martinou J.C, Medema J.P, Meier P, Melino S, Mizushima N, Moll U, Muñoz-Pinedo C, Nuñez G, Oberst A, Panaretakis T, Penninger J.M, Peter M.E, Piacentini M, Pinton P, Prehn J.H, Puthalakath H, Rabinovitch G.A, Ravichandran K.S, Rizzuto R, Rodrigues C.M, Rubinstein M, Rudel T, Shi Y, Simon H.U, Stockwell B.R, Szabadkai G, Tait S, Tang H.L,

Tavernarakis N, Tsujimoto Y, Vanden Berghe T, Vandenabeele P, Villunger A, Wagner E.F, Walczak H, White E, Wood G, Yuan J, Zakeri Z, Zhivotovsky B, Melino G, Kroemer G (2015) Essential versus accessory aspects of cell death: recommendations of the NCCD 2015. *Cell Death Differ.* 22, 58–73.

Galluzzi L, Kepp O, Trojel-Hansen C, Kroemer G (2012) Mitochondrial control of cellular life, stress, and death. *Circ. Res.* 111, 1198-1207.

Gaudio E, Taddei G, Vetuschi A, Sferra R, Frieri G, Ricciardi G, Caprilli R (1999) Dextran sulfate sodium (DSS) colitis in rats: clinical structural, and ultrastructural aspects. *Dig Dis Sci* 44, 1458-1475.

Gautheron J, Vucur M, Reisinger F, Cardenas D.V, Roderburg C, Koppe C, Kreggenwinkel K, Schneider A.T, Bartneck M, Neumann U.P, Canbay A, Reeves H.L, Luedde M, Tacke F, Trautwein C, Heikenwalder M, Luedde T (2014) A positive feedback loop between RIPK3 and JNK controls non-alcoholic steatohepatitis. *EMBO Mol. Med.* 6, 1062–1074.

Goldmacher V.S (2002) vMIA a viral inhibitor of apoptosis targeting mitochondria. *Biochimie* 84, 177-185

González-Juarbe N, Gilley R.P, Hinojosa C.A, Bradley K.M, Kamei A, Gao G, Dube P.H, Bergman M.A, Orihuela C.J (2015) Pore-forming toxins induce macrophage necroptosis during acute bacterial pneumonia. *PLoS Pathog.* 11, e1005337.

Gulbins E, Palmada M, Reichel M, Lüth A, Böhmer C, Amato D, Müller C.P, Tischbirek C.H, Groemer T.W, Tatabai G, Becker K.A, Tripal P, Staedtler S, Ackermann T.F, van Brederode J, Alzheimer C, Weller M, Lang U.E, Kleuser B, Grassmé H, Kornhuber J (2013) Acid sphingomyelinase-ceramide system mediates effects of antidepressant drugs. *Nat. Med.* 19(7), 934–938.

Günther C, Martini E, Wittkopf N, Amann K, Weigmann B, Neumann H, Waldner M.J, Hedrick S.M, Tenzer S, Neurath M.F, Becker C (2011) Caspase-8 regulates TNF-alpha-induced epithelial necroptosis and terminal ileitis. *Nature* 477, 335–339.

Hartkamp J, Carpenter B, Roberts S.G.E (2010) The Wilms' Tumor Suppressor Protein WT1 Is Processed by the Serine Protease HtrA2/Omi. *Mol. Cell* 37(2), 159-171.

He L, Peng K, Liu Y, Xiong J, Zhu F.F (2013) Low expression of mixed lineage kinase domain-like protein is associated with poor prognosis in ovarian cancer patients. *Onco. Targets Ther.* 6, 1539–1543.

He S, Liang Y, Shao F, Wang X (2011) Toll-like receptors activate programmed necrosis in macrophages through a receptor-interacting kinase-3-mediated pathway. *Proc. Natl. Acad. Sci. U.S.A.* 108, 20054–20059.

He S, Wang L, Miao L, Wang T, Du F, Zhao L, Wang X (2009) Receptor interacting protein kinase-3 determines cellular necrotic response to TNF-alpha. *Cell* 137, 1100–1111.

Holler N, Zaru R, Micheau O, Thomé M, Attinger A, Valitutti S, Bodmer J.L, Schneider P, Seed B, Tschopp J (2000) Fas triggers an alternative, caspase-8-independent cell death pathway using the kinase RIP as effector molecule. *Nat. Immunol.* 1, 489–495.

Huang Z, Wu S.Q, Liang Y, Zhou X, Chen W, Li L, Wu J, Zhuang Q, Chen C, Li J, Zhong C.Q, Xia W, Zhou R, Zheng C, Han J (2015) RIPK1/RIPK3 binding to HSV-1 ICP6 initiates necroptosis to restrict virus propagation in mice. *Cell Host Microbe* 17, 229–242.

Hurwitz R, Ferlinz K, Vielhaber G, Moczall H, Sandhoff K (1994) Processing of human acid sphingomyelinase in normal and I-cell fibroblasts. *J. Biol. Chem.* 269, 5440-5445.

Irun P, Mallén M, Dominguez C, Rodriguez-Sureda V, Alvarez-Sala LA, Arslan N, Bermejo N, Guerrero C, Perez de Soto I, Villalón L, Giraldo P, Pocovi M (2013) Identification of seven novel SMPD1 mutations causing Niemann–Pick disease types A and B. *Clin. Genet.* 84(4):356–61.

Jurjus A.R, Khoury N.N, Reimund J.M (2004) Animal models of inflammatory bowel disease. *J. Pharm. Tox. Methods* 50, 81-92.

Kaiser W.J, Upton J.W, Long A.B, Livingston-Rosanoff D, Daley-Bauer L.P, Hakem R, Caspary T, Mocarski E.S (2011) RIPK3 mediates the embryonic lethality of caspase-8-deficient mice. *Nature* 471, 368–372.

-
- Kanfer, J.N, Young, O.M, Shapiro D, Brady R.O** (1966) The metabolism of sphingomyelin I. Purification and properties of a sphingomyelin-cleaving enzyme from rat liver tissue. *J. Biol. Chem.* 241, 1081-1084.
- Kawahara R, Lima R.N, Domingues R.R, Pauletti B.A, Meirelles G.V, Assis M, Figueira A.C, Paes Leme A.F** (2014) Deciphering the role of ADAM17-dependent secretome in cell signalling. *J. Proteome Res.* 13, 2080-2093.
- Kelliher M.A, Grimm S, Ishida Y, Kuo F, Stanger B.Z, Leder P** (1998) The death domain kinase RIP mediates the TNF-induced NF- κ B signal. *Immunity* 8, 873-882.
- Kerr J.F, Wyllie A.H, Currie A.R** (1972) Apoptosis: a basic biological phenomenon with wide-ranging implications in tissue kinetics. *Br. J. Cancer* 26, 239–257.
- King M.D, Whitaker-Lea W.A, Campbell J.M, Alleyne Jr C.H, Dhandapani K.M** (2014) Necrostatin-1 reduces neurovascular injury after intracerebral haemorrhage. *Int. J. Cell Biol.* 2014, 495817.
- Kriegler M, Perez C, DeFay K, Albert I, Lu S.D** (1988) A novel form of TNF/cachectin is a cell surface cytotoxic transmembrane protein: ramifications for the complex physiology of TNF. *Cell* 53, 45-53.
- Laemmli U.K** (1970) Cleavage of structural proteins during the assembly of the head of bacteriophageT4. *Nature* 227, 680-685.
- Lansmann S, Schuette C.G, Bartelsen O, Hoernschemeyer J, Linke T, Weisgerber J, Sandhoff K** (2003) Human acid sphingomyelinase. *Eur. J. Biochem.* 270, 1076-1088.
- Leist M, Jäättelä M** (2001) Four deaths and a funeral: from caspases to alternative mechanisms. *Nat. Rev. Mol. Cell Biol.* 2, 589-598.
- Levrán O, Desnick RJ, Schuchman EH** (1991). A frequent missense mutation in the acid sphingomyelinase gene of Ashkenazi Jewish type A and B patients. *Proc. Natl. Acad. Sci. U.S.A* 88(9), 3748–3752.
-

-
- Li X, Gulbins E, Zhang Y** (2012) Oxidative stress triggers Ca-dependent lysosome trafficking and activation of acid sphingomyelinase. *Cell Physiol. Biochem.* 30(4), 815–826.
- Lin J, Li H, Yang M, Ren J, Huang Z, Han F, Huang J, Ma J, Zhang D, Zhang Z, Wu J, Huang D, Qiao M, Jin G, Wu Q, Huang Y, Du J, Han J** (2013) A role of RIPK3-mediated macrophage necrosis in atherosclerosis development. *Cell Rep.* 3, 200–210.
- Lin Y, Devin A, Rodriguez Y, Liu Z.G** (1999) Cleavage of the death domain kinase RIP by caspase-8 prompts TNF-induced apoptosis. *Genes Dev.* 13, 2514-2526.
- Linkermann A, Bräsen J.H, Darding M, Jin M.K, Sanz A.B, Heller J.O, De Zen F, Weinlich R, Ortiz A, Walczak H, Weinberg J.M, Green D.R, Kundendorf U, Krautwald S** (2013) Two independent pathways of regulated necrosis mediate ischemia- reperfusion injury. *Proc. Natl. Acad. Sci. U. S. A.* 110, 12024–12029.
- Linkermann A, Bräsen J.H, De Zen F, Weinlich R, Schwendener R.A, Green D.R, Kundendorf U, Krautwald S** (2012) Dichotomy between RIPK1- and RIPK3-mediated necroptosis in tumor necrosis factor-alpha-induced shock. *Mol. Med.* 18, 577–586.
- Lo S.C and Hannink M** (2006) PGAM5, a Bcl-XL-interacting protein, is a novel substrate for the redox-regulated Keap1-dependent ubiquitin ligase complex. *J. Biol. Chem.* 281 (49), 37893-37903.
- Lo S.C and Hannink M** (2008) PGAM5 tethers a ternary complex containing Keap1 and Nrf2 to mitochondria. *Exp. Cell. Res.* 314 (8), 1789-1803.
- Luedde M, Lutz M, Carter N, Sosna J, Jacoby C, Vucur M, Gautheron J, Roderburg C, Borg N, Reisinger F, Hippe H.J, Linkermann A, Wolf M.J, Rose-John S, Lüllmann-Rauch R, Adam D, Flögel U, Heikenwalder M, Luedde T, Frey N** (2014) RIPK3, a kinase promoting necroptotic cell death, mediates adverse remodelling after myocardial infarction. *Cardiovasc. Res.* 103, 206–216.
- Mahmood Z, Shukla Y** (2010) Death receptors: Targets for cancer therapy. *Exp. Cell Res.* 316, 887- 899.
-

Manshadi MD, Kamalidehghan B, Keshavarzi F, Aryani O, Dadgar S, Arastehkani A, Tondar M, Ahmadipour F, Meng GY, Houshmand M (2015) Four novel p.N385K, p.V36A, c.1033-1034insT and c.1417-1418delCT mutations in the sphingomyelin phosphodiesterase 1 (SMPD1) gene in patients with types A and B Niemann–Pick disease (NPD). *Int. J. Mol. Sci.* 16(4), 6668–6676.

Martins L.M, Morrison A, Klupsch K, Fedele V, Moiso N, Teisman P, Abuin A, Grau E, Geppert M, Livi G.P, Creasy C.L, Martín A, Gargreaves I, Heales S.J, Okada H, Brandner S, Schulz J.B, Mak T, Downward J (2004) Neuroprotective Role of the Reaper-Related Serine Protease HtrA2/Omi Revealed by Targeted Deletion in Mice. *Mol. Cell Biol.* 24(22), 9848-9862.

Martins L.M, Iaccarino I, Tenev T, Gschmeissner S, Totty NF, Lemoine NR, Svopoulos J, Gray C.W, Creasy C.L, Dingwall C, Downward J (2002) The serine protease Omi/HtrA2 regulates apoptosis by binding XIAP through a reaper-like motif. *J. Biol. Chem.* 277(1), 439-444.

Maskos K, Fernandez-Catalan C, Huber R, Bourenkov G.P, Bartunik H, Ellestad G.A, Reddy P, Wolfson M.F, Rauch C.T, Castner B.J, Davies R, Clarke H.R, Petersen M, Fitzner J.N, Cerretti D.P, March C.J, Paxton R.J, Black R.A, Bode W (1998) Crystal Structure of the catalytic domain of human tumor necrosis factor-alpha-converting enzyme. *Proc. Natl. Acad. Sci. U.S.A.* 96, 3408-3412.

McComb S, Cheung H.H, Korneluk R.G, Wang S, Krishnan L, Sad S (2012) cIAP1 and cIAP2 limit macrophage necroptosis by inhibiting RIPK1 and RIPK3 activation. *Cell Death Differ.* 19, 1791–1801.

Meng L, Jin W, Wang X (2015) RIPK3-mediated necrotic cell death accelerates systematic inflammation and mortality. *Proc. Natl. Acad. Sci. U. S. A.* 112, 11007–11012.

Meyer-Schwesinger C, Meyer T.N, Sievert H, Hocha E, Sachs M, Klupp E.M, Münster S, Balabanov S, Carrier L, Helmchen U, Thaiss F, Stahl R.A (2011) Ubiquitin C-terminal hydrolase-L1 activity induces polyubiquitin accumulation in podocytes and increases proteinuria in rat membranous nephropathy. *Am. J. Pathol.* 178, 2044-2057.

Micheau O, Tschopp J (2003) Induction of TNF receptor I-mediated apoptosis via two sequential signaling complexes. *Cell* 114, 181-190.

Michel V, Yuan Z, Ramsubir S, Bakovic M (2006) Choline transport for phospholipid synthesis. *Exp. Biol. Med. (Maywood)* 231, 490-504.

Moquin D.M, McQuade T, Chan F.K (2013) CYLD deubiquitinates RIPK1 in the TNF α -induced necrosome to facilitate kinase activation and programmed necrosis. *PLoS One* 8, e76841.

Moriwaki K, Balaji S, Chan FK (2016) Border security: The role of RIPK3 in epithelium homeostasis. *Front. Cell. Dev. Biol.* 4: 70.

Moriwaki K, Balaji S, McQuade T, Malhotra N, Kang J, Chan F.K (2014) The necroptosis adaptor RIPK3 promotes injury-induced cytokine expression and tissue repair. *Immunity.* 41, 567-78.

Moriwaki K, Chan F.K (2016) Regulation of RIPK3- and RHIM-dependent necroptosis by the proteasome. *J. Biol. Chem.* 291, 5948–5959.

Moriwaki K, Chan F.K (2017) The inflammatory signal adaptor RIPK3: Functions beyond necroptosis. *Int. Rev. Cell. Mol. Biol.* 328, 253-75.

Moriwaki K, Farias Luz N, Balaji S, De Rosa M.J, O'Donnell C.L, Gough P, Bertin J, Welsh R.M, Chan F.K (2016) The Mitochondrial Phosphatase PGAM5 Is Dispensable for Necroptosis but Promotes Inflammasome Activation in Macrophages. *J. Immunol.* 196, 407-415.

Moss M.L, Catherine Jin S.L, Milla M.E, Burkhart W, Luke Carter H, Chen W-J, Clay W.C, Didsbury J.R, Hassler D, Hoffman C.R, Kost T.A, Lambert M.H, Leesnitzer M.A, McCauley P, McGeehan G, Mitchell J, Moyer M, Pahel G, Rocque W, Overton L.K, Schoenen F, Seaton T, Su J-L, Warner J, Willard D, Becherer J.D (1997) Cloning of a disintegrin metalloproteinase that processes precursor tumour-necrosis-factor- α . *Nature* 385, 733-736.

Moujalled D.M, Cook W.D, Murphy J.M, Vaux D.L (2014) Necroptosis induced by RIPK3 requires MLKL but not Drp1. *Cell Death Dis* 5, e:1086.

Müllberg J, Althoff K, Jostock T, Rose-John S (2000) The importance of shedding of membrane proteins for cytokine biology. *Eur. Cytokine Netw.* 11, 27-38.

Murphy J.M, Lucet I.S, Hildebrand J.M, Tanzer M.C, Young S.N, Sharma P, Lessene G, Alexander W.S, Babon J.J, Silke J, Czabotar P.E (2014) Insights into the evolution of divergent nucleotide-binding mechanisms among pseudokinases revealed by crystal structures of human and mouse MLKL. *Biochem. J.* 457, 369–377.

Nagata S, Tanaka M (2017) Programmed cell death and the immune system. *Nat. Rev. Immunol* 17, 333–340.

Newrzella D and Stoffel W (1992) Molecular cloning of the acid sphingomyelinase of the mouse and the organization and complete nucleotide sequence of the gene. *Biol. Chem. Hoppe Seyler* 373, 1233-1238.

Newton K, Sun X, Dixit V.M (2004) Kinase RIP3 is dispensable for normal NF-kappa Bs, signalling by the B-cell and T-cell receptors, tumor necrosis factor receptor 1, and Toll-like receptors 2 and 4. *Mol. Cell Biol.* 24, 1464-1469.

Newton K, Manning G (2016a) Necroptosis and Inflammation. *Annu. Rev. Biochem.* 85, 593-743-63.

Newton K, Dugger D.L, Maltzman A, Greve J.M, Hedehus M, Martin-McNulty B, Carano R.A, Cao T.C, van Bruggen N, Bernstein L, Lee W.P, Wu X, DeVoss J, Zhang J, Jeet S, Peng I, McKenzie B.S, Roose-Girma M, Caplazi P, Diehl L, Webster J.D, Vucic D (2016b) RIPK3 deficiency or catalytically inactive RIPK1 provides greater benefit than MLKL deficiency in mouse models of inflammation and tissue injury. *Cell Death Differ.* 23, 1565-76.

Ni J, Chen S.F, Hollander D (1996) Effects of dextran sulfate sodium on intestinal epithelial cells and intestinal lymphocytes. *Gut* 39, 234-241.

Nomura M, Ueno A, Saga K, Fukuzawa M, Kaneda Y (2014) Accumulation of cytosolic calcium induces necroptotic cell death in human neuroblastoma. *Cancer Res.* 74, 1056–1066.

Oberst A, Dillon C.P, Weinlich R, McCormick L.L, Fitzgerald P, Pop C, Hakem R, Salvesen G.S, Green D.R (2011) Catalytic activity of the caspase-8-FLIP(L) complex inhibits RIPK3-dependent necrosis. *Nature* 471, 363–367.

Ohtani R, Tomimoto H, Kondo T, Wakita H, Akiguchi I, Shibasaki H, Okazaki T (2004) Upregulation of ceramide and its regulating mechanism in a rat model of chronic cerebral ischemia. *Brain Res.* 1023(1), 31–40.

Osborn S.L, Diehl G, Han S.J, Xue L, Kurd N, Hsieh K, Cado D, Robey E.A, Winoto A (2010) Fas-associated death domain (FADD) is a negative regulator of T-cell receptor-mediated necroptosis. *Proc. Natl. Acad. Sci. U. S. A.* 107, 13034–13039.

Pasparakis M and Vandenabeele P (2015) Necroptosis and its role in inflammation. *Nature* 517, 311–320.

Pearson J.S, Giogha C, Mühlen S, Nachbur U, Pham C.L, Zhang Y, Hildebrand J.M, Oates C.V, Lung T.W, Ingle D, Dagley L.F, Bankovacki A, Petrie E.J, Schroeder G.N, Crepin V.F, Frankel G, Masters S.L, Vince J, Murphy J.M, Sunde M, Webb A.I, Silke J, Hartland E.L (2017) EspL is a bacterial cysteine protease effector that cleaves RHIM proteins to block necroptosis and inflammation. *Nat. Microbiol.* 2, 16258.

Peschon J.J, Slack J.L, Reddy P, Stocking K.L, Sunnaborg S.W, Lee D.C, Russel W.E, Castner B.J, Johnson R.S, Fitzner J.N, Boyce R.W, Nelson N, Kozlosky C.J, Wolfson M.F, Rauch C.T, Cerretti D.P, Paxton R.J, March C.J, Black R.A (1998) An essential role for ectodomain shedding in mammalian development. *Science* 282, 1281-1284.

Pierdomenico M, Negroni A, Stronati L, Vitali R, Prete E, Bertin J, Gough P.J, Aloï M, Cucchiara S (2014) Necroptosis is active in children with inflammatory bowel disease and contributes to heighten intestinal inflammation. *Am. J. Gastroenterol.* 109, 279-87.

Poon I.K, Lucas C.D, Rossi A.G, Ravichandran K.S (2014) Apoptotic cell clearance: basic biology and therapeutic potential. *Nat. Rev. Immunol* 14, 166–180.

Qinli Z, Meiqing L, Xia J, Li X, Weili G, Xiuliang J, Junwei J, Hailan Y, Ce Z, Qiao N (2013) Necrostatin-1 inhibits the degeneration of neural cells induced by aluminum exposure. *Restor. Neurol. Neurosci.* 31, 543–555.

Qiu H, Edmunds T, Baker-Malcolm J, Karey K.P, Estes S, Schwarz C, Hughes H, Van Patten S.M (2003) Activation of human acid sphingomyelinase through modification or deletion of C-terminal cysteine. *J. Biol. Chem.* 278, 32744-32752.

Randhawa P.K, Singh K, Singh N, Jaggi A.S (2014) A review on chemical-induced inflammatory bowel disease models in rodents. *J. Physiol. Pharmacol.* Vol 18, 279-288.

Rodriguez D.A, Weinlich R, Brown S, Guy C, Fitzgerald, Dillon C.P, Oberst A, Quarato G, Low J, Cripps J.G, Chen T, Green D.R (2016) Characterization of RIPK3-mediated phosphorylation of the activation loop of MLKL during necroptosis. *Cell Death Differ.* 23, 76–88.

Rosenbaum D.M, Degterev A, David J, Rosenbaum P.S, Roth S, Grotta J.C, Cuny G.D, Yuan J, Savitz S.I (2010) Necroptosis, a novel form of caspase-independent cell death, contributes to neuronal damage in a retinal ischemia-reperfusion injury model. *J. Neurosci. Res.* 88, 1569–1576.

Roychowdhury S, McMullen M.R, Pisano S.G, Liu X, Nagy L.E (2013) Absence of receptor interacting protein kinase 3 prevents ethanol-induced liver injury. *Hepatology* 57, 1773–1783.

Sato K, Li S, Gordon W.C, He J, Liou G.I, Hill J.M, Travis G.H, Bazan N.G, Jin M (2013) Receptor interacting protein kinase-mediated necrosis contributes to cone and rod photoreceptor degeneration in the retina lacking interphotoreceptor retinoid-binding protein. *J. Neurosci.* 33, 17458–17468.

Scheiffele P and Fullekrug J (2000) Glycosylation and protein transport. *Essays Biochem.* 36, 27-35.

Scheller J, Chalaris A, Garbers C, Rose-John S (2011) ADAM17: a molecular switch to control inflammation and tissue regeneration. *Trends Immunol.* 32, 380-387.

Schildkopf P, Frey B, Mantel F, Ott O.J, Weiss E.M, Sieber R, Janko C, Sauer R, Fietkau R, Gaipl U.S (2010) Application of hyperthermia in addition to ionizing irradiation fosters necrotic cell

death and HMGB1 release of colorectal tumor cells. *Biochem. Biophys. Res. Commun.* 391, 1014–1020.

Schock S.N, Chandra N.V, Sun Y, Irie T, Kitagawa Y, Gotoh B, Coscoy L, Winoto A (2017) Induction of necroptotic cell death by viral activation of the RIG-I or STING pathway. *Cell Death Differ.* 24, 615–625.

Schuchman E.H, Suchi M, Takahashi T, Sandhoff K, Desnick R.J (1991) Human acid sphingomyelinase. Isolation, nucleotide sequence and expression of the full-length and alternatively spliced cDNAs. *J. Biol. Chem.* 266(13), 8531–8539.

Seifert L, Werba G, Tiwari S, Gao Ly N.N, Alothman S, Alqunaibit D, Avanzi A, Barilla R, Daley D, Greco S.H, Torres-Hernandez A, Pergamo M, Ochi A, Zambirinis C.P, Pansari M, Rendon M, Tippens D, Hundeyin M, Mani V.R, Hajdu C, Engle D, Miller G (2016) The necrosome promotes pancreatic oncogenesis via CXCL1 and Mincle-induced immune suppression. *Nature* 532, 245–249.

Soeda S, Tsuji Y, Ochiai T, Mishima K, Iwasaki K, Fujiwara M, Yokomatsu T, Murano T, Shibuya S, Shimeno H (2004) Inhibition of sphingomyelinase activity helps to prevent neuron death caused by ischemic stress. *Neurochem. Int.* 45(5), 619–626.

Sommer A, Kordowski F, Büch J, Marezky T, Evers A, Andrä J, Düsterhöft S, Michalek M, Lorenzen I, Somasundaram P, Tholey A, Sönnichsen F.D, Kunzelman K, Heinbockel I, Nehls C, Gutsmann T, Grötzinger J, Bhakdi S, Reiss K (2016) Phosphatidylserine exposure is required for ADAM17 sheddase function. *Nat. Commun.* 7, 11523.

Sosna J, Phillipp S, Fuchslocher Chico J, Saggau C, Fritsch J, Föll A, Plenge J, Arenz C, Pinkert T, Kalthoff H, Trauzold A, Schmitz I, Schütze S, Adam D (2016) Differences and similarities in TRAIL- and TNF-mediated necroptotic signalling in cancer cells. *Mol. Cell. Biol.* 36(20), 2626–2644.

Sosna J, Voigt S, Mathieu S, Kabelitz D, Trad A, Janssen O, Meyer-Schwesinger C, Schütze S, Adam D (2013) The proteases HtrA2/Omi and UCH-L1 regulate TNF-induced necroptosis. *Cell Commun. Signal.* 11, 76.

Strilic B, Yang L, Albarrán-Juárez J, Wachsmuth L, Han K, Müller U.C, Pasparakis M, Offermanns S (2016) Tumour-cell-induced endothelial cell necroptosis via death receptor 6 promotes metastasis. *Nature* 536, 215–218.

Sun L and Wang X (2014) A new kind of cell suicide: mechanisms and functions of programmed necrosis. *Trends in Biochemical Sciences* Vol 39, No. 12, 587-593.

Sun L, Wang H, Wang Z, He S, Chen S, Liao D, Wang L, Yan J, Liu W, Lei X, Wang X (2012) Mixed lineage kinase domain-like protein mediates necrosis signalling downstream of RIPK3 kinase. *Cell* 148, 213–227.

Suzuki Y, Imai Y, Nakayama H, Takahashi K, Takio K, Takahashi R (2001) A serine protease, HtrA2, is released from the mitochondria and interacts with XIAP, inducing cell death. *Mol. Cell* 8, 613–621.

Tait S.W.G, Oberst A, Quarato G, Milasta S, Haller M, Wang R, Karvela M, Ichim G, Yatim N, Albert M.L, Kidd G, Wakefield R, Frase S, Krautwald S, Linkermann A, Green D.R (2013) Widespread mitochondrial depletion via mitophagy does not compromise necroptosis. *Cell Rep.* 5(4), 878-885.

Tan S, Schubert D, Maher P (2001) Oxytosis: A novel form of programmed cell death. *Curr. Top. Med. Chem.* 1, 497–506.

Thapa R.J, Nogusa S, Chen P, Maki J.L, Lerro A, Andrade M, Rall G.F, Degterev A, Balachandran S (2013) Interferon-induced RIPK1/RIPK3-mediated necrosis requires PKR and is licensed by FADD and caspases. *Proc. Natl. Acad. Sci. U. S.A.* 110, E3109–E3118.

Thon L, Möhlig H, Mathieu S, Lange A, Bulanova E, Winoto-Mohrbach S, Schütze S, Bulfone-Paus S, Adam D (2005) Ceramide mediates caspase-independent programmed cell death. *FASEB J.* 19(14), 1945-1956.

Thon L, Mathieu S, Kableitz D, Adam D (2006) The murine TRAIL receptor signals caspase-independent cell death through ceramide. *Exp. Cell Res.* 312, 3808-3821.

Trad A, Riese M, Scomali M, Hedeman N, Effenberger T, Grötzinger J, Lorenzen I (2013) The disintegrin domain of ADAM17 antagonizes fibroblastcarcinoma cell interactions. *Int. J. Oncol.* 42, 1793-1800.

Trichonas G, Murakami Y, Thanos A, Morizane Y, Kayama M, Debouck C.M, Hisatomi T, Miller J.W, Vavvas D.G (2010) Receptor interacting protein kinases mediate retinal detachment-induced photoreceptor necrosis and compensate for inhibition of apoptosis. *Proc. Natl. Acad. Sci. U. S. A.* 107, 21695–21700.

Upton J.W, Kaiser W.J, Mocarski E.S (2012) DAI/ZBP1/DLM-1 complexes with RIPK3 to mediate virus-induced programmed necrosis that is targeted by murine cytomegalovirus vIRA. *Cell Host Microbe* 11, 290–297.

van Loo G, van Gurp M, Depuydt B, Srinivasula S.M, Rodriguez I, Alnemri E.S, Gevaert K, Vandekerckhove J, Declercq W, Vandenabeele P (2002) The serine protease Omi/HtrA2 is released from mitochondria during apoptosis. Omi interacts with caspase-inhibitor XIAP and induces enhanced caspase activity. *Cell Death Differ.* 9, 20–26.

Vande Walle L, Van Damme P, Lamkanfi M, Saelens X, Vandekerckhove J, Gevaert K, Vandenabeele P (2007) Proteome-wide identification of HtrA2/Omi Substrates. *Journal of Proteome Research* 6, 1006-1015.

Vande Walle L, Wirawan E, Lamkanfi M, Festjens N, Verspurten J, Saelens X, Vanden Berghe T, Vandenabeele P (2010) The mitochondrial serine protease HtrA2/Omi cleaves RIPK1 during apoptosis of Ba/F3 cells induced by growth factor withdrawal. *Cell Research* 20, 421-433.

Vanden Berghe T, Linkermann A, Jouan-Lanhouet S, Walczak H, Vandenabeele P (2014) Regulated necrosis: the expanding network of non-apoptotic cell death pathways. *Nat. Rev. Mol. Cell Biol.* 15, 135–147.

Vanhaesebroeck B, Decoster E, Van Ostade X, Van Bladel S, Lenaerts A, Van Roy F, Fiers W (1992) Expression of an exogenous tumor necrosis factor (TNF) gene in TNF-sensitive cell lines confers resistance to TNF-mediated cell lysis. *J. Immunol.* 148(9), 2785-2794.

Vitner E.B, Salomon R, Farfel-Becker T, Meshcheriakova A, Ali M, Klein A.D, Platt F.M, Cox T.M, Futerman A.H (2014) RIPK3 as a potential therapeutic target for Gaucher's disease. *Nat. Med.* 20, 204–208.

Wang H, Sun L, Su L, Rizo J, Liu L, Wang L.F, Wang F.S, Wang X (2014a) Mixed lineage kinase domain-like protein MLKL causes necrotic membrane disruption upon phosphorylation by RIPK3. *Mol. Cell* 54, 133–146.

Wang S, Ni H.M, Dorko K, Kumer S.C, Schmitt T.M, Nawabi A, Komatsu M, Huang H, Ding W.X (2016) Increased hepatic receptor interacting protein kinase 3 expression due to impaired proteasomal functions contributes to alcohol-induced steatosis and liver injury. *Oncotarget* 7 17681–17698.

Wang Y, Wang H, Tao Y, Zhang S, Wang J, Feng X (2014b) Necroptosis inhibitor necrostatin-1 promotes cell protection and physiological function in traumatic spinal cord injury. *Neuroscience* 266, 91–101.

Wang Z, Jiang H, Chen S, Du F, Wang X (2012) The mitochondrial phosphatase PGAM5 functions at the convergence point of multiple necrotic death pathways. *Cell* 148, 228-243.

Welz P.S, Wullaert A, Vlantis K, Kondylis V, Fernández-Majada V, Ermolaeva M, Kirsch P, Sterner-Kock A, van Loo G, Pasparakis M (2011) FADD prevents RIP3-mediated epithelial cell necrosis and chronic intestinal inflammation. *Nature.*; 477: 330-4.

Wen S, Ling Y, Yang W, Shen J, Li C, Deng W, Liu W, Liu K (2017) Necroptosis is a key mediator of enterocytes loss in intestinal ischaemia/reperfusion injury. *J. Cell. Mol. Med.* 21, 432–443.

Wertz I.E, O'Rourke K.M, Zhou H, Eby M, Aravind L, Seshagiri S, Wu P, Wiesmann C, Baker R, Boone D.L, Ma A, Koonin E.V, Dixit V.M (2004) De-ubiquitination and ubiquitin ligase domains of A20 downregulate NF-kappaB signalling. *Nature* 430, 694–699.

Willingham S.B, Bergstralh D.T, O'Connor W, Morrison A.C, Taxman D.J, Duncan J.A, Barnoy S, Venkatesan M.M, Flavell R.A, Deshmukh M, Hoffman H.M, Ting J.P (2007) Microbial pathogen-induced necrotic cell death mediated by the inflammasome components CIAS1/cryopyrin/NLRP3 and ASC. *Cell Host Microbe* 2, 147–159.

-
- Wong E, Maretzky T, Peleg Y, Blobel C.P, Sagi I** (2015) The functional maturation of a disintegrin and metalloproteinase (ADAM) 9, 10 and 17 requires processing at a newly identified protein convertase (PC) cleavage site. *J. Biol. Chem.* 290, 12135-12146.
- Woo Cho S, Kim S, Kim Y, Kweon J, Seok Kim H, Bae S, Kim J-S** (2014) Analysis of off-target effects of CRISPR/Cas-derived RNA-guided endonucleases and nickases. *Genome Res.* 24(1), 132-141.
- Yang Q.H, Church-Hajduk R, Ren J, Newton M.L, Du C** (2003) Omi/HtrA2 catalytic cleavage of inhibitor of apoptosis (IAP) irreversibly inactivates IAPs and facilitates caspase activity in apoptosis. *Genes Dev.* 17, 1487–1496.
- You Z, Savitz S.I, Yang J, Degterev A, Yuan J, Cuny G.D, Moskowitz M.A, Whalen M.J** (2008) Necrostatin-1 reduces histopathology and improves functional outcome after controlled cortical impact in mice. *J. Cereb. Blood Flow Metab.* 28, 1564–1573.
- Zeidan Y.H, Hannun Y.A** (2010) The acid sphingomyelinase/ceramide pathway: Biomedical significance and mechanisms of regulation. *Curr. Mol. Med.* 10 (5), 454-466.
- Zhang D.W, Shao J, Lin J, Zhang N, Lu B.J, Lin S.C, Don M.Q, Han J** (2009) RIPK3, an energy metabolism regulator that switches TNF-induced cell death from apoptosis to necrosis. *Science* 325, 332–336.
- Zhang T, Zhang Y, Cui M, Jin L, Wang Y, Lv F, Liu Y, Zheng W, Shang H, Zhang J, Zhang M, Wu H, Guo J, Zhang X, Hu X, Cao C.M, Xiao R.P** (2016) CaMKII is a RIPK3 substrate mediating ischemia- and oxidative stress-induced myocardial necroptosis. *Nat. Med.* 22, 175–182.
- Zhang Y, Su S.S, Zhao S, Yang Z, Zhong C.Q, Chen X, Cai Q, Yang Z.H, Huang D, Wu R, Han J** (2017) RIPK1 autophosphorylation is promoted by mitochondrial ROS and is essential for RIPK3 recruitment into necrosome. *Nat. Commun.* 8, 14329.
- Zhang X-H, Tee L.Y, Wang X-G, Huang Q-S, Yang S-H** (2015) Off-target effects in CRISPR/Cas9-mediated Genome Engineering. *Mol. Ther. Nucleic Acids* 4(11), e264.
- Zhu S, Zhang Y, Bai G, Li H** (2011) Necrostatin-1 ameliorates symptoms in R6/2 transgenic mouse model of Huntington's disease. *Cell Death Dis.* 2, e115.
-

Zhu X, Tao L, Tejima-Mandeville E, Qiu J, Park J, Garber K, Ericsson M, Lo E.H, Whalen M.J (2012) Plasmalemma permeability and necrotic cell death phenotypes after intracerebral hemorrhage in mice. *Stroke* 43, 524–531.

Zunke F, Rose-John S (2017) The shedding protease ADAM17: Physiology and pathophysiology. *Biochim. Biophys. Acta* 1864, 2059-2070.

7 List of publications

Fuchslocher Chico J, Saggau C, Adam D (2017) Proteolytic control of regulated necrosis. *Biochim. Biophys. Acta* 1864, 2147-2161.

Sommer A, Düppe M, Baumecker L, Kordowski F, Büch J, Fuchslocher Chico J, Fritsch J, Schütze S, Adam D, Sperrhacke M, Bhakdi S, Reiss K (2017) Extracellular sphingomyelinase activity impairs TNF-alpha signalling in endothelial cells via ADAM 17 activation and TNF receptor 1 shedding. *Oncotarget* 8(42), 72584-72596.

Sosna J, Phillipp S, Fuchslocher Chico J, Saggau C, Fritsch J, Föll A, Plenge J, Arenz C, Pinkert T, Kalthoff H, Trauzold A, Schmitz I, Schütze S, Adam D (2016) Differences and similarities in TRAIL- and TNF-mediated necroptotic signalling in cancer cells. *Mol. Cell. Biol.* 36(20), 2626-2644.

Submitted for publication

Fuchslocher Chico J, Falk-Paulsen M, Luzius A, Saggau C, Ruder B, Bolik J, Schmidt-Arras D, Linkermann A, Becker C, Rosenstiel P, Rose-John S, Adam D (2017) The enhanced susceptibility of ADAM-17 hypomorphic mice to DSS-induced colitis is not ameliorated by loss of RIPK3, revealing an unexpected function of ADAM-17 in necroptosis.

8 Curriculum Vitae

Personal data

First name(s): Johaiber Ilich
Family name(s): Fuchslocher Chico
Birthdate: 09/ 09/ 1989
Birthplace: Caracas, Venezuela
Nationality: German

Scientific Career

School

09/2005 – 08/2007 Graduation from High School
Colegio Escuelas Pías Quisisana (Tenerife, Spain)

University

09/2007 - 08/2010 Basic studies (Biology), six semesters
Universidad La Laguna (Tenerife, Spain)

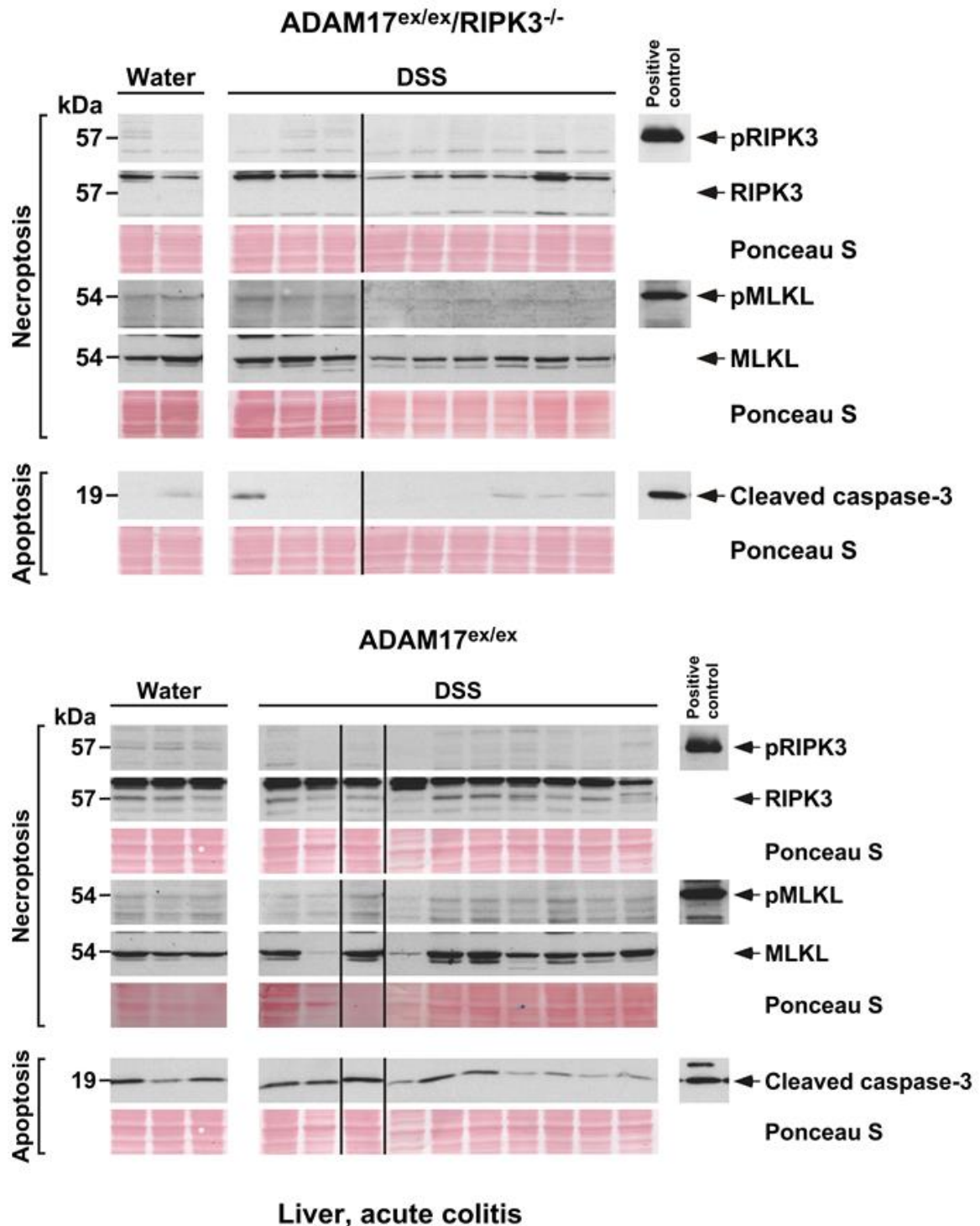
09/2010 - 08/2012 Main studies and graduation (Biology)
Focus: Genetics and cellular biology, four semesters
Universidad Autónoma de Madrid (Madrid, Spain)

Graduation thesis
Development of an experimental method to detect genomic
deletions, duplications and SNV's
INGEMM, Hospital Universitario La Paz (Madrid, Spain).

09/2012 – 02/2014 Master of Science
Christian-Albrechts-Universität zu Kiel (Kiel, Germany)
Focus: Genetics and cellular biology, three semesters,
interrupted to start the PhD

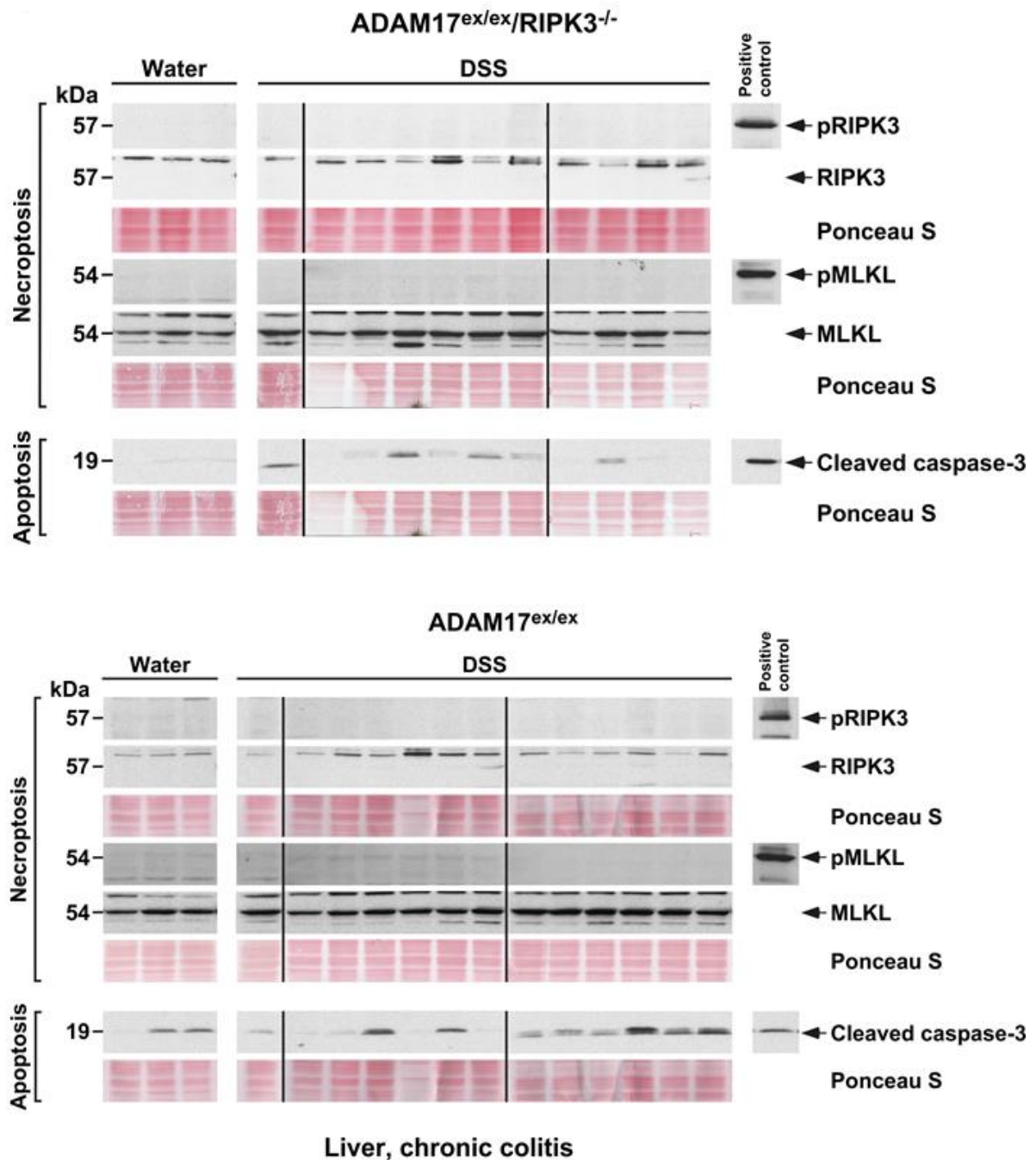
PhD

07/2014 – 12/2017 Proteolytic control of necroptosis
Christian-Albrechts-Universität zu Kiel, Institut für Immunologie
(Kiel, Germany)

9 Appendix**Appendix figure 1**

Western blot analysis of lysates isolated from liver tissue samples of the ADAM17^{ex/ex} RIPK3^{-/-} and ADAM17^{ex/ex} mice participating in the DSS-induced acute colitis experiment. Performed in separate gels to avoid overlapping of pMLKL/MLKL and pRIPK3/RIPK3 signals. Ponceau S staining was performed as a loading control.

Positive control for necroptosis are lysates from MEF pre-stimulated with 1 μ g/mL CHX and 20 μ M zVAD for 30 min, and then stimulated with 100 ng/mL TNF for 16 h to induce necroptosis. Positive control for apoptosis is made of lysates from MEF pre-stimulated with 1 μ g/mL CHX for 30 min, and then stimulated with 100 ng/mL TNF for 16 h to induce apoptosis.

**Appendix figure 2**

Western blot analysis of lysates generated from liver tissue samples of the ADAM17^{ex/ex} RIPK3^{-/-} and ADAM17^{ex/ex} mice participating in the DSS-induced chronic colitis experiment. Performed in separate gels to avoid overlapping of signals corresponding to pMLKL/MLKL and pRIPK3/RIPK3. Ponceau S staining was performed to serve as a loading control. Positive control for necroptosis consists of lysates from MEF pre-stimulated with 1 μ g/mL CHX and 20 μ M zVAD for 30 min, and then stimulated with 100 ng/mL TNF for 16 h to elicit necroptosis. Positive control for apoptosis consists of lysates from MEF pre-stimulated with 1 μ g/mL CHX for 30 min, and then stimulated with 100 ng/mL TNF for 16 h to elicit apoptosis.